INFORMATION TO USERS

This manuscript has been reproduced from the microfilm master. UMI films the text directly from the original or copy submitted. Thus, some thesis and dissertation copies are in typewriter face, while others may be from any type of computer printer.

The quality of this reproduction is dependent upon the quality of the copy submitted. Broken or indistinct print, colored or poor quality illustrations and photographs, print bleedthrough, substandard margins, and improper alignment can adversely affect reproduction.

In the unlikely event that the author did not send UMI a complete manuscript and there are missing pages, these will be noted. Also, if unauthorized copyright material had to be removed, a note will indicate the deletion.

Oversize materials (e.g., maps, drawings, charts) are reproduced by sectioning the original, beginning at the upper left-hand corner and continuing from left to right in equal sections with small overlaps.

Photographs included in the original manuscript have been reproduced xerographically in this copy. Higher quality 6" x 9" black and white photographic prints are available for any photographs or illustrations appearing in this copy for an additional charge. Contact UMI directly to order.

ProQuest Information and Learning
300 North Zeeb Road, Ann Arbor, MI 48106-1346 USA
800-521-0600

Evaluation of the Uniform Theory of Diffraction for Edge Diffraction at Low Frequency

Riman Shukayr

A Thesis
In
The Department
of
Electrical and Computer Engineering

Presented in Partial Fulfillment of the Requirements

For the Degree of Master of Applied Science at

Concordia University

Montréal, Québec, Canada

August, 2001

ABSTRACT

Evaluation of the Uniform Theory Of Diffraction
for Edge Diffraction at Low Frequency

Riman Shukayr

This thesis examines the UTD diffraction coefficient's limitations in accuracy for a half plane and a wedge at low frequency. The UTD solutions are developed for scattering by a strip and a square cylinder with diffraction considered as a local phenomenon. Single and multiple diffractions are considered, and both TE and TM polarizations are done.

As a benchmark, moment method solutions are developed for the strip and square cylinder. Pulse basis point matching is used after investigating its adequacy: some moment method codes that are available in the open literature were examined; in one instance some modifications were required to obtain satisfactory results. For the infinite edge, comparison is done with modal solutions and Sommerfeld's exact solution. The UTD diffraction solution reduces to Sommerfeld's exact solution when the edge is a half plane and the incident field is a plane wave. The equivalence of these cases is not obvious and is derived as part of this work. Other comparisons are made with results that are available in the literature.

It was found that UTD, when multiple diffraction is taken into account, can be used to compute scattered fields and surface currents for scatterers as small as

0.1 λ in dimension, with a very high degree of accuracy. This is quite surprising, as UTD is generally expected to only work well with electrically large structures on the order of 1 λ in size or larger.

ACKNOWLEDGEMENT

I am grateful to E. A. Poe and C. Beaudelaire for indirectly causing me to attend my first EMC course. A special tribute is owed to Dr. S. Kubina whose great enthusiasm and knowledge in teaching the EMC course at Concordia university triggered my interest and convinced me to pursue research in electromagnetics.

I wish to thank my supervisor Dr. R. Paknys for sharing his knowledge and spending time on long, interesting and inspiring conversations. His understanding of my academic inactivity during periods of business travel was greatly appreciated and permitted me to pursue a demanding career in parallel with research.

I am in debt to J. Jolicoeur for typing this manuscript in a record time after overcoming two computer viruses.

Finally, I would like to dedicate this work to my parents who more than 50 years after the amateur installation of the "radio à galène" antenna in Arsoun, never suspected that their son will be dealing with waves and their scattering.

TABLE OF CONTENTS

TABLE OF CONTENTS (continued)

LIST OF FIGURES

LIST OF FIGURES (continued)

LIST OF FIGURES (continued)

LIST OF FIGURES (continued)

LIST OF FIGURES (continued)

LIST OF TABLES

1 INTRODUCTION

The analysis of scattering problems using the uniform theory of diffraction (UTD) is used usually for objects with dimensions of many wavelengths or larger. This stems from the fact that UTD solutions are generated by high frequency asymptotic techniques.

The purpose of this work is to evaluate the behavior of UTD at low frequency. The UTD Edge diffraction solution is one of the most used tools [1] to solve problems dealing with modeling of antennas on complex platforms. Proving the accuracy of UTD at low frequencies could be very advantageous. A typical application would be to predict the radiation pattern and hence the performance of an antenna mounted on the fuselage of an airplane when the frequency used is low or the airplane structure is electrically small. This will minimize the usage of measurements requiring expensive scale modeling to design and locate antennas.

To achieve this evaluation, a well proven independent method is needed to be established and used for comparison with UTD. It is of great importance also to study many scattering cases to be able to establish the major reasons that cause UTD to fail. At a first glance, going low in frequency by itself is supposed to be a sufficient cause for UTD solutions to degrade. It will be shown however that UTD solutions for some electrically small scatterers are adequate and major parameters affecting the success of UTD are the scattering problem geometry, the incidence angle and the field polarization.

Both TEz and TMz plane wave illumination with different angles of incidence are considered here. Different scatterer shapes also are used. These shapes are of simple geometry and they include the infinite edge, the strip and the rectangular cylinder. The choice of these shapes is not arbitrary since they are considered building blocks for more complex geometries and they can be considered as a series of tests, ascending in difficulty, for UTD to pass.

The edge is a canonical problem. The strip is a combination of two back to back half planes where diffraction is the most severe and multiple diffraction is existent but for which UTD is an exact solution to first order diffraction (special case). The rectangular cylinder is the combination of four 90° edges for which diffraction is in a sense halfway between the highest diffraction (half plane) and no diffraction at all (full plane) but for which UTD is not an exact solution and where multiple diffraction is present. Radiation patterns are usually the results thought of in a scattering problem. Since a low frequency is used however, the radiation patterns for such small electrical scatterers hold few surprises. The surface current density distributions are the most sensitive variables to changes on an electrically small scatterer.

In the next chapters, the surface current densities on edges, strips and rectangular cylinders for different illumination incidence angles and polarization are plotted and a conclusion is made regarding the results obtained.

Through out this work the $e^{j\omega t}$ time variation is understood and suppressed.

2 BACKGROUND

2.1 UTD AS A HIGH FREQUENCY METHOD

The fields generated by radiation and scattering of electromagnetic waves incident upon conducting two-dimensional wedges could be found using modal solutions. Most of these solutions however consist of infinite series, which are poorly convergent [2]. To overcome this limitation, the Uniform Theory of Diffraction (UTD) which is an extension of the Geometrical Theory of Diffraction (GTD) uses high frequency asymptotic techniques to make the modal solution mathematically manageable.

Typically, GTD transforms the modal solution infinite series into integrals and then obtains a high frequency ($k\rho$ large) asymptotic expansion for them by means of residue complex calculus contour integration (geometrical optics terms) and the conventional method of steepest descent (diffraction terms) [2]. Even though this method separates and defines clearly the total geometrical optics and total diffracted fields, the formulation of the diffracted fields is valid only for observations made far from the incident and reflected shadow boundaries (kLa large).

UTD is based on GTD but uses the so-called Pauli-Clemmow modified method of steepest descent [3], which compensates for singularities along the corresponding shadow boundaries. This compensation is done by an additional discontinuous function (transition function) proportional to a Fresnel integral. Away from shadow boundaries, this integral is nearly unity and the UTD formulation reduces to the GTD formulation. UTD provides the total field solution for the 2-D scattering problem shown in fig 2.1a as

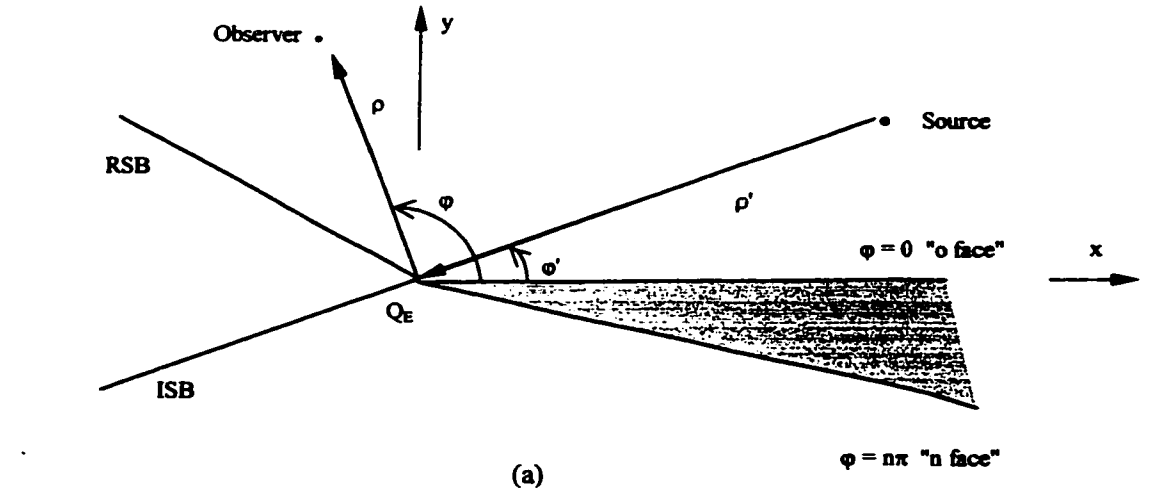

(a)

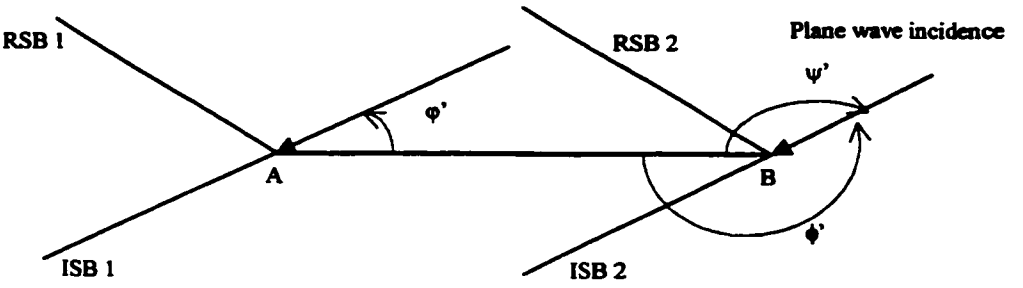

(b)

Figure 2.1: UTD 2-D wedge diffraction geometry.(a) Canonical edge. (b) Combination of two edges (half planes, n=2) back to back to evaluate the local diffraction of each edge of a strip.

$$E_z = E_z^i + E_z^r + E_z^d \quad \text{for the TMz (soft) case} \tag{2.1}$$

$$H_z = H_z^i + H_z^r + H_z^d \quad \text{for the TEz (hard) case} \tag{2.2}$$

The incident field is nonexistent beyond the incident shadow boundary (ISB), the reflected field is nonexistent beyond the reflected shadow boundary (RSB) and the diffracted field is given by the following [3]:

$$E_z^d = E_z^i(Q_E) \times \frac{e^{-jk\rho}}{\sqrt{\rho}} \times D_s(\rho, L, \varphi, \varphi', n) \tag{2.3}$$

$$H_z^d = H_z^i(Q_E) \times \frac{e^{-jk\rho}}{\sqrt{\rho}} \times D_h(\rho, L, \varphi, \varphi', n) \tag{2.4}$$

Where $E_z^i(Q_E)$ or $H_z^i(Q_E)$ is the field incident on the edge and the diffracted field appearing to be generated by the edge Q_E as a cylindrical wave. The UTD diffraction coefficient is given by [3]:

$$D_{s,h} = \frac{e^{-j\frac{\pi}{4}}}{2n\sqrt{2\pi k}\sin\beta_0} \times \left[\begin{array}{l} \cot\left(\frac{\pi + (\varphi - \varphi')}{2n}\right) F\left(kLa^+(\varphi - \varphi')\right) \\ + \cot\left(\frac{\pi - (\varphi - \varphi')}{2n}\right) F\left(kLa^-(\varphi - \varphi')\right) \\ \mp \left\{ \begin{array}{l} \cot\left(\frac{\pi + (\varphi + \varphi')}{2n}\right) F\left(kLa^+(\varphi + \varphi')\right) \\ + \cot\left(\frac{\pi - (\varphi + \varphi')}{2n}\right) F\left(kLa^-(\varphi + \varphi')\right) \end{array} \right\} \end{array} \right] \tag{2.5}$$

The - and the + signs in $\mp$ correspond to the soft (TMz) and hard (TEz) case respectively. For the 2-D case we have always $\beta_0 = \frac{\pi}{2}$. The distance parameter L is given by [3]:

$L=\rho$ for plane wave incidence or

$$L=\frac{\rho\rho'}{\rho+\rho'} \quad \text{for cylindrical wave incidence} \tag{2.6}$$

the transition function F is

$$F(X)=2j\sqrt{X}e^{jX}\int_{\sqrt{X}}^{\infty}e^{-j\tau^2}d\tau \tag{2.7}$$

with the expression for $a^{\pm}(\varphi\pm\varphi')$ being

$$a^{\pm}(\varphi\pm\varphi')=2\cos^2\left(\frac{2n\pi N^{\pm}-(\varphi\pm\varphi')}{2}\right) \tag{2.8}$$

in this expression, $N^{\pm}$ are the integers which most satisfy the equations:

$$2n\pi N^{+}-(\varphi\pm\varphi')=\pi \quad \text{and} \quad 2n\pi N^{-}-(\varphi\pm\varphi')=-\pi \tag{2.9}$$

It is a measure of the angular separation between the observation point and the shadow boundaries. Away from the boundaries *kLa* is large and it is easy to show that the transition function becomes unity and the diffraction coefficient reduces to its GTD formulation.

In words, UTD shows that the scattered field by an infinite edge is the same as the one obtained by geometrical optics with the addition of the local edge diffraction effect. This concept of treating the edge diffraction as a local phenomenon is very interesting and could be utilized in making the edge part of a building block of more complex shapes than the canonical infinite edge itself. Figure 2.1(b) shows an example of how this concept is used. The strip shown in Figure 2.1(b) is illuminated by a plane wave at an angle of incidence of φ'. In

geometrical optics terms it is easy to see that the incident field is present everywhere except between ISB 1 and ISB 2 below the strip The reflected field is present only between RSB 1 and RSB 2 above the strip. To evaluate the diffracted field however, the strip is considered to be a combination of two edges (back to back) one at A and the other at B. These edges are half planes (n=2). The diffracted fields from A and B can be computed from equations 2.3 and 2.4. The diffraction coefficient parameters must however be properly defined. For the case of Figure 2.1(a), they are:

$D^{A}_{..}(\rho_A, L_A, \varphi, \varphi', n)$ and $D^{B}_{..}(\rho_B, L_B, \psi, \psi', n)$

where,

ρ_A = distance from the observer to A

ρ_B = distance from the observer to B

$L_A=\rho_A$ (plane wave incidence)

$L_A=\rho_B$ (plane wave incidence)

φ'= angle of incident wave with 'o face' of edge A

φ= angle of $\vec{\rho}_A$ with 'o face' of edge A

ψ'= angle of incident wave with 'o face' of edge B

ψ =angle of $\vec{\rho}_B$ with 'o face' of edge B

n=2 (half plane)

For this case, the strip upper surface was considered to be the 'o face' of edge B but if it was the lower surface to be used, ψ and ψ' should be replaced by ϕ and ϕ' respectively.

The building of more complex geometries can be done also by considering A and B to be 90° edges (back to back) and add to them another two 90° edges C and D below to form a rectangular cylinder. The same analysis followed above applies to the rectangular cylinder with additional RSBs and ISBs to respect all the surfaces and with diffraction coefficient parameters evaluated with respect to

the distance from each edge and the angle from each edge 'o face' surface with n being representative of the angle of the edge.

The above listed UTD formulation was derived using asymptotic approximations for high frequencies. It should not be forgotten here that by high frequency approximation, it is meant that kL is assumed to be large. This means that the observation point is far away from the edge. No deep investigation however has shown yet to what extent this formulation can be used with success when going lower in frequency. In [3] it is mentioned that the diffraction coefficient obtained by UTD for an incident plane wave ($L=\rho$) is found to be accurate for $kL>1.0$. In [4], the field error computed by UTD as close as 0.25 λ near the edge of a 90° wedge was found to be very small.

The goal of the present work is to show to what extent the frequency can be reduced, with the UTD formulation still being accurate. Practically speaking this does not imply verifying only the total UTD field solution accuracy near the edge of scattering created by incident plane waves on infinite wedges, it consists of the following:

a) Verifying the accuracy of UTD when used on electrically small scatterers. Since diffraction is a local phenomenon, the infinite edge canonical solution can be used as a building block solution for different 2-D shapes scatterers like plates and rectangular cylinders.
b) Verifying UTD success when used to figure the current singularity at the edge, which exists in the TMz case
c) Verifying UTD success when used on electrically small scatterers where the phenomenon of multiple diffraction due to nearby edges becomes important. In this case not only incidence of plane waves (at low

frequency) on edges is present only but cylindrical-like waves also and this is of great significance.

To establish the success criteria of UTD at low frequency the following needs to be defined:

- The type of UTD derived results to be assessed (i.e. radiation patterns, field values, surface currents on scatterers, etc.)
- The formulation of UTD to be used specially in computer programs.
- The independent method (able to solve similar problems as UTD) and its computer formulation to be used to test the UTD results. Obviously this method should be totally UTD independent from the theoretical formulation point of view. It should be also a well-proven method already used with success.

The above mentioned subjects will be covered in the following sections.

2.2 CHOICE BETWEEN UTD RADIATION PATTERNS & SURFACE CURRENTS

At the beginning of this investigation, radiation patterns were considered to be more practical as a UTD end result. Since the interest however was to explore the low frequency limit of UTD, the scatterers to be used must be electrically small (dimension below 1λ). Several computer FORTRAN codes (some already existent and some created specifically for this task) were used to plot radiation patterns of line sources above electrically small plates and cylinders. The results compared well between themselves.

The patterns however were almost isotropic. This was something to expect for a far field pattern when the only scatterers disturbing the incident fields had dimensions of 0.2λ or below. Figure 2.2 shows the radiation pattern of a magnetic line source above an infinite strip (plate) and also above an infinite rectangular cylinder. Both the plate and the rectangular cylinder have a width of 0.2λ. The magnetic line source is 0.05λ above the plate or cylinder surface. The code used is based on the moment method. Figure 2.3 shows the radiation pattern of a magnetic line source above an infinite plate with the same geometry as for Figure 2.2 except that the code used is based on UTD.

It is quite obvious that both methods emphasize the fact that at such a low frequency (electrically small scatterers) the radiation patterns are almost uniform and omni directional. Some plots also were done for the surface currents and they were almost identical non withstanding the method used to produce them. It is interesting to note however that changes made to moment method codes to use a smaller number of segments resulted in noticeable differences in the surface current plots but almost none in the radiation pattern ones. After this observation it was decided to use surface current values and plots as the criteria

to be based upon to establish UTD results success at low frequency. After all, currents are the building blocks for a multitude of practical results used by industry and research. It is important to note at this stage the discontinuity at the edges in Figure 2.3. Since the code used depends on a model of two simple half plane diffractions (back to back), if $\varphi = 0$ deg and $\varphi = 360^{o}$ the diffracted fields are very different. The same edge, as part of a strip, is expected to be continuous as we go from $\varphi = 359.9°$ to $\varphi = 0.1°$. Double diffraction will eliminate this problem, but this, with additional details on computer codes used, will be discussed in later sections.

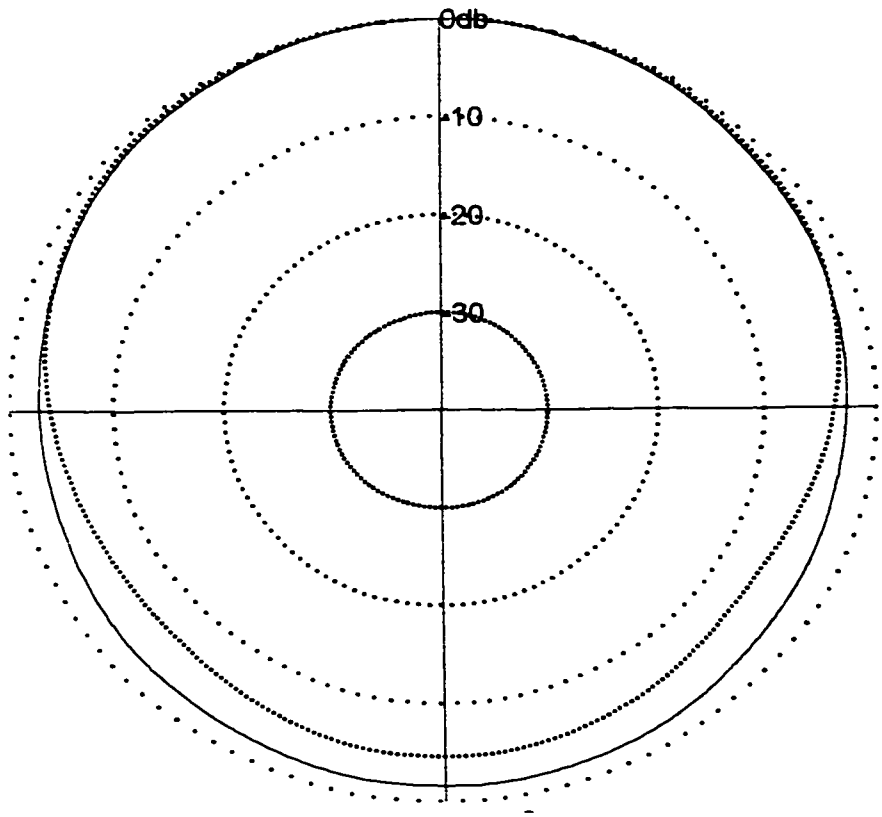

Figure 2.2: Radiation pattern (Normalized power in dB) for a magnetic line source above (height = 0.0012) a strip (width = 0.2 λ , solid line) and a rectangular cylinder (by 0.2 λ) using moment method.

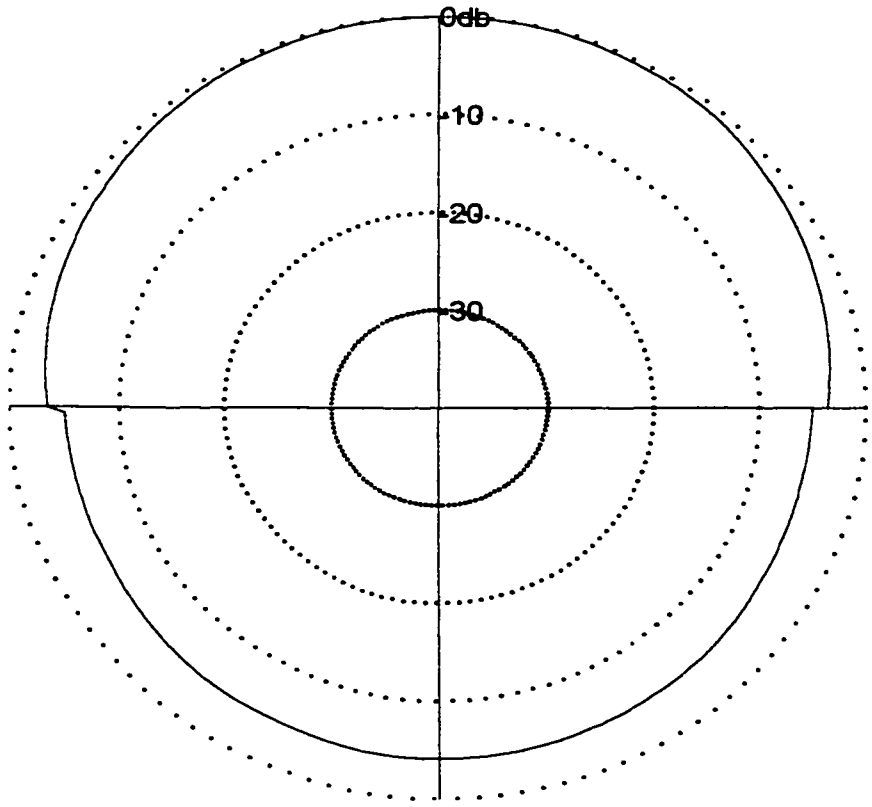

Figure 2.3: Radiation pattern (Normalized power in dB) for a magnetic line source above (height = 0.001 λ) a strip (by 0.2 λ) using first order diffraction (UTD).

2.3 COMPARING UTD GENERAL FORMULATION AND AN EXACT SOLUTION

The formulation of the diffracted field in section 2.1 was taken from [3]. The present work uses this formulation as the basis for all computer codes created to compute and plot surface currents on scatterers derived from a UTD solution. As mentioned earlier, an independent method will be used to compare results. Before starting however to use the codes based on UTD it was important to gain a high level of confidence in the formulation and its corresponding subroutine codes. As stated in [3], for half planes illuminated with a perpendicular to edge plane wave, there is an exact solution (obtained by Sommerfeld). The goal in this section is to prove that the UTD formulation in section 2.1 reduces to an exact solution for the special case of a half plane illuminated by a plane wave and to compute and plot the exact solution results. These results will be used to validate results obtained by the UTD general formulation and subroutine code especially.

2.3.1 Reduction of the UTD Formulation:

For a half plane illuminated by a plane wave, as shown in Figure 2.1, n=2 and $L=\rho$. This leads to the following reductions:

Equation 2.8 becomes: $$a^{\pm}(\varphi\pm\varphi')=2\cos^2\left(\frac{\varphi\pm\varphi'}{2}\right)$$

Using this reduces equation 2.5 to:

$$D_{s,h}=\frac{e^{-j\frac{\pi}{4}}}{4\sqrt{2\pi k}}\times\left[\begin{array}{l}\cot\left(\frac{\pi+(\varphi-\varphi')}{4}\right)F\left(k\rho 2\cos^2\left(\frac{(\varphi-\varphi')}{2}\right)\right)\\+\cot\left(\frac{\pi-(\varphi-\varphi')}{4}\right)F\left(k\rho 2\cos^2\left(\frac{(\varphi-\varphi')}{2}\right)\right)\\\mp\left\{\begin{array}{l}\cot\left(\frac{\pi+(\varphi+\varphi')}{4}\right)F\left(k\rho 2\cos^2\left(\frac{(\varphi+\varphi')}{2}\right)\right)\\+\cot\left(\frac{\pi-(\varphi+\varphi')}{4}\right)F\left(k\rho 2\cos^2\left(\frac{(\varphi+\varphi')}{2}\right)\right)\end{array}\right\}\end{array}\right]$$

Now since [5]

$$\cot\left(\frac{\pi+X}{4}\right)+\cot\left(\frac{\pi-X}{4}\right)=\frac{1-\tan\left(\frac{\pi}{4}\right)\times\tan\left(\frac{X}{4}\right)}{\tan\left(\frac{\pi}{4}\right)+\tan\left(\frac{X}{4}\right)}+\frac{1+\tan\left(\frac{\pi}{4}\right)\times\tan\left(\frac{X}{4}\right)}{\tan\left(\frac{\pi}{4}\right)-\tan\left(\frac{X}{4}\right)}$$

$$=\frac{1-\tan\left(\frac{X}{4}\right)}{1+\tan\left(\frac{X}{4}\right)}+\frac{1+\tan\left(\frac{X}{4}\right)}{1-\tan\left(\frac{X}{4}\right)}=\frac{2+2\tan^2\left(\frac{X}{4}\right)}{1-\tan^2\left(\frac{X}{4}\right)}$$

which after expansion in sine and cosine terms becomes = $\frac{2}{\cos(X/2)}$;

then taking into consideration equation 2.7 this will lead to a diffraction coefficient

$$D_{s,h}=\frac{e^{-j\frac{\pi}{4}}}{4\sqrt{2\pi k}}\times\left[\begin{array}{l}\frac{2}{\cos\left(\frac{\varphi-\varphi'}{2}\right)}\times\left\{2j\sqrt{k\rho 2\cos^2\left(\frac{\varphi-\varphi'}{2}\right)}e^{jk\rho 2\cos^2\left(\frac{\varphi-\varphi'}{2}\right)}\int_{\sqrt{k\rho 2\cos^2\left(\frac{\varphi-\varphi'}{2}\right)}}^{\infty}e^{-j\tau^2}d\tau\right\}\\\mp\frac{2}{\cos\left(\frac{\varphi+\varphi'}{2}\right)}\times\left\{2j\sqrt{k\rho 2\cos^2\left(\frac{\varphi+\varphi'}{2}\right)}e^{jk\rho 2\cos^2\left(\frac{\varphi+\varphi'}{2}\right)}\int_{\sqrt{k\rho 2\cos^2\left(\frac{\varphi+\varphi'}{2}\right)}}^{\infty}e^{-j\tau^2}d\tau\right\}\end{array}\right]$$

The diffracted field of equations 2.3 and 2.4 reduces to

$$\begin{pmatrix} Diffracted \\ field\ at\ \rho \end{pmatrix}_{s,h} = \begin{pmatrix} Incident \\ field\ at \\ edge \end{pmatrix}_{s,h} \times \frac{-e^{-j\left(k\rho-\frac{\pi}{4}\right)}}{\sqrt{\pi}} \times \left[\begin{array}{l} \mathrm{sgn}\left(\pi-(\varphi-\varphi')\right) \times \left\{ e^{jk\rho 2\cos^2\left(\frac{\varphi-\varphi'}{2}\right)} \int_{\sqrt{2k\rho}\cos\left|\frac{\varphi-\varphi'}{2}\right|}^{\infty} e^{-j\tau^2} d\tau \right\} \\ \mp \mathrm{sgn}\left(\pi-(\varphi+\varphi')\right) \times \left\{ e^{jk\rho 2\cos^2\left(\frac{\varphi+\varphi'}{2}\right)} \int_{\sqrt{2k\rho}\cos\left|\frac{\varphi+\varphi'}{2}\right|}^{\infty} e^{-j\tau^2} d\tau \right\} \end{array} \right]$$

Since $2\cos^2\left(\frac{\varphi\pm\varphi'}{2}\right) = \left(\cos(\varphi\pm\varphi')\right)+1$

and $e^{j\frac{\pi}{4}} = \frac{\sqrt{2}}{2}(1+j)$

the final formulation of equations 2.3 and 2.4 is:

(Diffracted field)$_{s,h}$ =

$$\begin{pmatrix} Incident \\ field \end{pmatrix}_{s,h} \times \left(\frac{-(1+j)}{2}\right)\sqrt{\frac{2}{\pi}} \times \left[\begin{array}{l} \mathrm{sgn}\left(\pi-(\varphi-\varphi')\right) \times \left\{ e^{jk\rho\cos(\varphi-\varphi')} \int_{\sqrt{2k\rho}\cos\left|\frac{\varphi-\varphi'}{2}\right|}^{\infty} e^{-j\tau^2} d\tau \right\} \\ \mp \mathrm{sgn}\left(\pi-(\varphi+\varphi')\right) \times \left\{ e^{jk\rho\cos(\varphi+\varphi')} \int_{\sqrt{2k\rho}\cos\left|\frac{\varphi+\varphi'}{2}\right|}^{\infty} e^{-j\tau^2} d\tau \right\} \end{array} \right] \quad (2.10)$$

2.3.2 Sommerfeld Exact Solution

for the case of a half plane illuminated by a perpendicular plane wave (ref. to fig. 2.1) Sommerfeld [6][7] resolved the problem by methods based on the concept of a two-sheeted Riemann surface. The solution for the total field (for a unity incident field) is:

$$\text{(Total Field at } \rho)_{s,h} = \begin{bmatrix} e^{jk\rho\cos(\varphi-\varphi')} \times \left(\frac{1+j}{2}\right) \times \int_{-\infty}^{2\sqrt{\frac{k\rho}{\pi}}\cos\left(\frac{\varphi-\varphi'}{2}\right)} e^{-j\frac{\pi\tau^2}{2}} d\tau \\ \mp e^{jk\rho\cos(\varphi+\varphi')} \times \left(\frac{1+j}{2}\right) \times \int_{-\infty}^{2\sqrt{\frac{k\rho}{\pi}}\cos\left(\frac{\varphi+\varphi'}{2}\right)} e^{-j\frac{\pi\tau^2}{2}} d\tau \end{bmatrix} \tag{2.11}$$

Since this is the total field solution, the goal in this section is to expand or reduce as necessary to obtain a geometrical optic term and a diffraction term (segregated) so that comparison could be made with equations in section 2.1. With a variable transformation $t=\sqrt{\frac{\pi}{2}}\tau$, the integral in equation 2.11 will be:

$$\sqrt{\frac{2}{\pi}} \int_{-\infty}^{\sqrt{2k\rho}\cos\left(\frac{\varphi\pm\varphi'}{2}\right)} e^{-jt^2} dt$$

With another variable transformation $U=-t$, the same integral will be:

$$\sqrt{\frac{2}{\pi}} \int_{-\sqrt{2k\rho}\cos\left(\frac{\varphi\pm\varphi'}{2}\right)}^{\infty} e^{-jU^2} dU \tag{2.12}$$

If the lower limit of the integral is negative and since the function is symmetrical, the integral can be written as:

$$\sqrt{\frac{2}{\pi}} \times \left[2\int_0^{\infty} e^{-jU^2} dU - \int_{-\sqrt{2k\rho}\cos\left(\frac{\varphi\pm\varphi'}{2}\right)}^{\infty} e^{-jU^2} dU \right]$$

Since [8][9] the Fresnel integral is $\int_0^{\infty} e^{-j\tau^2} d\tau = \sqrt{\frac{\pi}{2}} \times \left(\frac{1-j}{2}\right)$

then the final integral will be:

$$\sqrt{\frac{2}{\pi}} \times \left[\sqrt{\frac{\pi}{2}}(1-j) - \int_{-\sqrt{2k\rho}\cos\left(\frac{\varphi\pm\varphi'}{2}\right)}^{\infty} e^{-jU^2} dU \right] \tag{2.13}$$

If the lower limit of the integral in (2.12) is positive, the result will be:

$$\sqrt{\frac{2}{\pi}} \times \left[\int_{-\sqrt{2kp}\cos\left(\frac{\varphi \pm \varphi'}{2}\right)}^{\infty} e^{-jU^2} dU \right] \qquad (2.14)$$

The following tables will show the integral to be used according to the sign of its lower limit.

$\varphi-\varphi'$	-2π	$-\pi$	o	$+\pi$	$+2\pi$
$\frac{(\varphi-\varphi')}{2}$	$-\pi$	$-\frac{\pi}{2}$	o	$+\frac{\pi}{2}$	$+\pi$
$\cos\left(\frac{\varphi-\varphi'}{2}\right)$	negative	positive	positive	negative	
Integral equation	eq 2.14	eq 2.13	eq 2.13	eq 2.14	

Table 2.1

$\varphi+\varphi'$	o	π	2π	3π	4π
$\frac{(\varphi+\varphi')}{2}$	o	$\frac{\pi}{2}$	π	$\frac{3\pi}{2}$	2π
$\cos\left(\frac{\varphi+\varphi'}{2}\right)$	positive	negative	negative	positive	
Integral equation	eq 2.13	eq 2.14	eq 2.14	eq 2.13	

Table 2.2

It is quite obvious that the integral formulation changes at the reflection shadow boundary and incident shadow boundary. This means that equation 2.13 includes a non continuous term existent for all φ before the RSB and another one existent for all φ before the ISB. The final formulation in equation. 2.11 can be written finally in a way to segregate between the individual geometrical optics and the diffraction terms. For simplicity, only incidence angles above the plane

will be considered here and unit magnitude incident fields. Taking into consideration tables 2.1 & 2.2 and using equations 2.13 and 2.14 accordingly transforms equation 2.11 to the following:

$$\text{(Total field)}_{s,h} = \left[\begin{array}{l} e^{jk\rho\cos(\varphi-\varphi')}U(\pi-(\varphi-\varphi')) \\ \mp e^{jk\rho\cos(\varphi+\varphi')}U(\pi-(\varphi+\varphi')) \\ \\ \dfrac{1+j}{2}\sqrt{\dfrac{2}{\pi}} \left\{ \begin{array}{l} e^{jk\rho\cos(\varphi-\varphi')} \times \displaystyle\int_{\sqrt{2k\rho}\cos\left(\frac{\varphi-\varphi'}{2}\right)}^{\infty} e^{-jU^2} dU \times \operatorname{sgn}(\pi-(\varphi-\varphi')) \\ \mp e^{jk\rho\cos(\varphi+\varphi')} \times \displaystyle\int_{\sqrt{2k\rho}\cos\left(\frac{\varphi+\varphi'}{2}\right)}^{\infty} e^{-jU^2} dU \times \operatorname{sgn}(\pi-(\varphi+\varphi')) \end{array} \right. \end{array} \right] \qquad (2.15)$$

The first two terms are the incident field and reflected fields respectively as determined from the geometrical optics solution. The last term is the diffracted field and is identical to equation 2.10. Hence we have shown that the UTD half plane solution and the exact Sommerfeld solution are identical.

2.3.3 Surface Current Computation Using Sommerfeld Exact Solution

For the case of a half plane (n=2) illuminated by a TEz plane wave with an angle of incidence of 90° and with a unit magnitude incident magnetic field at the edge of the plane, let's compute and plot the surface current on the lit and shadow side of the plane using Sommerfeld's exact solution.

Since we are dealing with the TEz case, the total magnetic field will be always in the z direction. This means also that $\bar{J}=\hat{n}\times\bar{H}_{Total}$ ($\hat{n}$ a normal unit vector to the surface of the plane) has only a ρ component. Hence the surface curent is :

$$\begin{cases} J_\rho = H_{Total}\ (lit\ side) \\ J_\rho = -H_{Total}\ (shadow\ side) \end{cases} \tag{2.16}$$

Using equation 2.15 (hard case), the total field for our example is:

a) <u>For the lit side:</u>

$$\varphi = 0°, \varphi' = 90° \Rightarrow \begin{cases} U(\pi - (\varphi - \varphi')) = 1 \\ U(\pi - (\varphi + \varphi')) = 1 \\ (\varphi - \varphi') = -\frac{\pi}{2}; \cos(\varphi - \varphi') = 0 \\ (\varphi + \varphi') = \frac{\pi}{2}; \cos(\varphi + \varphi') = 0 \\ \frac{(\varphi - \varphi')}{2} = -\frac{\pi}{4}; \cos\left(\frac{(\varphi - \varphi')}{2}\right) = \frac{\sqrt{2}}{2} \\ \frac{(\varphi + \varphi')}{2} = \frac{\pi}{4}; \cos\left(\frac{(\varphi + \varphi')}{2}\right) = \frac{\sqrt{2}}{2} \end{cases}$$

hence the total field is:

$$H_{Total} = 1+1-(1+j)\times\sqrt{\frac{2}{\pi}}\times\int_{\sqrt{k\rho}}^{\infty} e^{-j\tau^2}d\tau$$

b) <u>For the Shadow side:</u>

$$\varphi = 360°, \varphi' = 90° \Rightarrow \begin{cases} U(\pi-(\varphi-\varphi')) = 0 \\ U(\pi-(\varphi+\varphi')) = 0 \\ (\varphi-\varphi') = -3\frac{\pi}{2}; \cos(\varphi-\varphi') = 0 \\ (\varphi+\varphi') = 5\frac{\pi}{2}; \cos(\varphi+\varphi') = 0 \\ \frac{(\varphi-\varphi')}{2} = 3\frac{\pi}{4}; \cos\left(\frac{(\varphi-\varphi')}{2}\right) = -\frac{\sqrt{2}}{2} \\ \frac{(\varphi+\varphi')}{2} = 5\frac{\pi}{4}; \cos\left(\frac{(\varphi+\varphi')}{2}\right) = -\frac{\sqrt{2}}{2} \end{cases}$$

hence the total field is:

$$H_{Total}=(1+j)\times\sqrt{\frac{2}{\pi}}\times\int_{\sqrt{k\rho}}^{\infty}e^{-j\tau^2}d\tau$$

Both surface current densities can be deduced directly using equation (2.16). Both are exact solutions.

A FORTRAN code called SOMMERFELD.FOR was created to compute and plot these current densities. The Fresnel integral subroutine in this case is based on [10], it had however to be customized to get C_1 and S_1 from C and S.
Figure 2.4 depicts the surface current density on the lit side of the plane illuminated by a TEz plane wave at 90° with a magnetic field of unit magnitude at the edge.
Figure 2.5 shows the surface current density on the shadow side of the plane. Since the incident field is $\vec{H}^i = \hat{z}e^{jky}$; the physical optics current on the lit side is then $\vec{J}_s = 2\hat{n}\times\vec{H}^i = 2\hat{y}\times\hat{z}e^{jk0} = \hat{x}\ 2\ A/m$. This is in fair agreement with Figure 2.4. On the shadow side of the strip, PO gives $J_s = 0$.
The plots of Figures 2.4 and 2.5 will be compared later to the ones in chapter 3 obtained by the general UTD formulation code. The importance of this stems from the fact that UTD is considered to be a high frequency solution for a local phenomenon. UTD, for the special case of a half plane and plane wave incidence, reduces to an exact solution and this will help in segregating between the low frequency limitation (near the edge)and the geometry limitation (local diffraction of multiple edges) when comparing solutions of electrically small scatterers considered to be building blocks of canonical solutions.

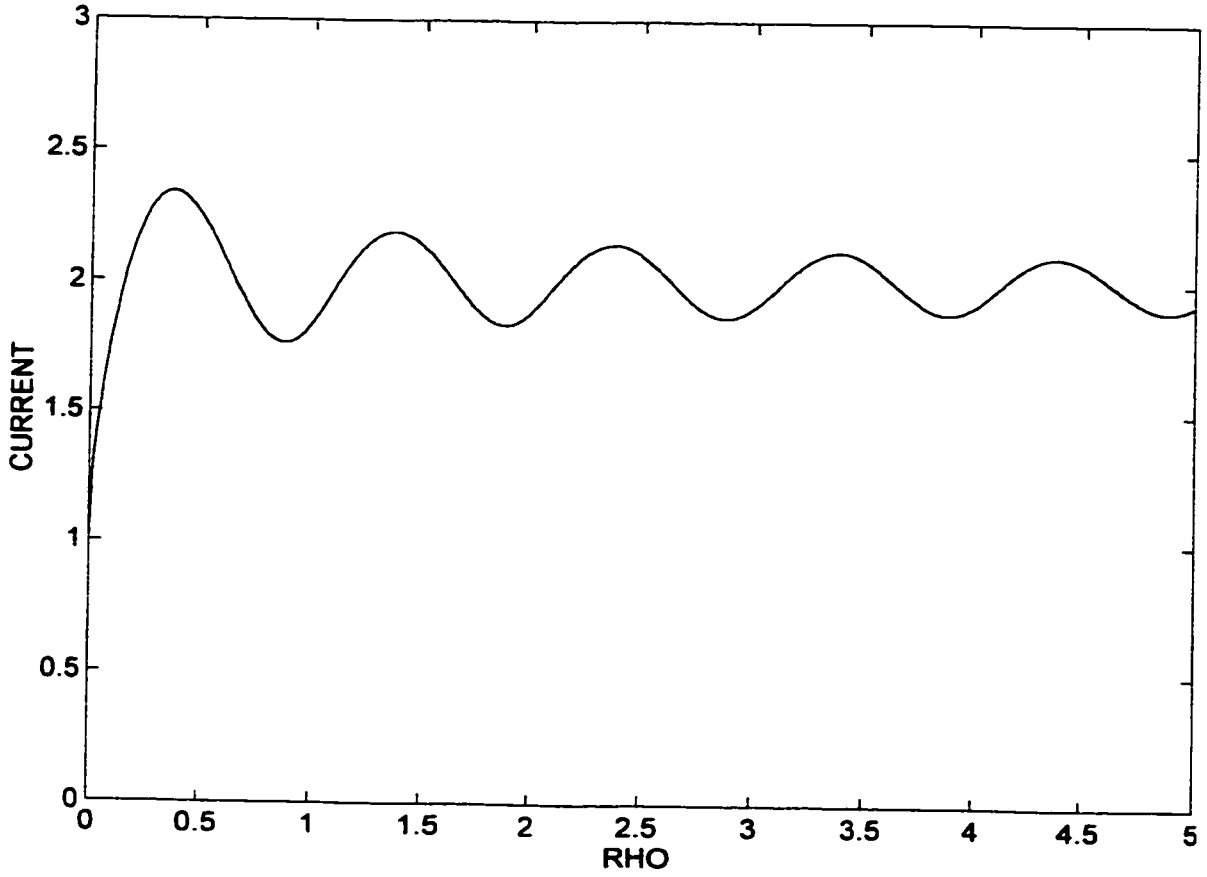

Figure 2.4: Magnitude of surface current density (A/m) on the lit side of a half plane illuminated by a TEz plane wave at 90° (Using SOMMERFELD.FOR).

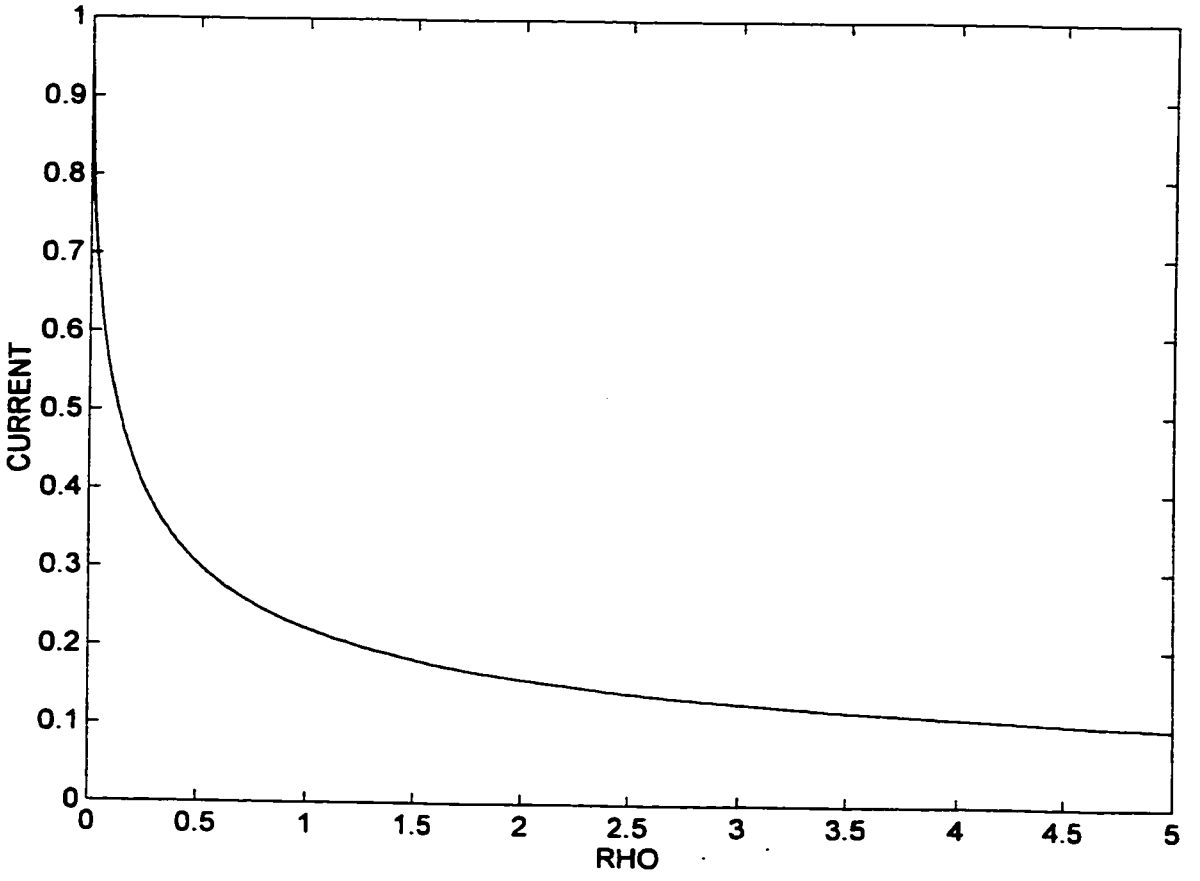

Figure 2.5: Magnitude of surface current density (A/m) on the shadow side of a half plane illuminated by a TEz plane wave at 90°(Using SOMMERFELD. FOR).

2.4 CHOICE OF AN INDEPENDENT METHOD FOR COMPARISON

Whenever possible, the UTD solutions in this work were compared to modal solutions, exact solutions and other approximate solutions found in the open literature. The moment method solutions however were the main ones that were used. The moment method was chosen because it is a well established method and computer codes were created and customized for almost each UTD case covered. The codes created used pulse basis functions and point matching. This section will review quickly the moment method formulation and describe two already existent independent moment method codes that were used in addition to created codes. It will also explain why pulse basis functions and point matching were chosen.

2.4.1 Two Dimensional Electric Field Integral Equation

In a typical scattering problem, the solution is the accurate prediction of the current density distributions on the surface of the scatterer. Radiation integrals are used afterwards to compute radiated or scattered fields. The prediction of current densities can be achieved by the integral equation method. The most popular equations are the electric field integral equation (EFIE) and the magnetic field integral equation (MFIE). The way they work is that the EFIE enforces the boundary condition on the surface of the perfectly electric conducting scatterrer for the tangential electric field. Like wise the MFIE enforces the boundary conditions on the tangential magnetic field.
In this work only EFIEs were used to create moment method computer codes, hence only the EFIE will be covered below. Since both TEz and TMz polarizations are used, it is best to cover the EFIE derivation for both 2-D polarization in two typical examples.

a) TMz Polarization:

Consider the two dimensional scatterer (finite width strip or cylinder of any shape) with a perimeter C, illuminated by a TMz uniform plane wave (it could be also a cylindrical wave). Since the incident electric field has only a z component which is independent of z variations (two dimensional), the scattered field and hence the surface currents densities are assumed to have only 2 components independent of z variations. This means that current on the surface of the scatterer is composed of infinite current line sources in the z direction. The field radiated by an infinite line source is [2][11]:

$$E_z^s = -I\frac{k\eta}{4}H_0^{(2)}(k\rho)$$

Where I is the current of the line source, and ρ is the distance from the line source to the observation point.

Similarly, the scattered field at a certain point due to the surface current of a 2-D scatterer illuminated by a TMz wave is:

$$E_z^s = \frac{-k\eta}{4}\int_C J_z(\vec{\rho}')H_0^{(2)}(k|\vec{\rho}-\vec{\rho}'|)dc'$$

Where J_z is the current density on the surface of the scatterer at a distance ρ' (from a specified origin point)

$\vec{\rho}$ is the vector from the origin to the observation point.

C is the perimeter of the 2-D scatterer.

To enforce the boundary conditions, the total tangential electric field must vanish on the surface of the scatterer, thus

$$E_z^i(\vec{\rho}_m) = \frac{k\eta}{4}\int_C J_z(\vec{\rho}')H_0^{(2)}(k|\vec{\rho}_m-\vec{\rho}'|)dc' \qquad (2.17)$$

where,

$E_z^i(\vec{\rho}_m)$ is the incident field on point m on the surface of the scatterer ,and

$\vec{\rho}_m$ is the vector from the origin to point m.

Equation (2.17) is the desired two-dimensional electric field integral equation to be solved for the current density J_z over the surface of the scatterer. The solution can be accomplished by using the moment method.

b) TEz Polarization:

Since the incident electric field has x and y components with no z variations, the scattered field is assumed also to have the same characteristics. This is actually what makes this example less straight forward then the TMz case. To derive the EFIE for the TEz case a specific example of a strip of finite width (aligned with the x axis) illuminated by a TEz type wave will be used. Even though this example seems to be specific, its solution is considered a building block for more complex scatterer geometries as it will be seen later.

Using vector potentials [2] the x and y components of the scattered electric field can be written as:

$$E_x^s = \frac{-k\eta}{8}\int_0^w J_x(x')\left[H_0^{(2)}(kR_m) + H_2^{(2)}(kR_m)\cos(2\varphi'')\right]dx' \qquad (2.18a)$$

$$E_y^s = \frac{-k\eta}{8}\int_0^w J_x(x')\left[H_2^{(2)}(kR_m)\sin(2\varphi'')\right]dx' \qquad (2.18b)$$

where

w = the width of the strip ($0 \le x \le w$)

J_x = Current density on the surface of the strip

x' = position of source current on the strip

R_m = Distance from the source x' to the observation point m. (on the scatterer)

φ"= Angle at x' between R_m and the strip.(positive when taken anticlockwise from strip)

This can be generalized to any scatterer made of strips as building blocks. The only difference is that the integration would be on the whole perimeter of the scatterer and the x and y components of the scattered field are replaced by the parallel and perpendicular (to the strip) component. For every strip (single building block) the proper axis rotation will have to be done depending on the angle of the strip relative to the actual coordinate axis.

The EFIE for this case is:

$$\vec{E}^s_{tan} = -\vec{E}^i_{tan} \qquad (2.19)$$

where the component of the scattered and incident field taken is tangential to the scatterer at point m.

Again equation 2.19 can be solved by the moment method.

2.4.2 The Moment Method

The current density J_z in equation 2.17 can be represented by [12][13]:

$$J_z(\rho') \cong \sum_{n=1}^{N} I_n \, g_n(\rho') \quad \text{(finite series)} \qquad (2.20)$$

Substituting this in equation 2.17 gives:

$$E^i_z(\rho_m) = \int_c \sum_{n=1}^{N} I_n \, g_n(\rho') H_0^{(2)}\left(k|\vec{\rho}_m - \vec{\rho}\,'|\right) dc'$$

$$\Rightarrow E^i_z(\rho_m) = \sum_{n=1}^{N} I_n \int_c g_n(\rho') H_0^{(2)}\left(k|\vec{\rho}_m - \vec{\rho}\,'|\right) dc'$$

This takes the general form:

$$V_m = \sum_{n=1}^{N} I_n Z_{mn} \qquad (2.21a)$$

where

$V_m = E_z^i(\vec{\rho}_m)$ (known excitation function) (2.21b)

I_n = constant coefficients set. (2.21c)

$Z_{mn} = \int_c g_n(\rho') H_0^{(2)}(k|\vec{\rho}_m - \vec{\rho}'|) dc'$ (2.21d)

g_n represent basis functions.

Equation 2.20 represents a numerical solution of the EFIE (equation 2.17). Since for a given observation point at ρ_m , it leads to one equation with N unknowns, the process can be repeated for N different observation points m=1 to m=N.The final outcome will be N linear equations each with N unknowns. This is better represented in matrix form:

$$[V_m] = [Z_{mn}][I_n] \quad (2.22)$$

$$[I_n] = [Z_{mn}]^{-1} [V_m]. \quad (2.23)$$

The [V] elements are known, the [Z] elements can be computed and the [I] vector can be determined. This will allows us to approximate $J_z(\rho')$ using equation 2.20 and hence permit the computation of the radiation integral to determine the scattered field anywhere. In words, equation 2.21 means that for each observation point, the total field consists of the sum of the direct E^i and scattered E^s components. To find the scattered component, the contribution of all segments of the scatterer, which include the one where the observation is made, must be added. The contribution of the local segment (where the observation is made) is called the self term or diagonal term (Z_{mn}). This is usually the hardest term to compute due to singularities existent when $\rho_n = \rho'$.

Other non diagonal terms are usually easier to compute and can be approximated.

Ideally the basis functions set should resemble and accurately represent the unknown current function. A limited number of basis sets are used typically in practice, the most popular being:

a) Functions which are nonzero only over a part of the domain (surface of the scatterer) of the function $g(\rho')$. The surface of the scatterer is divided into N segments and the basis function is defined relatively to the limit of one or more segments. Typical shapes of these functions include: the pulse type, the piecewise linear or sinusoidal types.

b) Functions which are nonzero over the entire perimeter of the scatterer. They are usually sinusoids and their use is similar to a Fourier series expansion of a function.

Determining the best basis functions set from the ones listed in a) is not obvious. It is believed [14] that increasing the sophistication of basis functions beyond the pulse shape will represent more smoothly the current and hence is more accurate. The price to pay however is computational complexity. In some cases also the use of sinusoid function could lead in an evaluation of the integral operator without numerical integration. The functions listed in b) are usually used when the current distribution is known to have mainly a sinusoidal distribution.

In this work the pulse basis function was used because it is simple and, as explained in the next section, several trials with pulse basis and piecewise sinusoid basis functions based codes were done in the early stage of this investigation: Both codes have similar accuracy for radiation patterns and current distributions.

Equation 2.11 is used as the numerical technique to solve for the current by satisfying the boundary condition (vanishing electric fields on the scatterer surface) only at discrete points. There is no guarantee that between these

points, the boundary conditions will be satisfied. A method to force the boundary conditions [13] (in an average sense at least on the entire scatterer surface) is to use weighting functions in the domain of the integral. This means that equation 2.21 becomes

$$\langle W_m, V_m \rangle = \sum_{n=1}^{N} I_n \langle W_m, Z_{mn} \rangle \qquad \text{m=1.2....,N.}$$

$\langle W_m, V_m \rangle$ is an inner product which is a scalar operation. When both weighting functions and basis functions are the same this is known as Galerkin method.

In the literature [15] this method is considered adequate but not superior to a method using weighting and basis function not equal but of the same order. Again trials with two different codes (one using the Galerkin method and the other not) did not prove the superiority of one method over the other. It was beyond the scope of this work to investigate residuals of tangent electric field over the surface of the scatterers used, but from a current density and radiation pattern point of view, accuracies of both codes (at least for the simple shape used) were similar.

The moment method codes created in this work use the point matching method and pulse basis functions. It should be noted that point matching is equivalent to using the impulse function as the weighting function.

2.4.3 Experience with TDRS and TECYL

Two independent codes based on the moment method were utilized during this investigation in addition to the codes created especially for each scattering case. The first code, TDRS (Two Dimensional Radiation and Scattering) was obtained from [2]. It uses the integral equation and moment method with equal

segmentation applied to all geometries and pulse basis functions and point matching. It covers TEz and TMz polarization scattering of strips and cylinders. The second code, TECYL (2-D TE radiation and scattering from conducting CYLinders) is based on [16][17][18]. It uses the integral equation and moment method. It deals only with the TEz case but covers open end closed conducting surfaces. It uses piecewise sinusoidal basis function and Galerkin's method.

In the early stages of this investigation TDRS and TECYL were used intensively to be able to determine the radiation patterns of electrically small scatterers but of different shapes.

In the case of a magnetic line source illuminating a strip of width = 5 λ (source heights=0.2 λ) the number of segments required by TDRS was at least 50 times higher than the number of segments required by TECYL to achieve the same accuracy. This finding was interesting because TDRS uses pulse basis and point matching and TECYL uses piecewise sinusoid basis and Galerkin method. Since at that point no decision was yet taken on the independent method to be used to compare UTD derived results, an investigation was due and what follows is the result.

For a 2-D thin plate (strip), illuminated by an infinite magnetic line source (TEz case), TDRS based on [2] has suggested the following impedance terms Z_{mn} (between segment m and segment n):

$$Z_{mn} \cong \frac{k\eta\Delta x_n}{8}\left\{1 - j\frac{1}{\pi}\left[-1 + 2\ln\left(\frac{1.781\,k\Delta x_n}{4e}\right) + \frac{16}{(k\Delta x_n)^2}\right]\right\} \quad \text{for m = n} \tag{2.24}$$

$$Z_{mn} \cong \frac{k\eta\Delta x_x}{8}\left\{1 + j\frac{4}{\eta k^2}\frac{1}{|x_m - x_n|^2 - \frac{(\Delta x_n)^2}{4}}\right\} \quad \text{for } m \neq n \;\&\; |m-n| \leq 2 \tag{2.25}$$

$$Z_{mn} = \frac{k\eta}{4}\int_{-\frac{\Delta x}{2}}^{\frac{\Delta x}{2}} \frac{H_1^{(2)}\left[k\left(|x_m - x_n| + x'\right)\right]}{k\left(|x_m - x_n| + x'\right)}dx' \qquad \text{for} \quad |m-n| > 2 \tag{2.26}$$

x_m and x_n being the middle points of segments *m* and *n* respectively.

Δx_n = width of segment *n*.

It should be noted here that equation (2.26) is an exact formula.

Equation (2.25) is derived from equation (2.26) using the approximation [2] of the Hankel function for small arguments: $H_1^{(2)}(k\rho) = J_1(k\rho) - jY_1(k\rho)$

$$\left.\begin{aligned} J_1(k\rho) &\to \frac{k\rho}{2} \\ Y_1(k\rho) &\to -\frac{1}{\pi}\frac{2}{\beta\rho} \end{aligned}\right\} \text{for } k\rho \to 0 \text{ (ρ being the distance from a point on segment n to } x_m)$$

This approximation converges for small segments ($k\rho \to 0$), but since it is used for adjacent segments ($|m-n| \leq 2; m \neq n$) and suppose that ($\Delta x = 0.1\lambda$), then kρ can vary from 0.1π to 5π. At $k\rho = 5\pi$, it is obvious that the Hankel function approximation is poor.

As for equation (2.24) it was derived directly from a mixed potential equation (refer to section 2.4.1b) leading to an exact formula consisting of an integral of Hankel $H_0^{(2)}$ *and* $H_1^{(2)}$ functions. Accurate approximations were used for the Hankel functions at that point: instead of using the crude approximation as was done in the case of equation 2.25, additional terms [5][8] were used in representing the Hankel function for small arguments.

It should be noted here that for the self term, (kρ) can vary from zero to 0.1π (if segment width is 0.1 λ). As expected, convergence of this term is much better than equation (2.25).

a) Plotting of the radiation pattern of this scattering problem was done using the moment method solution based on equations (2.24), (2.25) and (2.26). Equation (2.26) was computed using numerical integration.

Figure 2.6 shows radiation patterns for a segment width of 0.1 λ. A comparison made with results computed by TECYL and also GTD showed that only at a segment width of less than 0.005 λ that the radiation pattern begins to be accurate.

b) The same problem was solved by the moment method with the following difference: TDRS equation (2.25) was replaced by the exact formula of equation (2.26) and it was integrated numerically.

Figures 2.7 shows the radiation patterns for a segment width of 0.1λ. The plot is identical to plots obtained by TECYL and GTD.

It is obvious that the method used in b) with segment width =0.1λ (50 segments) achieved the same result as method in a) with segment width = 0.001λ (5000segments). Hence, it is safe to say that the approximations in [2] for Z_{mn} are bad, and that the integral should be done numerically or a more accurate closed form used.

Great care must be taken when computing impedance terms in moment method solutions for scattering problems. Not only the self term must be formulated accurately but also mutual impedance terms accuracy for adjacent segments must be taken into account to obtain acceptable results using typical segment width of 0.1λ to 0.2 λ.

It should be noted that the penalty paid (because of loop computing adjacent term impedances) is normally less than the penalty paid because of the increase in the simultaneous linear equations number (due to fine slicing of segments). It was decided after this investigation that pulse basis functions and point matching were adequate enough for the customized moment method codes to be created throughout this work

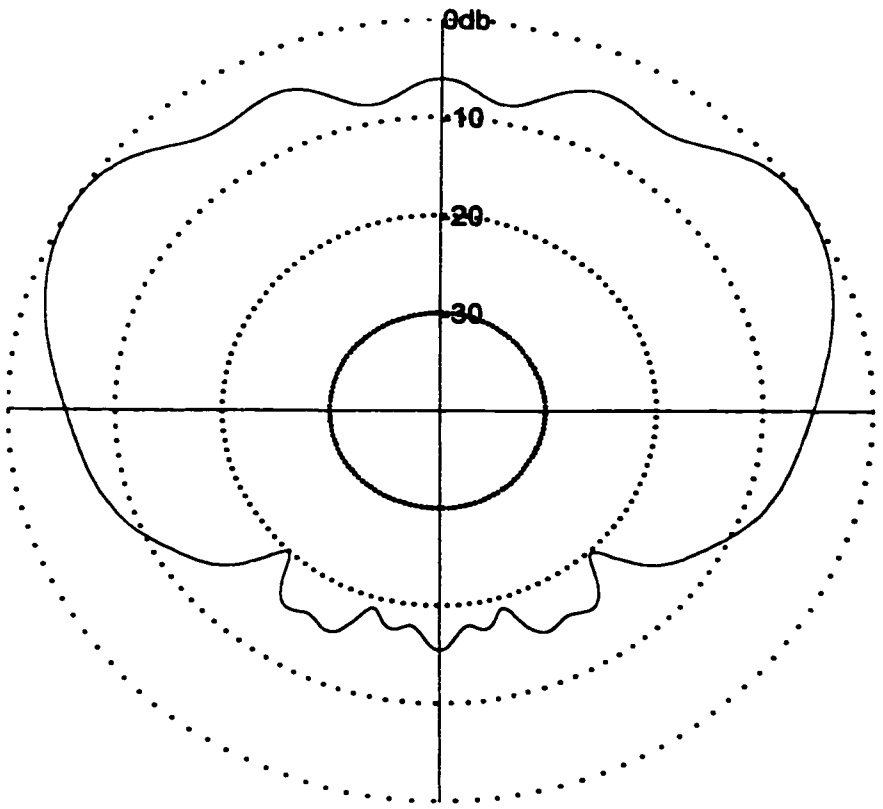

Figure 2.6: Normalized radiation pattern of a 2-D strip (width = 5λ) illuminated by a magnetic line source (height = 0.2λ) at the center of the strip, with Zmn poor approximation for |m-n|<2 and m≠n (segment = 0.1λ, N=50) using TDRS.

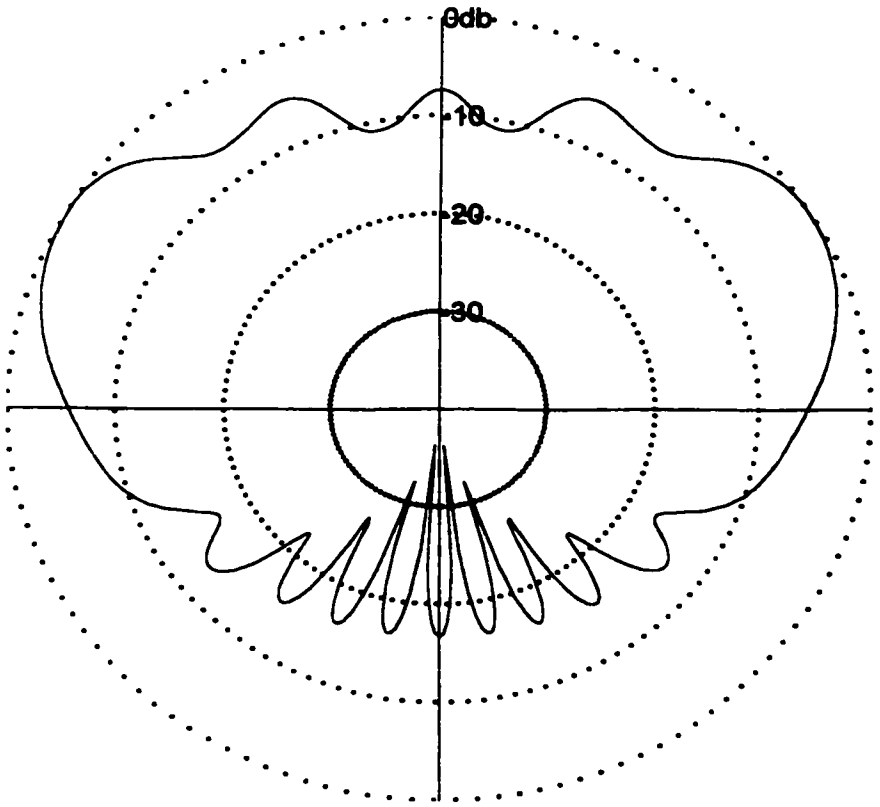

Figure 2.7: Normalized radiation pattern of a 2-D strip (width = 5λ) illuminated by a magnetic line source (height = 0.2λ). with corrected expressions for Zmn (numerical integration) for m≠ n (segment = 0.1λ, N=50) using TDRS.

2.4.4 Evaluation of TMz & TEz Z_{mn} Terms

As shown in section 2.4.3, the evaluation of Z_{mn} terms is very important and could lead easily to misleading results if not done properly. Approximations and closed forms of typical Z_{mn} terms can be found in the open literature [2] [12], but since the accuracy of results will be extremely sensitive to the adequacy of Z_{mn} evaluation, the derivation of all Z_{mn} impedance terms in closed or integral and approximate forms will be done here. Only scatterers made of surfaces parallel to the x or y axis are dealt with in this work.

a)TMz case

From equation 2.17 and 2.21d with pulse basis functions and point matching, the impedance term of a strip segment n of width Δ_x (aligned with the x axis) is:

$$Z_{mn} = \frac{k\eta}{4} \int_{x_n-\frac{\Delta_x}{2}}^{x_n+\frac{\Delta_x}{2}} H_0^{(2)}(kR_m)dx \qquad (2.27)$$

where,

$$R_m=\sqrt{(x_m-x)^2+(y_m-y)^2}$$

The integral in equation 2.27 experiences a singularity when m=n and it becomes:

$$Z_{mn} = \frac{k\eta}{2} \int_0^{\frac{\Delta_x}{2}} H_0^{(2)}(k\rho)d\rho \qquad (2.28)$$

Now since Δ_x is small, $k\rho$ is a small argument. The approximation of the Hankel function when $k\rho \to 0$ is [2] (γ=1.781):

$$H_0^{(2)}(k\rho) \cong 1 - j\frac{2}{\pi}\ln\left(\frac{\gamma k\rho}{2}\right) \qquad (2.29)$$

If we insert 2.29 in 2.28 we have:

$$Z_{mn} = \frac{k\eta}{2}\left[\frac{\Delta_x}{2} - j\frac{2}{\pi}\left[\rho\ln\left(\frac{\gamma k\rho}{2}\right) - \rho\right]_0^{\frac{\Delta_x}{2}}\right]$$

Now since $x\ln(x)\cong 0$ when $x\to 0$, then

$$Z_{mn} \cong \frac{k\eta}{4}\Delta_x\left[1 - j\frac{2}{\pi}\left[\ln\left(\frac{\gamma k\Delta_x}{4}\right) - 1\right]\right] = \frac{k\eta}{4}\Delta_x\left[1 - j\frac{2}{\pi}\ln\left(\frac{\gamma k\Delta_x}{4e}\right)\right] \qquad (2.30)$$

the same analysis applies to strip segments aligned with the y axis but with Δ_y replacing Δ_x Hence the Z_{mn} evaluations suggested are:

- if m=n, $$Z_{mn} \cong \frac{k\eta}{4}\Delta_x\left[1 - j\frac{2}{\pi}\ln\left(\frac{\gamma k\Delta_x}{4e}\right)\right] \qquad (2.31)$$

-if m≠n, $$Z_{mn} = \frac{k\eta}{4}\int_{\rho_n}^{\rho_n+1} H_0^{(2)}(kR_m)d\rho \qquad (2.32)$$

or $$Z_{mn} \cong \frac{k\eta}{4} \times \Delta \times H_0^{(2)}(kR_{mn}) \qquad (2.33)$$

Equation 2.32 is to be evaluated by numerical integration on a small segment n of a strip on the scatterer with ρ being the linear distance on the surface of the strip (usually its fixed origin is one edge of the strip).

In equation 2.32, $R_{mn}=\sqrt{(x_m-x_n)^2+(y_m-y_n)^2}$ and the expression is a crude approximation but yields in general good results.

It should be noted that the ρ is a linear distance that can be in the x or y direction.

b) TEz case – non diagonal terms;

Equation 2.18 gives an expression with Hankel functions of 0 and 2nd orders. Since most subroutines limit their output to Hankel functions of 0 and 1st order only and since [2]

$$\alpha H_2^{(2)}=\frac{2}{x}H_1^{(2)}(\alpha x)-\alpha H_0^{(2)}(\alpha x)$$

the Z_{mn} from equations 2.18 and 2.19 can be written as:

-For m and n on parallel but not the same surfaces

$$Z_{mn}=\frac{k\eta}{8}\int_{\rho_m}^{\rho_m+1}\left[(1-\cos(2\varphi''))H_0^{(2)}(kR_m)+\frac{2}{kR_m}H_1^{(2)}(kR_m)\cos 2\varphi''\right]d\rho \quad (2.34)$$

- For m and n on the same surface (cos(2φ")=1)

$$Z_{mn}=\frac{k\eta}{8}\int_{\rho_m}^{\rho_m+1}\left[\frac{2}{kR_m}H_1^{(2)}(kR_m)\right]d\rho \quad (2.35)$$

- For m and n on perpendicular surfaces

$$Z_{mn}=\frac{k\eta}{8}\int_{\rho_m}^{\rho_m+1}\left[\left\{\frac{2}{kR_m}H_1^{(2)}(kR_m)-H_0^{(2)}(kR_m)\right\}\sin(2\varphi'')\right]d\rho \quad (2.36)$$

The terms in equations 2.34, 2.35 and 2.36 can all be computed by numerical integration.

c)TEz case- Diagonal term (self impedance):

When m=n, the integral in equation 2.18 a, experiences a singularity. To be able to evaluate this term, we need to follow its derivation since the beginning. The vector potential equation can be written as

$$\vec{E}=-j\omega\vec{A}-\nabla V$$

In two dimensional cases and at a certain match point m [2]

$\left(\nabla^2 + k^2\right)\vec{A}(\vec{\rho}_m) = -\mu\vec{J}(\vec{\rho}_m)$ and

$$\vec{A}(\vec{\rho}_m) = -\frac{j\mu}{4}\int_C \vec{J}(\rho)H_0^{(2)}\left(k\left|\vec{\rho}_m - \vec{\rho}\right|\right)d\rho$$

where C is the perimeter of the scatterer and ρ is the linear distance from the origin. Similarly [11][12] the same can be stated for the scalar voltage potential

$$\left(\nabla^2 + k^2\right)V(\vec{\rho}_m) = -\frac{1}{\varepsilon}\rho_s(\vec{\rho}_m)$$

$$V(\vec{\rho}_m) = -\frac{j}{4\varepsilon}\int_C \rho_s(\rho)H_0^{(2)}\left(k\left|\vec{\rho}_m - \vec{\rho}\right|\right)d\rho$$

Where ρ_s is the surface charge density.

If the surface of the scatterer is divided into segments of width Δ and the current is represented by pulse basis functions and point matching is used, the contribution of the vector potential $\vec{A}$ to the electric field and hence to the impedance from a segment n to a point m located at the middle of the segment is

$$Z_{mn}^{A} = \frac{k\eta}{4}\int_{\frac{-\Delta}{2}}^{\frac{\Delta}{2}} H_0^{(2)}\left(k\left|\rho\right|\right)d\rho \qquad (2.37)$$

Equation 2.37 is equivalent to equation 2.30.

Since ρ directed surface current is related to the charge by $\frac{dJ_\rho}{d\rho} = -j\omega\rho_s$, then

$$V(\vec{\rho}_m) = -\frac{j}{4\omega\varepsilon}\int_C J'_\rho(\rho)H_0^{(2)}\left(k\left|\vec{\rho}_m - \vec{\rho}\right|\right)d\rho \qquad (2.38)$$

Since the current is represented by a pulse, its derivative with respect to ρ is a positive impulse (delta function) at ρ_n and a negative one at ρ_{n+1}. Now if m=n,

and since $E_\rho^V(m=n)=-\frac{dV}{d\rho}$ then the contribution of the scalar voltage potential to the self term is

$$Z_{mn}^V = -\frac{\eta}{2} H_1^{(2)}\left(k\frac{\Delta}{2}\right) \tag{2.39}$$

since Δ is small we can use the small argument approximation of J_0 and Y_0 from [8] and and by using $J_0' = -J_1$ and $Y_0' = -Y_1$ we can write

$$J_1(x) \approx \frac{1}{2}x - \frac{1}{16}x^3 + \cdots \tag{2.40}$$

$$\pi Y_1(x) \approx x\ln\left(\frac{\gamma x}{2}\right) - \frac{2}{x} - \frac{1}{2}x + \frac{6}{32}x^3 + \cdots \tag{2.41}$$

Retaining terms of order x only (small argument) results in

$$Z_{mn}^V \cong \frac{k\eta\Delta}{8}\left[-1 - j\frac{1}{\pi}\left\{-2\ln\left(\frac{\gamma\ k\Delta}{4e}\right) - 1 + \frac{16}{(k\Delta)^2}\right\}\right] \tag{2.42}$$

Since $Z_{mn} = Z_{mn}^A + Z_{mn}^V$, from equations 2.30 and 2.42

$$Z_{mn} \cong \frac{\eta k\Delta}{8}\left[1 - \frac{j}{\pi}\left\{-1 + 2\ln\left(\frac{\gamma k\Delta}{4e}\right) + \frac{16}{(k\Delta)^2}\right\}\right] \tag{2.43}$$

Throughout this work the impedance terms derived in this section will be used when applying moment method to a scattering problem.

3 SCATTERING - TEz CASE

In this chapter TEz plane waves are used to illuminate scatterers. UTD obtained surface current densities are plotted for the infinite edges, strips and rectangular cylinders. The edge results are compared with Sommerfeld's solution. The strip and cylinder results are compared with the moment method results.

3.1 EDGE SURFACE CURRENT USING UTD

To obtain the edge surface current density of Figure 2.1, we need to calculate the total magnetic field on the surface. Since the wedge is a perfect electric conductor and the incident plane wave is of the TEz type, the magnetic field has only a z component and hence the current density has a ρ component only,

$\vec{J}_s = \hat{n} \times \vec{H}$.

a) On the "0" side

For a unity TEz plane wave impinging on the wedge at angle $\varphi' \leq \frac{n}{2}\pi$:

$\varphi_o = o^o$, and from equation 2.1 we have $\vec{H}_Z = \vec{H}_z^i + \vec{H}_z^r + \vec{H}_z^d$

$H_z^i = 1 \times e^{jk\rho\cos(\varphi_o - \varphi')}$ incident wave

$H_z^r = 1 \times e^{jk\rho\cos(\varphi_o + \varphi)}$ reflected wave

from equation 2.4

$H_z^d = 1 \times \frac{e^{-jk\rho}}{\sqrt{\rho}} \times D_h(\rho, L, \varphi, \varphi', n)$ diffracted field.

D_h is the diffraction coefficient expanded in equation 2.5

φ = 0° ('o' face)

L= ρ (plane wave incidence)

n = 2 represents the angle of the wedge (2-n)π

b) On the 'n' face

$\varphi_n = n\pi$

For simplicity, $\varphi' \le \frac{n\pi}{2}$. The reason is that for larger values of φ', the geometry of the problem is symmetric and the result could be deduced.

$$H_z^i = U(\varphi' - (n-1)\pi) \times \frac{e^{jk\rho\cos(\varphi n - \varphi')}}{\sqrt{\rho}}$$

$$H_z^r = U(\varphi' - (n-1)\pi) \times \frac{e^{-jk\rho\cos(-\varphi n + \varphi')}}{\sqrt{\rho}}$$

$$H_z^d = 1 \times \frac{e^{-jk\rho}}{\sqrt{\rho}} \times D_s(\rho, L, \varphi, \varphi', n) \qquad \varphi = \varphi_n \text{ here}$$

The computer code INFEDGE.FOR was created to compute and plot the surface current density Jρ on the 'o' face and on the 'n' face of a wedge. The code is based on the equations listed above and hence uses the generic formulation of the UTD diffraction coefficient.

Several cases were plotted (ρ is in λ), J_o in A/m is the surface current density on the 'o' face and J_n is the one on the 'n' face.

Figure 3.1 depicts the half plane case (n=2) illuminated by a broadside incident TEz plane wave (φ'= 90°). It is identical to the Sommerfeld solution graph in Figures 2.4 and 2.5.

Figure 3.2 is the infinite plane case (n=1) illuminated by a incident TEz plane wave (φ'= 90°). As expected, there is no diffraction in this case and the graph reduces to the geometrical optic solution.

Figures 3.3 and 3.4 are for wedge and angles of 45° and 90° respectively. For these angles, diffraction is existent and the solution is not exact.

Figure 3.5 was produced to check the robustness of the code, the incident angle of 135° on a 90° wedge leads to similar illumination of both faces. As expected, both current densities are the same.

Figures 3.6 and 3.7 plot the current density on the surface of a 90° wedge for incidence angles of 60 ° and 0.7° (almost grazing incidence) respectively.

It is clear from the results obtained that the UTD generic formulation code produced the expected solutions for the Sommerfeld case (n=2) and the non diffraction case (n=1).

The created UTD code is considered adequate to be used as a building block for more complex scatterer shapes.

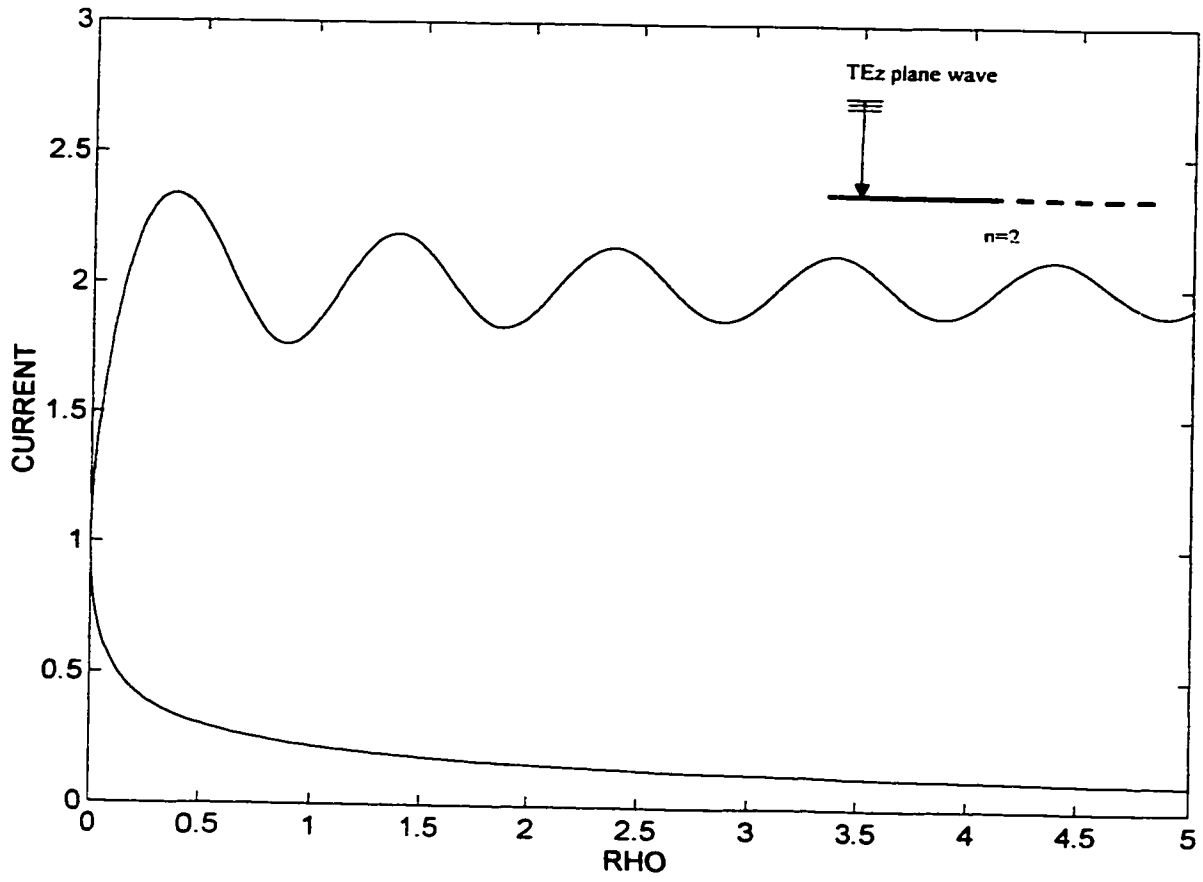

Figure 3.1: Magnitude of current density induced on the 'o' face and 'n' face of an infinite half plane illuminated by a TEz plane wave at normal incidence $\varphi'=90°$ (J in A/m, ρ in λ).

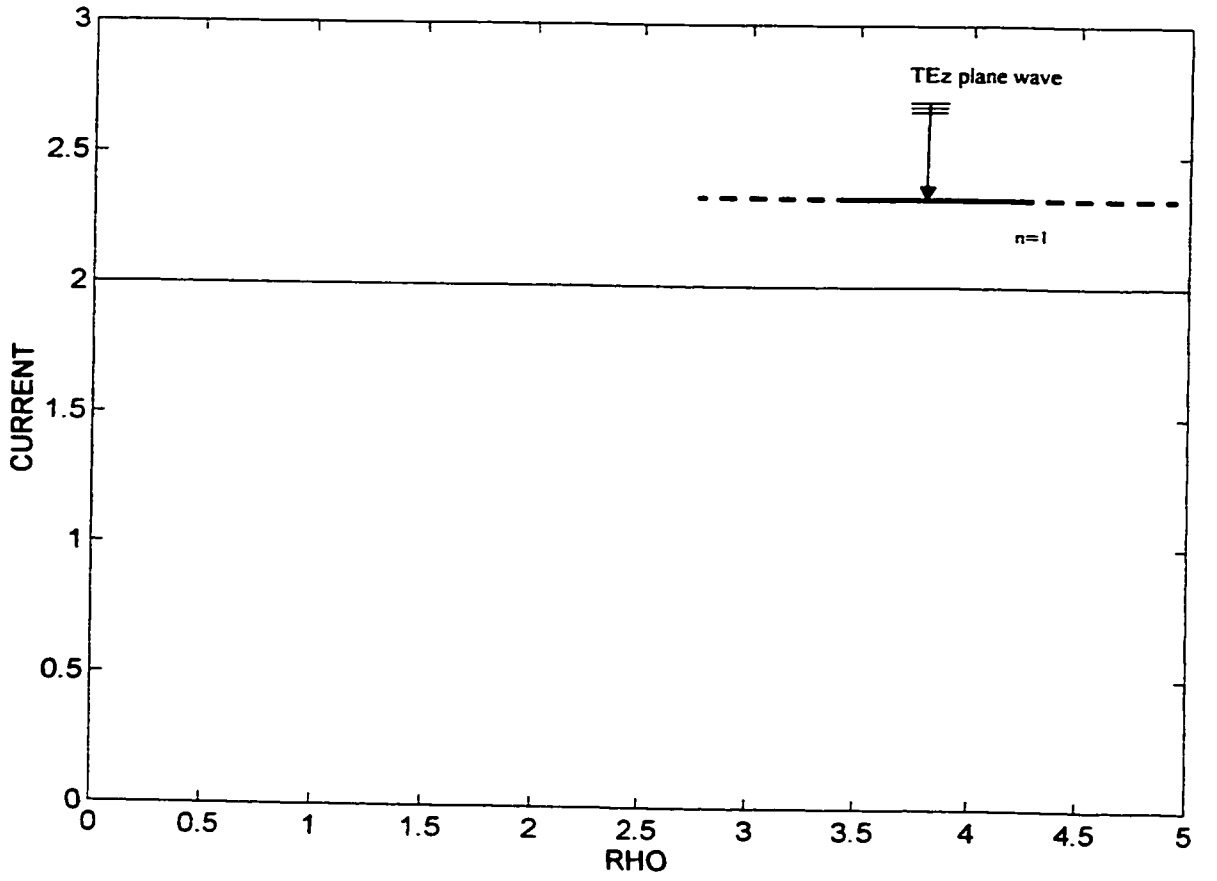

Figure 3.2: Magnitude of current density induced on the 'o' face and 'n' face of a wedge (n=1, infinite plane) illuminated by a TEz plane wave at normal incidence $\varphi'=90°$ (J in A/m, ρ in λ).

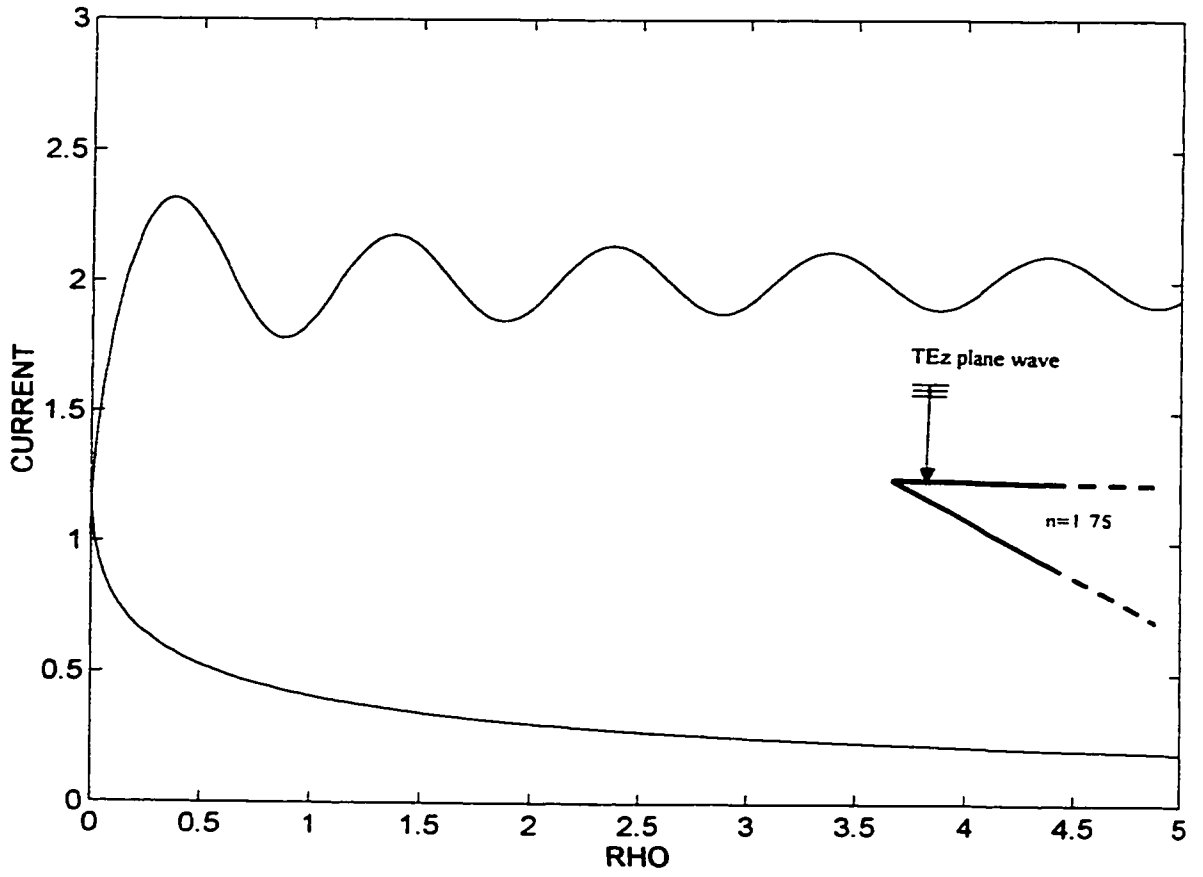

Figure 3.3: Magnitude of current density induced on the 'o' face and 'n' face of a wedge (n=1.75) illuminated by a TEz plane wave at normal incidence $\varphi'=90°$ (J in A/m, ρ in λ).

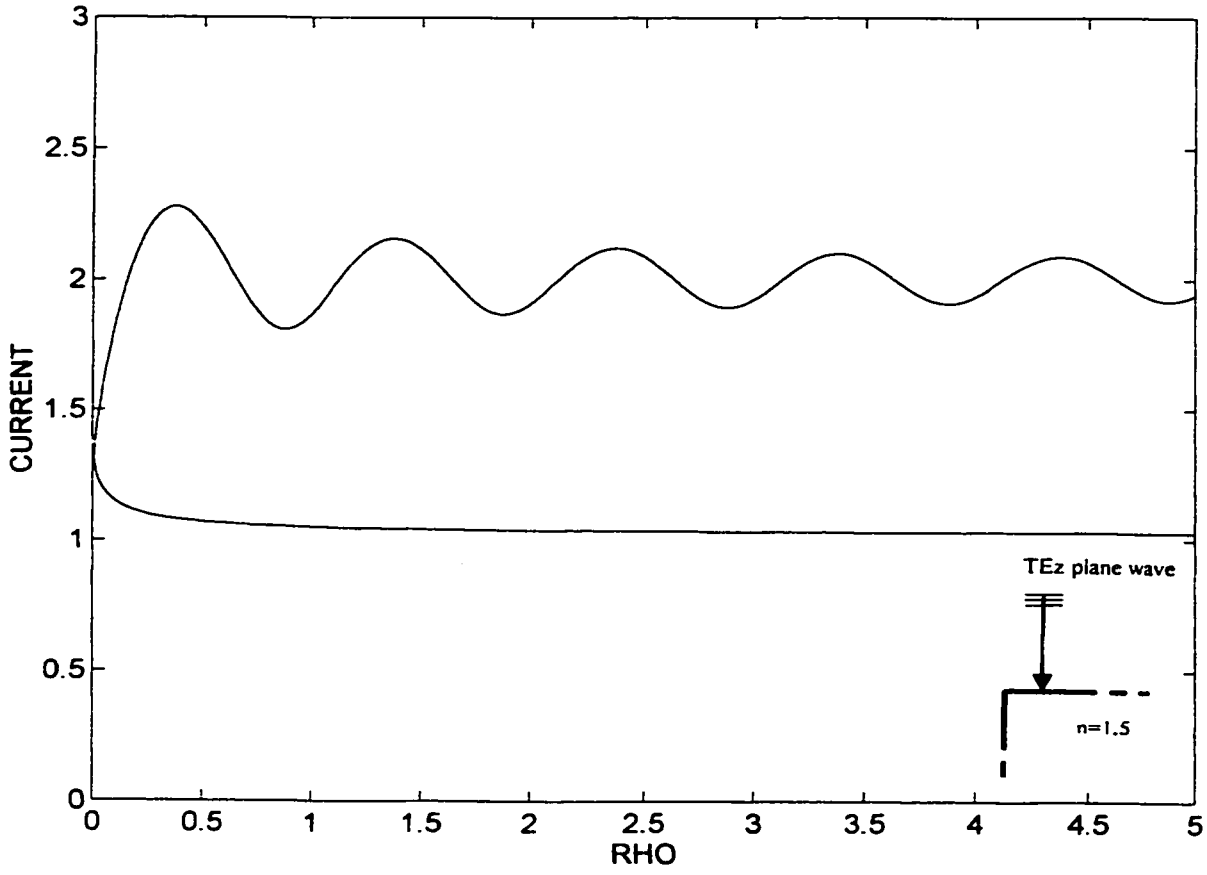

Figure 3.4: Magnitude of current density induced on the 'o' face and 'n' face of a wedge (n=1.5) illuminated by a TEz plane wave at normal incidence $\varphi'=90°$ (J in A/m, ρ in λ).

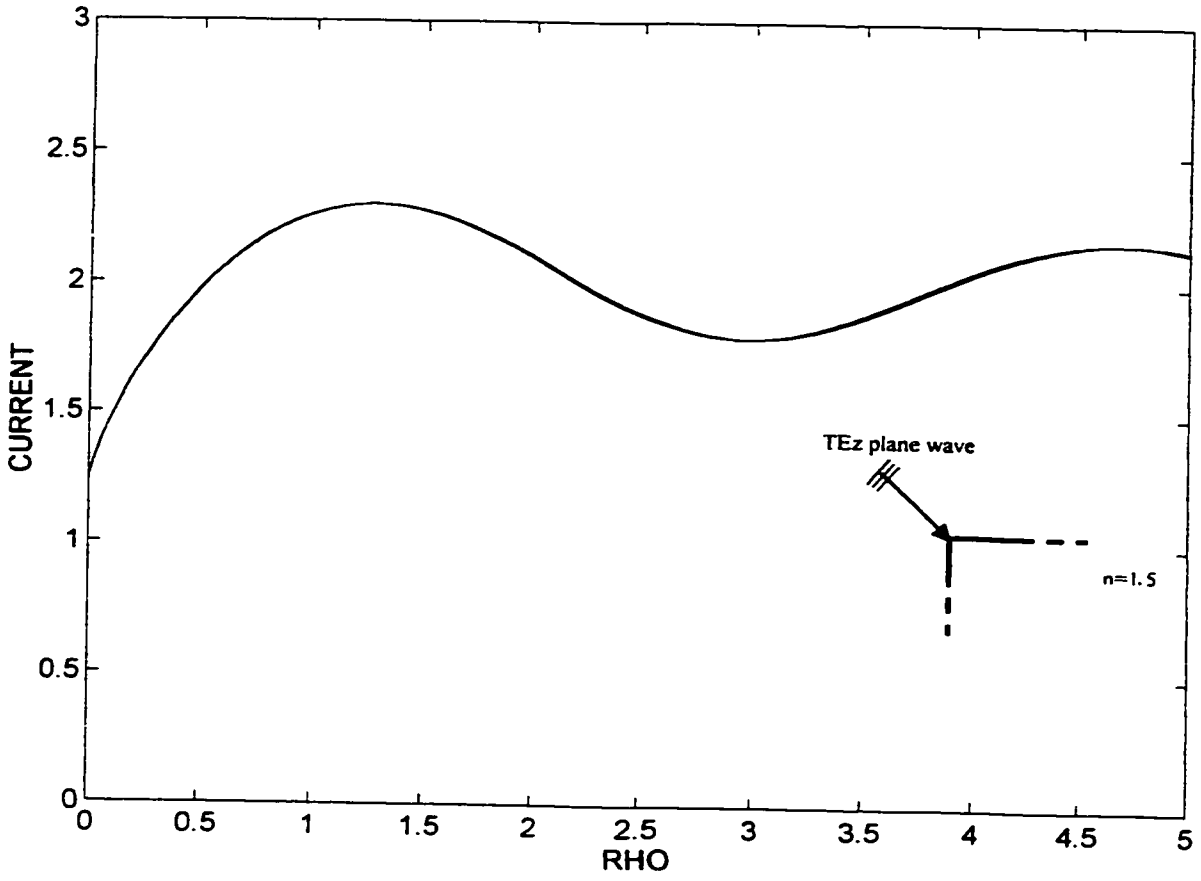

Figure 3.5: Magnitude of current density induced on the 'o' face and 'n' face of a wedge (n=1.5) illuminated by a TEz plane wave at $\varphi'=135°$ (J in A/m, ρ in λ).

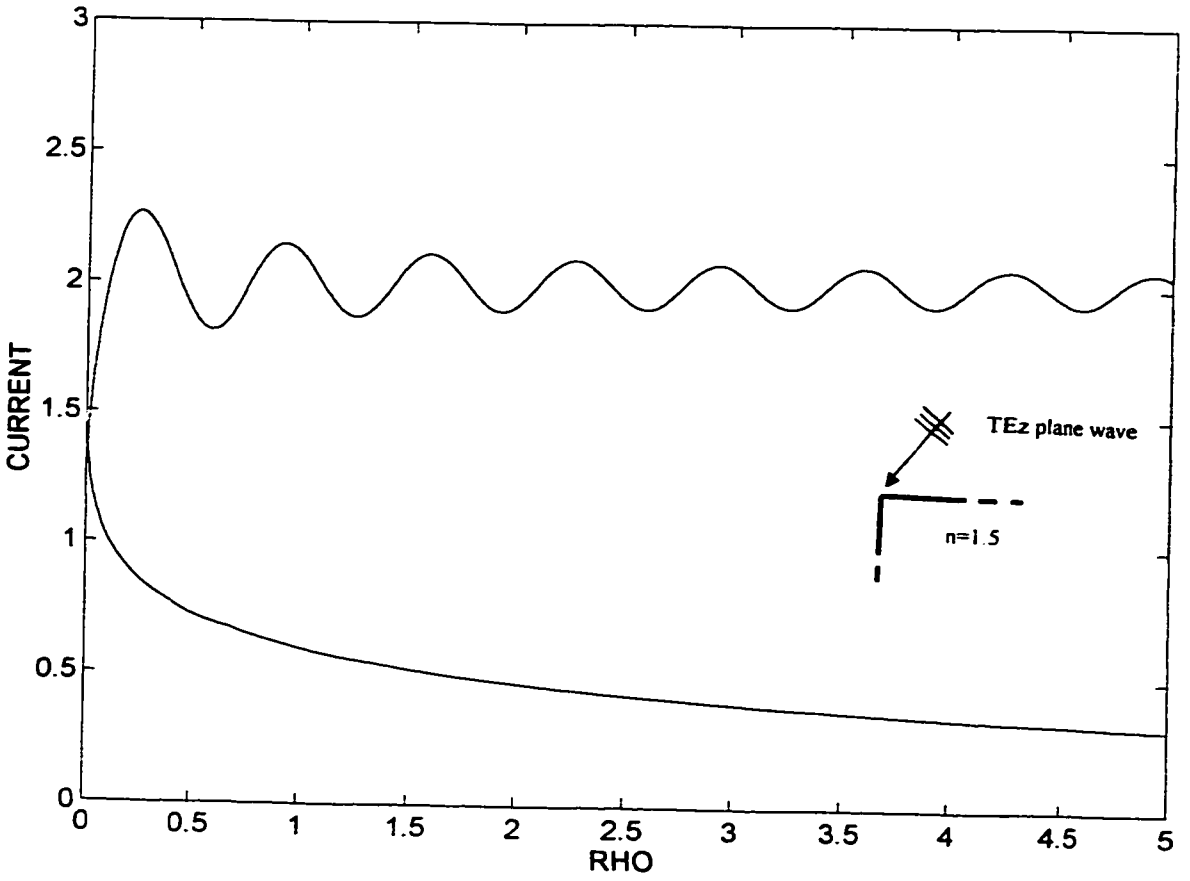

Figure 3.6: Magnitude of current density induced on the 'o' face and 'n' face of a wedge (n=1.5) illuminated by a TEz plane wave at $\varphi'=60°$ (J in A/m, ρ in λ).

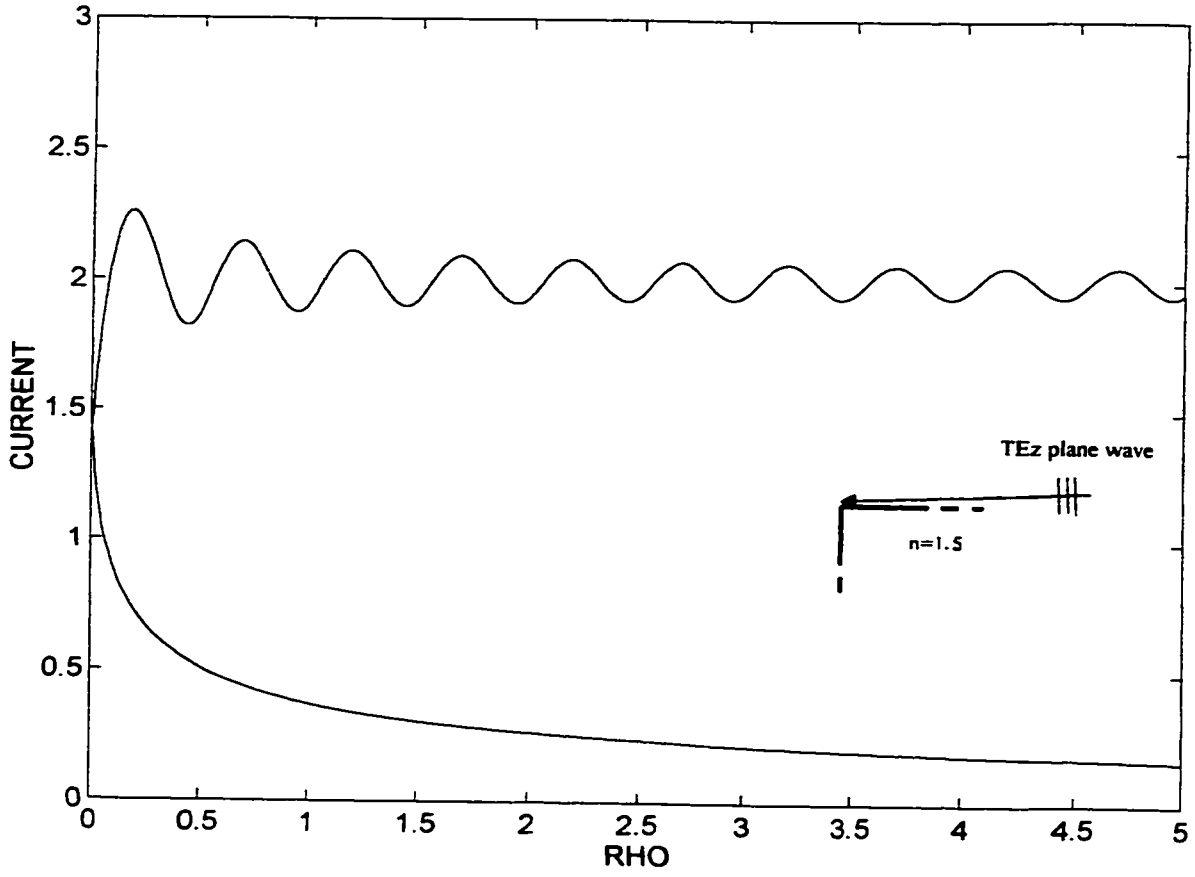

Figure 3.7: Magnitude of current density induced on the 'o' face and 'n' face of a wedge (n=1.5) illuminated by a TEz plane wave at almost grazing incidence $\varphi'=0.7°$ (J in A/m, ρ in λ).

3.2 STRIP SURFACE CURRENT USING UTD

3.2.1 Formulation

To obtain the current density on the upper and lower face of a strip illuminated by a plane wave, the total magnetic field must be computed on these surfaces. The strip (refer to Figure 3.8) is along the x axis with edge A at the origin and has a width w.

The incident TEz plane wave has a unity magnetic field at the origin and has an angle of incidence φ'. The formulation of the solution consists in considering the strip as a combination of two back to back infinite edges (one at A and one at B). Cases of φ' between 0 and 180 degrees only will be covered here (other cases can be deduced from symmetry). The total magnetic field on the surface of the strip could be formulated as follows:

$$H^{Total} = H^{i} + H^{r} + H^{d}$$

where H^{i} and H^{r} are the incident and reflected fields respectively from geometrical optics.

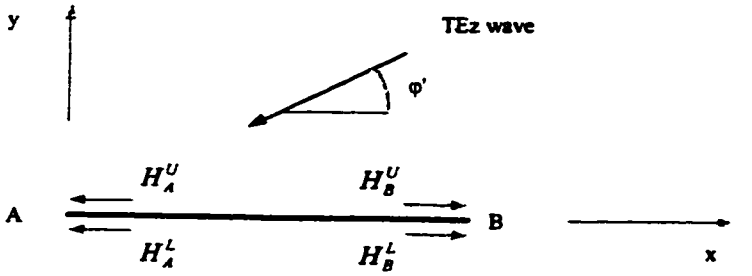

Figure 3.8 : Strip of width w illuminated by a TEz plane wave at an angle φ'.

H^d Is the total diffracted field by edge A and edge B including multiple diffractions.

Position along the x axis (with A as the origin) is denoted by ρ.

a) Geometrical optics fields:

-On the upper surface $H^i = e^{jk\rho\cos\varphi'}$

and $H^r = e^{jk\rho\cos\varphi'}$

-On the lower surface $H^i = H^r = 0$

b) Diffracted fields :

The diffracted fields are generated by the diffraction of the incident field by edges A and B and consequently by additional multiple diffractions of the diffracted fields themselves. The formulation of multiple diffractions is based on the "self consistent" principle [19]. In other words, the following fields (ready to be diffracted) are existent at the edges: an incident field, a multiple diffraction field component coming to the edge from the upper side and another one from the lower side.

If we define the following:

H_A^u = Total of fields generated by multiple diffractions only coming towards edge A from the upper side at grazing incidence

H_A^L = Total of fields generated by multiple diffractions only coming towards edge A from the lower side at grazing incidence

H_B^u = Total of fields generated by multiple diffractions only coming from the upper side towards edge B at grazing incidence.

H_B^L = Total of fields generated by multiple diffractions only coming from the lower side towards edge B at grazing incidence.

H_A^i = Incident field at A (Unit magnitude).

H^{i}_{B} = Incident field at B $= \left(e^{-jk\rho\cos\varphi'}\right)$.

L_p = Distance parameter L for a plane wave = ρ or w-ρ

L_c = Distance parameter L for a cylindrical wave = $\frac{\rho\rho'}{\rho+\rho'}$ or $\frac{(w-\rho)\rho'}{(w-\rho)+\rho'}$

(If the source and the observer are the same, then $L_c = \frac{ww}{2w} = \frac{w}{2}$)

the following could be stated :

$$H^{u}_{A} = \begin{bmatrix} H^{i}_{B} \times D_h(w, L_\rho, 0, \pi-\varphi', 2) \times \frac{e^{-jkw}}{\sqrt{w}} \\ +\frac{1}{2} H^{u}_{B} \times D_h(w, L_c, 0, 0, 2) \times \frac{e^{-jkw}}{\sqrt{w}} \\ +\frac{1}{2} H^{L}_{B} \times D_h(w, L_c, 0, 2\pi, 2) \times \frac{e^{-jkw}}{\sqrt{w}} \end{bmatrix} \quad (3.1)$$

$$H^{L}_{A} = \begin{bmatrix} H^{i}_{B} \times D_h(w, L_\rho, 2\pi, \pi-\varphi', 2) \times \frac{e^{-jkw}}{\sqrt{w}} \\ +\frac{1}{2} H^{u}_{B} \times D_h(w, L_c, 2\pi, 0, 2) \times \frac{e^{-jkw}}{\sqrt{w}} \\ +\frac{1}{2} H^{L}_{B} \times D_h(w, L_c, 2\pi, 2\pi, 2) \times \frac{e^{-jkw}}{\sqrt{w}} \end{bmatrix} \quad (3.2)$$

$$H^{U}_{B} = \begin{bmatrix} H^{i}_{A} \times D_h(w, L_\rho, 0, \varphi', 2) \times \frac{e^{-jkw}}{\sqrt{w}} \\ +\frac{1}{2} H^{u}_{A} \times D_h(w, L_c, 0, 0, 2) \times \frac{e^{-jkw}}{\sqrt{w}} \\ +\frac{1}{2} H^{L}_{A} \times D_h(w, L_c, 2\pi, 0, 2) \times \frac{e^{-jkw}}{\sqrt{w}} \end{bmatrix} \quad (3.3)$$

$$H^{L}_{B} = \begin{bmatrix} H^{i}_{A} \times D_h(w, L_\rho, 2\pi, \varphi', 2) \times \frac{e^{-jkw}}{\sqrt{w}} \\ +\frac{1}{2} H^{u}_{A} \times D_h(w, L_c, 2\pi, \varphi, 2) \times \frac{e^{-jkw}}{\sqrt{w}} \\ +\frac{1}{2} H^{L}_{A} \times D_h(w, L_c, 2\pi, 2\pi, 2) \times \frac{e^{-jkw}}{\sqrt{w}} \end{bmatrix} \quad (3.4)$$

note that a factor of ½ is multiplied with fields at grazing incidence.

Equations 3.1 to 3.4 are four equations with four unknowns that can be solved for H_A^u , H_A^L, H_B^u and H_B^L.

Once these four unknowns are computed, and since $\vec{J}_s = \hat{n} \times \vec{H}$, the current density on the surface of the strip can be obtained from:

<u>i) On the upper surface</u>:

$$H^{Total} = \left[\begin{array}{l} 2 \times e^{jk\rho\cos\varphi'} \\ + H_A^L D_h(\rho, L_p, 0, \varphi', 2) \times \frac{e^{-jk\rho}}{\sqrt{\rho}} \\ + \frac{1}{2} H_A^u D_h(\rho, L_c, 0, 0, 2) \times \frac{e^{-jk\rho}}{\sqrt{\rho}} \\ + \frac{1}{2} H_A^L D_h(\rho, L_c, 0, 2\pi, 2) \times \frac{e^{-jk\rho}}{\sqrt{\rho}} \\ + H_B^L D_h(w-\rho, L_p, 0, \pi - \varphi', 2) \times \frac{e^{-jk(w-\rho)}}{\sqrt{w-\rho}} \\ + \frac{1}{2} H_B^u D_h(w-\rho, L_c, 0, 0, 2) \times \frac{e^{-jk(w-\rho)}}{\sqrt{w-\rho}} \\ + \frac{1}{2} H_B^L \times D_h(w-\rho, L_c, 0, 2\pi, 2) \times \frac{e^{-jk(w-\rho)}}{\sqrt{w-\rho}} \end{array} \right] \quad (3.5)$$

ii)On the lower surface:

$$H^{Total} = \begin{bmatrix} H_A^{i} D_h(\rho, L_p, 2\pi, \varphi', 2) \times \frac{e^{-jk\rho}}{\sqrt{\rho}} \\ + \frac{1}{2} H_A^{u} D_h(\rho, L_c, 2\pi, 0, 2) \times \frac{e^{-jk\rho}}{\sqrt{\rho}} \\ + \frac{1}{2} H_A^{L} D_h(\rho, L_c, 2\pi, 2\pi, 2) \times \frac{e^{-jk\rho}}{\sqrt{\rho}} \\ + H_B^{i} D_h(w-\rho, L_p, 2\pi, \pi-\varphi', 2) \times \frac{e^{-jk(w-\rho)}}{\sqrt{w-\rho}} \\ + \frac{1}{2} H_B^{u} D_h(w-\rho, L_c, 2\pi, 0, 2) \times \frac{e^{-jk(w-\rho)}}{\sqrt{w-\rho}} \\ + \frac{1}{2} H_B^{L} D_h(w-\rho, L_c, 2\pi, 2\pi, 2) \times \frac{e^{-jk(w-\rho)}}{\sqrt{w-\rho}} \end{bmatrix} \quad (3.6)$$

3.2.2 Code and Results

The formulation of section 3.2.1 was used to create the MGTD1.FOR code. It contains the generic UTD diffraction coefficient subroutine. The set of linear equations was solved by forward/backward substitution method based on [20]. The code was made flexible so that the total magnetic field could be computed with or without multiple diffraction. Results from the moment method solution described in section 3.3 are plotted (in small circles) for comparison:

a) 90^0 angle of plane wave incidence:

Several cases were considered for a 90^0 angle of incidence. The idea behind that is to be able to evaluate the causes that would prevent the success of UTD at low frequency. Since the UTD solution for a half plane illuminated by a incident plane wave at 90^0 is an exact one, it would be expected that the UTD solution success of an electrically small strip (illuminated by a plane wave at 90^0 and considered to be the combination of two edges) would depend on how low a

frequency can be used, with diffraction still being considered as a local phenomenon.

Figures 3.9, 3.11, 3.13 and 3.15 depict the current density on strips of width 1.λ, 0.5λ, 0.2λ and 0.1λ respectively. Multiple diffraction was taken into account for current computation.

Figures 3.10, 3.12, 3.14 and 3.16 depict the current density on strips of width 1.λ, 0.5λ, 0.2λ and 0.1λ respectively. Only simple diffraction was considered for current computation.

It is obvious that when multiple diffraction is not taken into account, relatively big errors begin to be introduced at edges for w=1λ to end up with a totally different current distribution at w=0.1λ.

When multiple diffraction is taken into account, UTD results are almost identical to moment method results. More surprising is that the UTD works quite well down to 0.1λ.

b) Other angles of incidence:

Figures 3.17, 3.18 and 3.19 depict the current distribution on a strip of width w=0.2λ illuminated by a plane wave at 60^0, 10^0 and 0.5^0 (near grazing) angle of incidence respectively.

Figures 3.20, 3.21 and 3.22 show the current distribution on a strip of width w=0.1λ illuminated by a plane wave incident at 60^0, 10^0 and 0.5^0 respectively. Both sets of figures take into account multiple diffractions in computing current densities. They show clearly that results still compare well, with the difference between the UTD and moment method results increasing at near grazing angles for smaller strip width. The maximum difference detected between the values of both methods (as a percentage of the moment method value) is still however less than 5%.

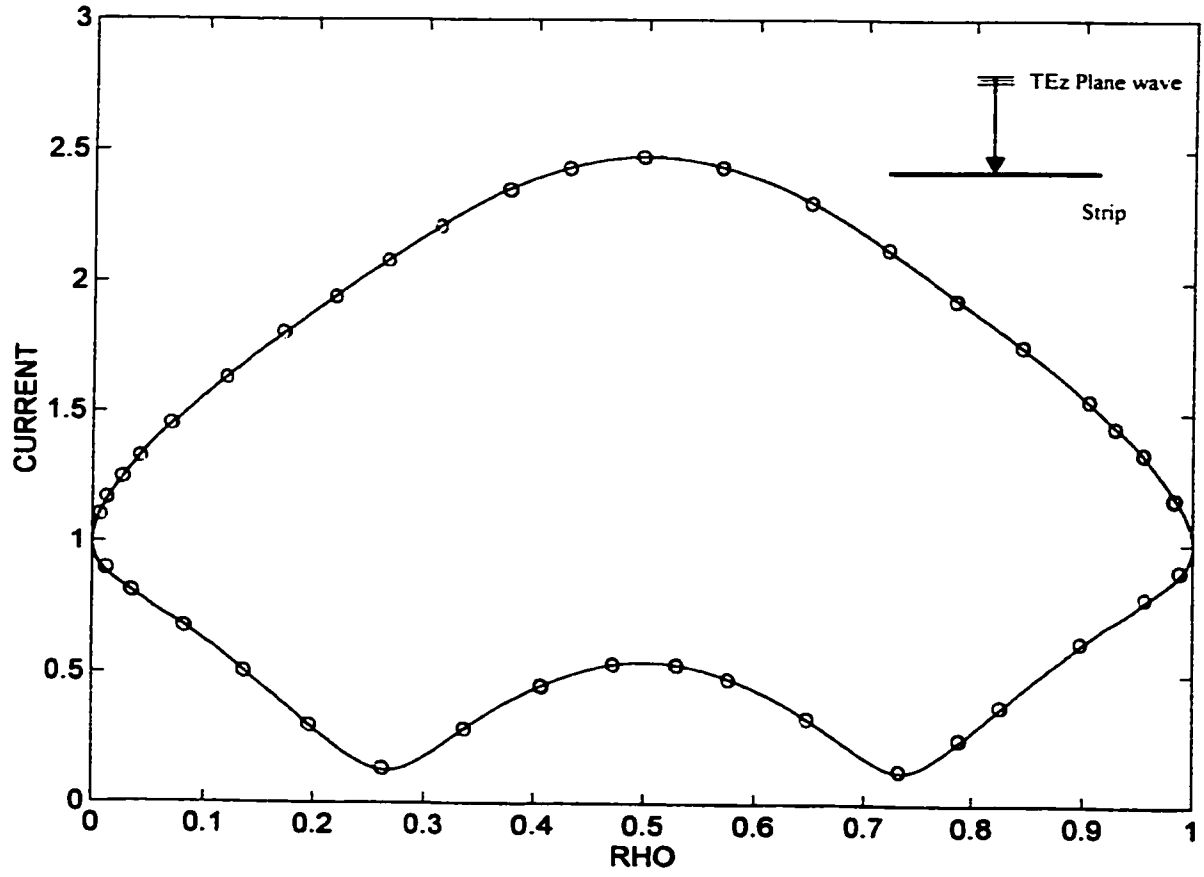

Fig 3.9: Magnitude of current density on both surfaces of a strip of width w=1 λ illuminated by a TEz plane wave incident at φ'=90° (J in A/m. ρ in λ.). [— Multiple diffraction UTD solution. ooo MM with 500 segments]

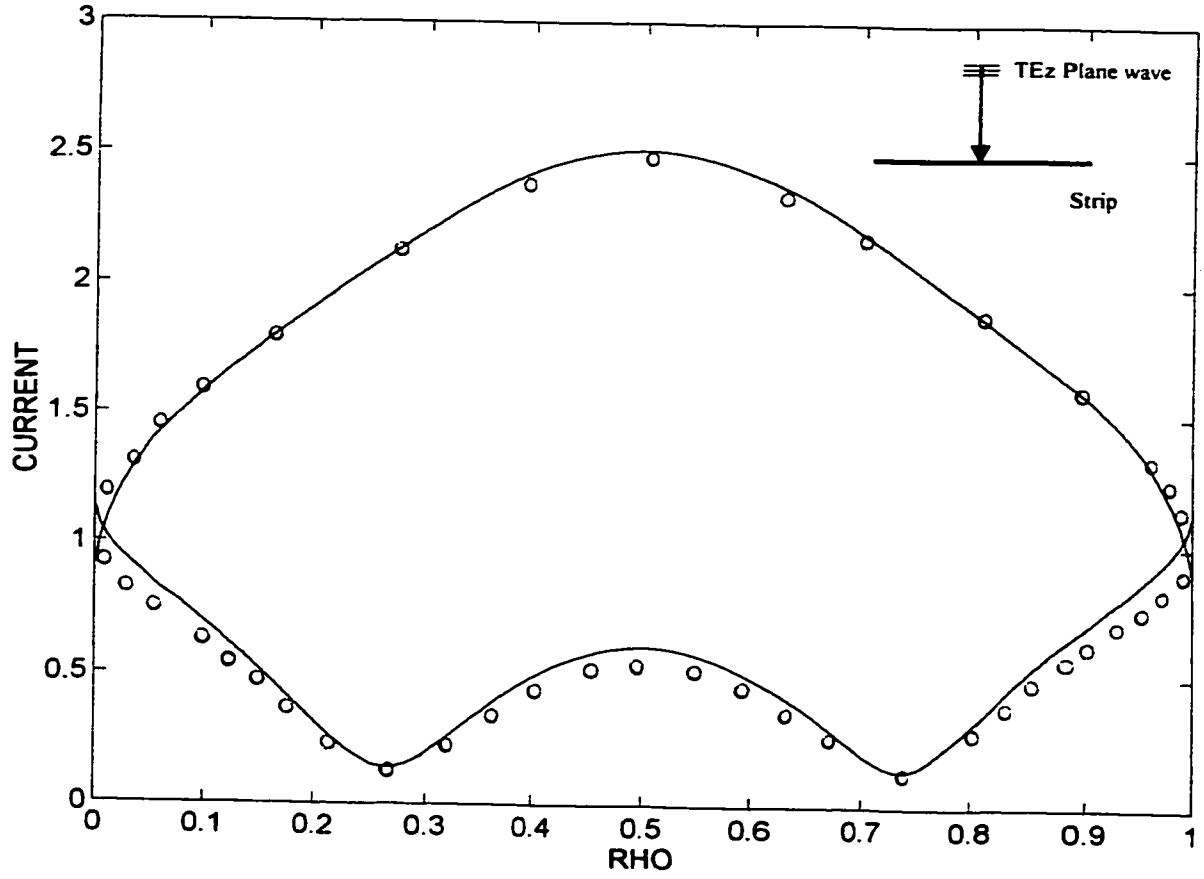

Fig 3.10: Magnitude of current density on both surfaces of a strip of width w=1 λ illuminated by a TEz plane wave incident at $\varphi'=90°$ (J in A/m, ρ in λ). [— Single diffraction UTD solution, ooo MM with 500 segments]

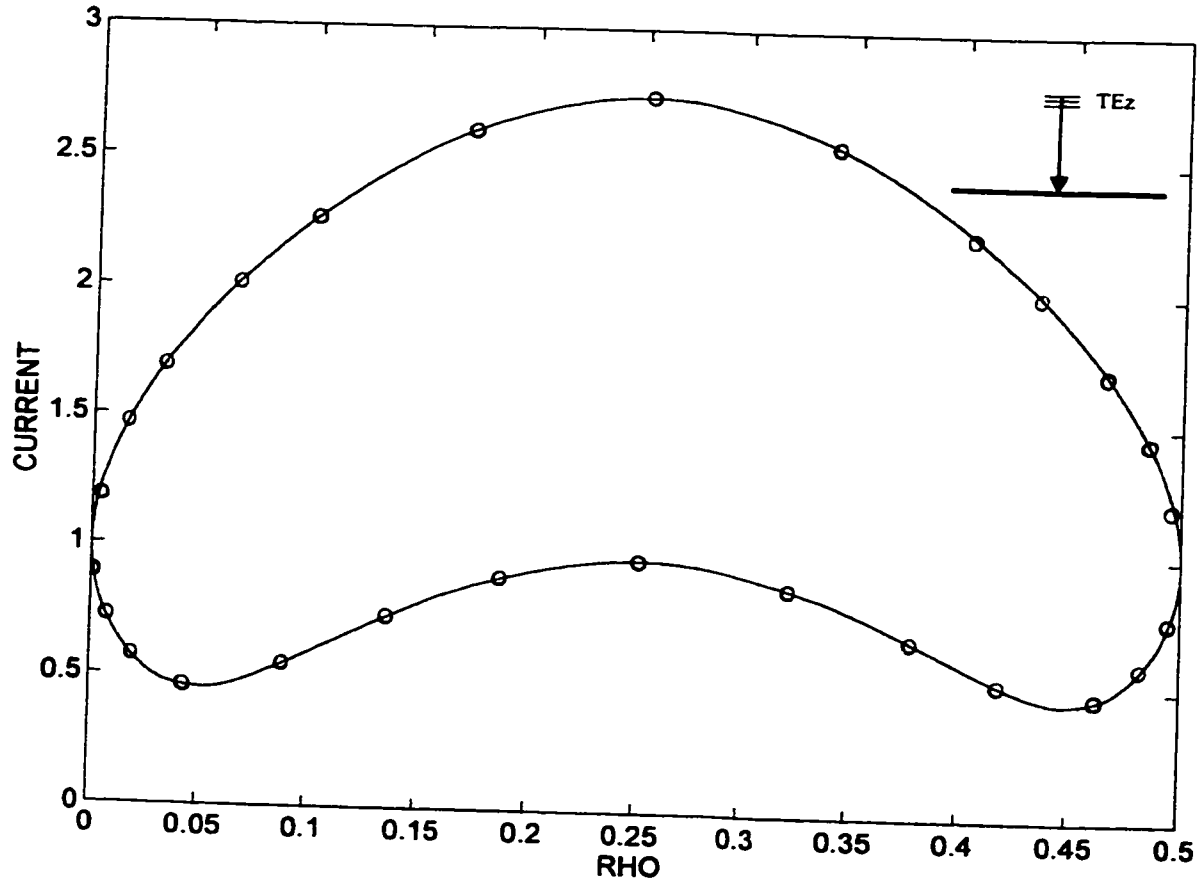

Fig 3.11 : Magnitude of current distribution on a strip of width w=0.5 λ illuminated by a TEz plane wave at φ'=90° (J in A/m, ρ in λ). [— Multiple diffraction UTD solution, ooo MM with 300 segments]

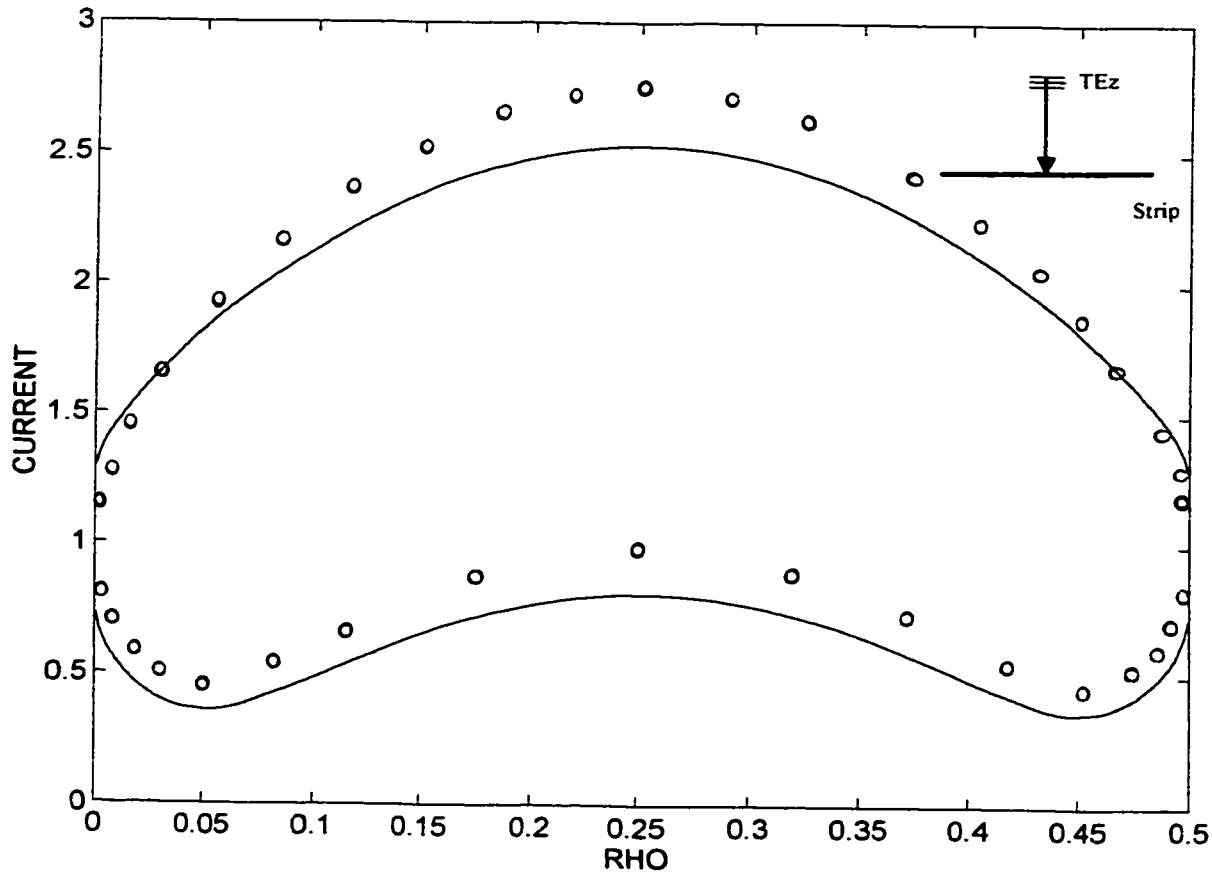

Fig 3.12: Magnitude of current density on a strip of width w=0.5λ illuminated by a TEz plane wave incident at φ'=90° (J in A/m, ρ in λ). [— Single diffraction UTD solution, ooo MM with 300 segments]

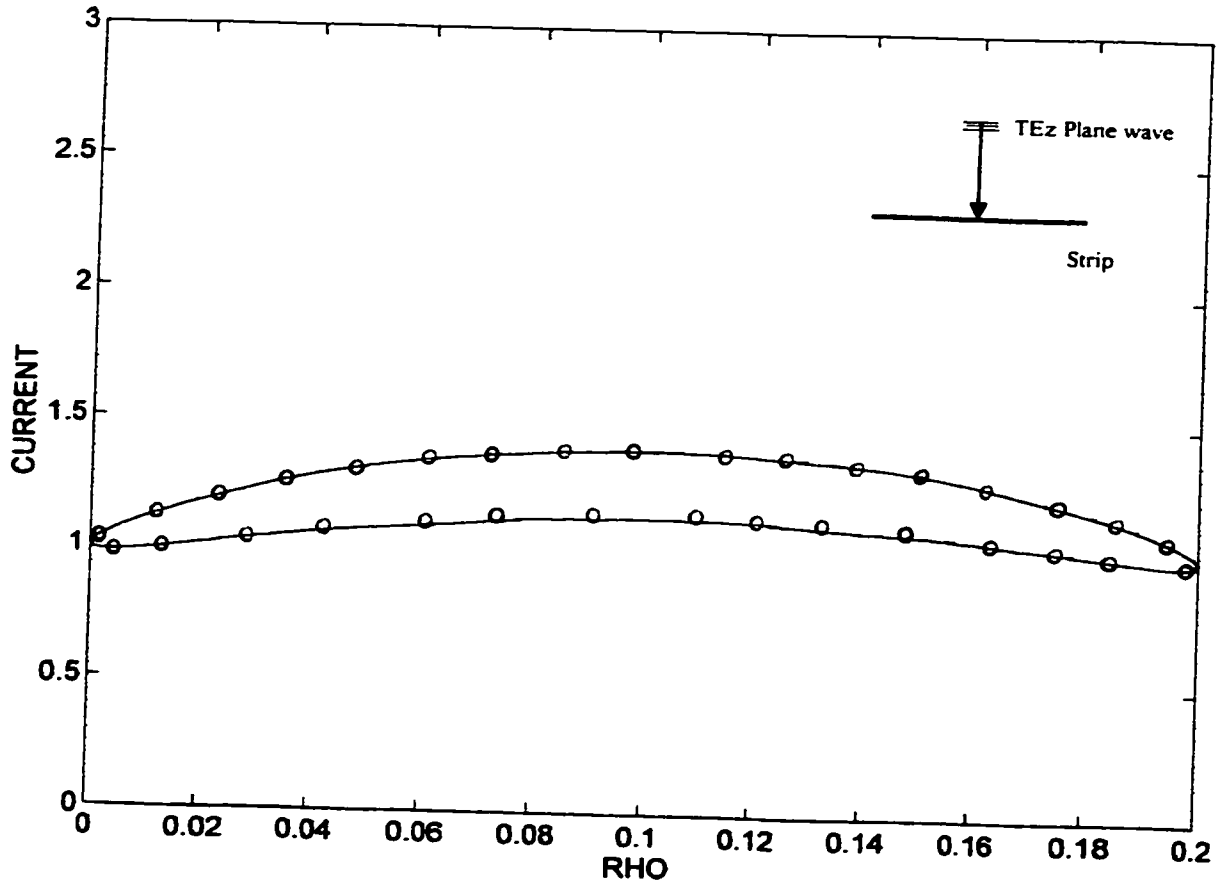

Fig 3.13: Magnitude of current density on a strip of width w=0.2λ illuminated by a TEz plane wave incident at φ'=90° (J in A/m, ρ in λ). [— Multiple diffraction UTD solution, ooo MM with 200 segments]

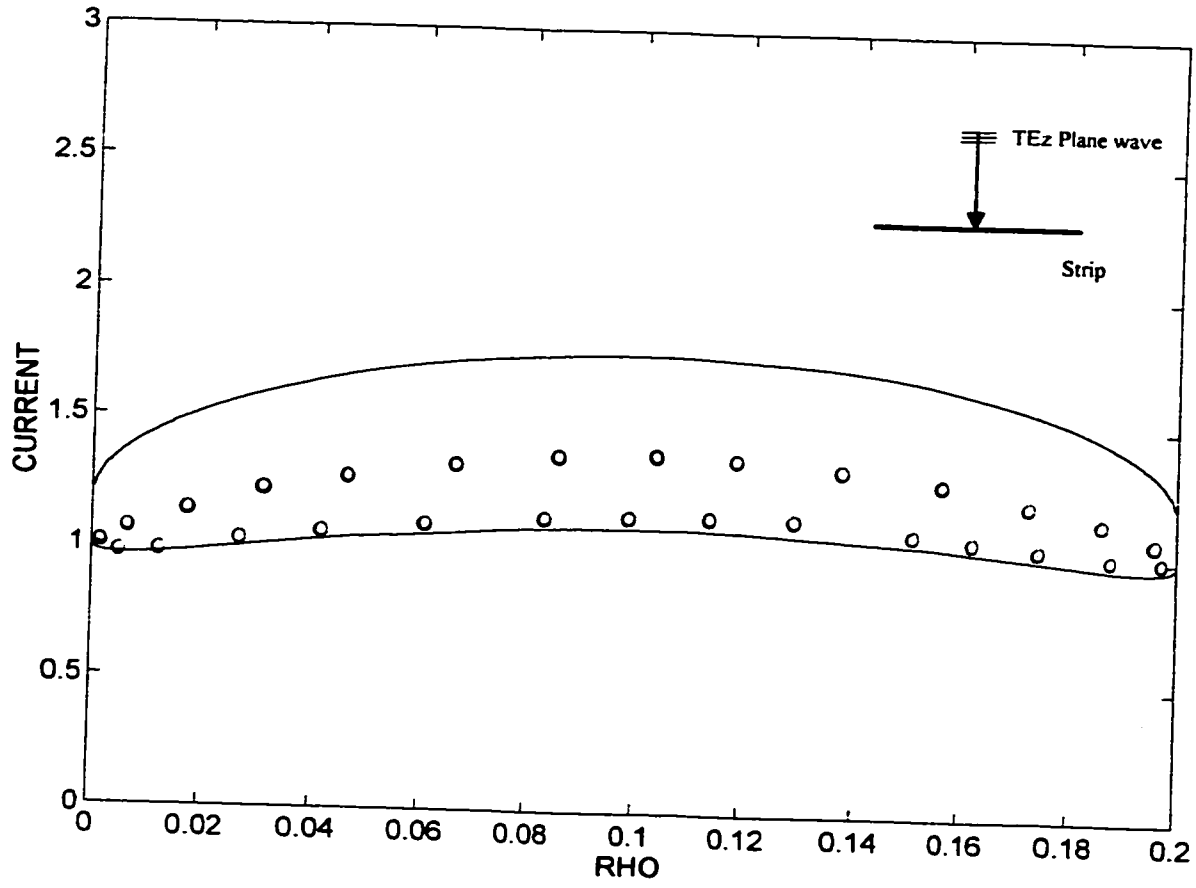

Fig 3.14: Magnitude of current distribution on a strip of width $w=0.2\lambda$ illuminated by a TEz plane wave incident at $\varphi'=90°$ (J in A/m, ρ in λ). [— Single diffraction UTD solution. ooo MM with 200 segments]

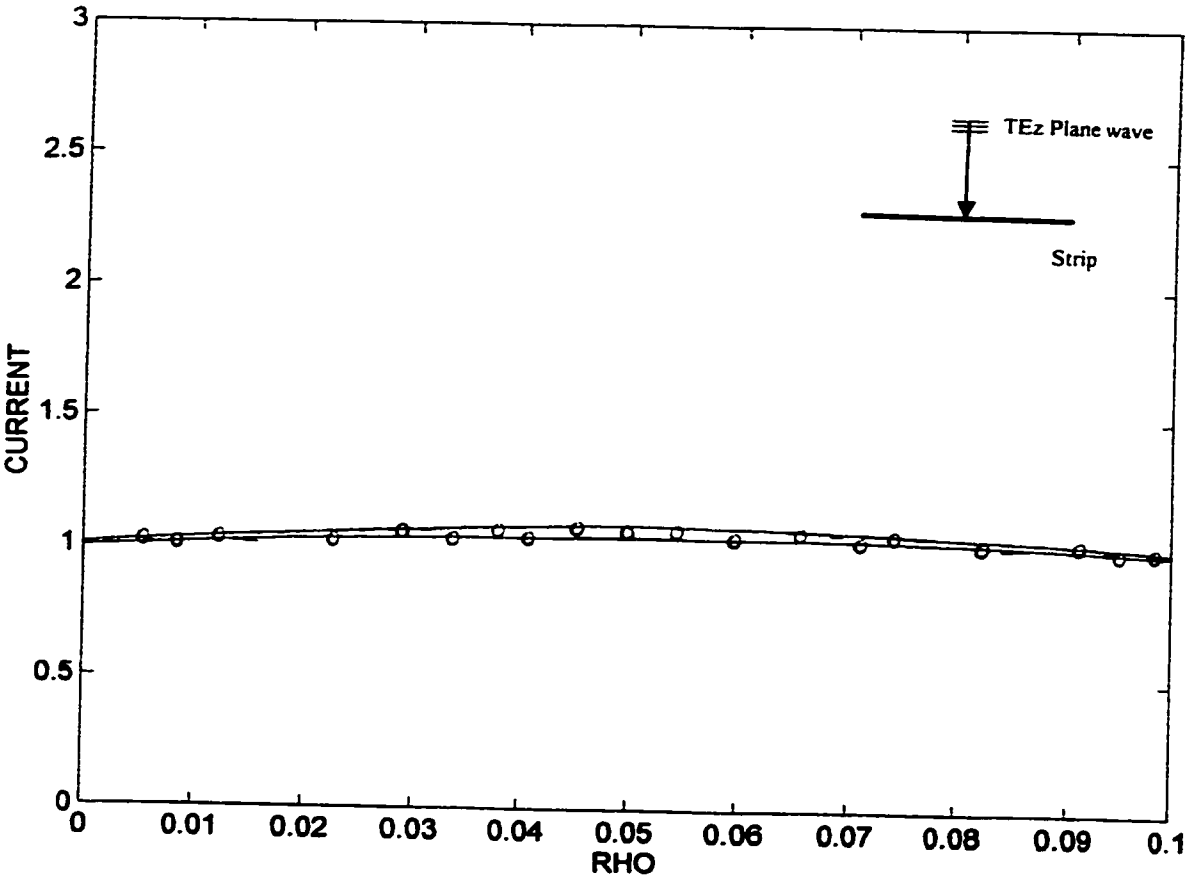

Fig 3.15 : Magnitude of current distribution on a strip of width w=0.1λ illuminated by a TEz plane wave incident at φ'=90° (J in A/m, ρ in λ). [— Multiple diffraction UTD solution, ooo MM with 200 segments]

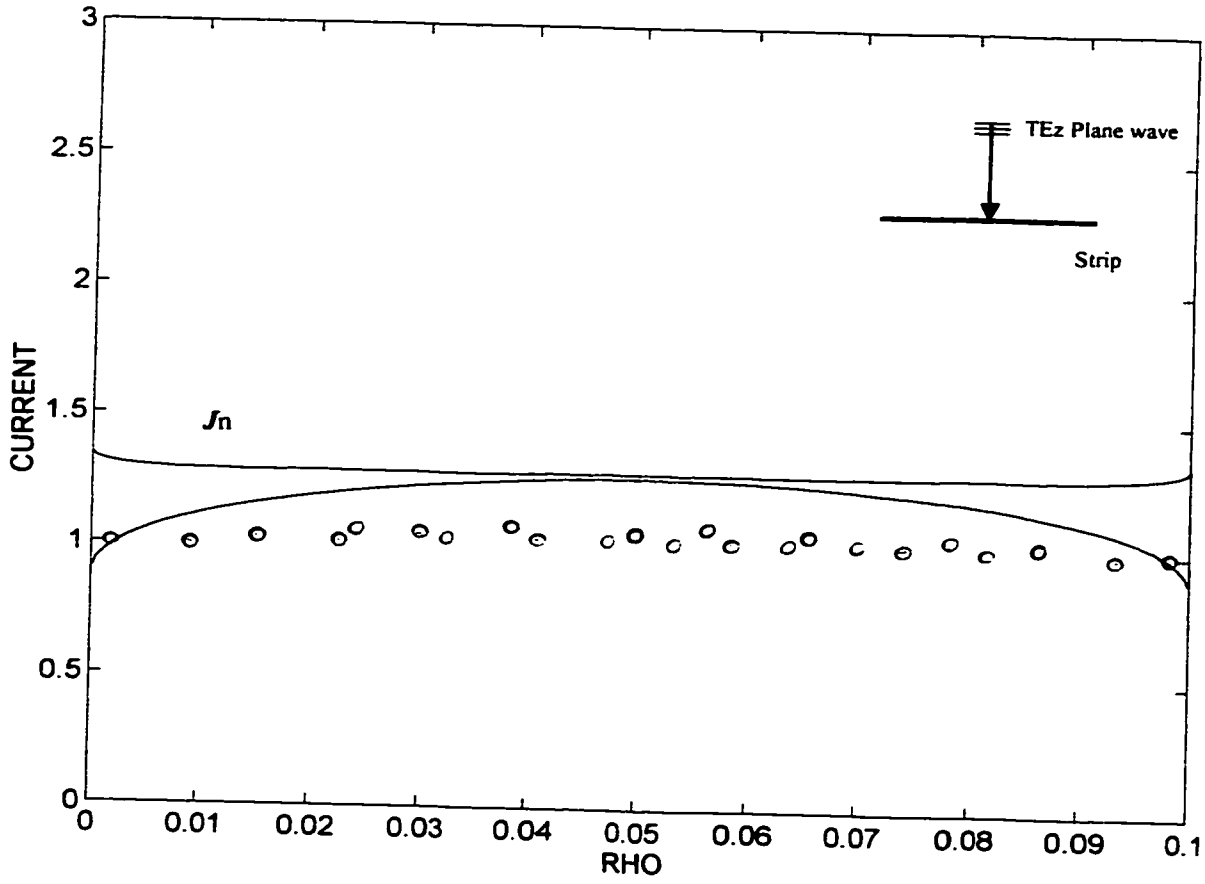

Fig 3.16: Magnitude of current distribution on a strip of width w=0.1 λ illuminated by a TEz plane wave incident at φ'=90° (J in A/m, ρ in λ). [— Single diffraction UTD solution, ooo MM with 200 segments]

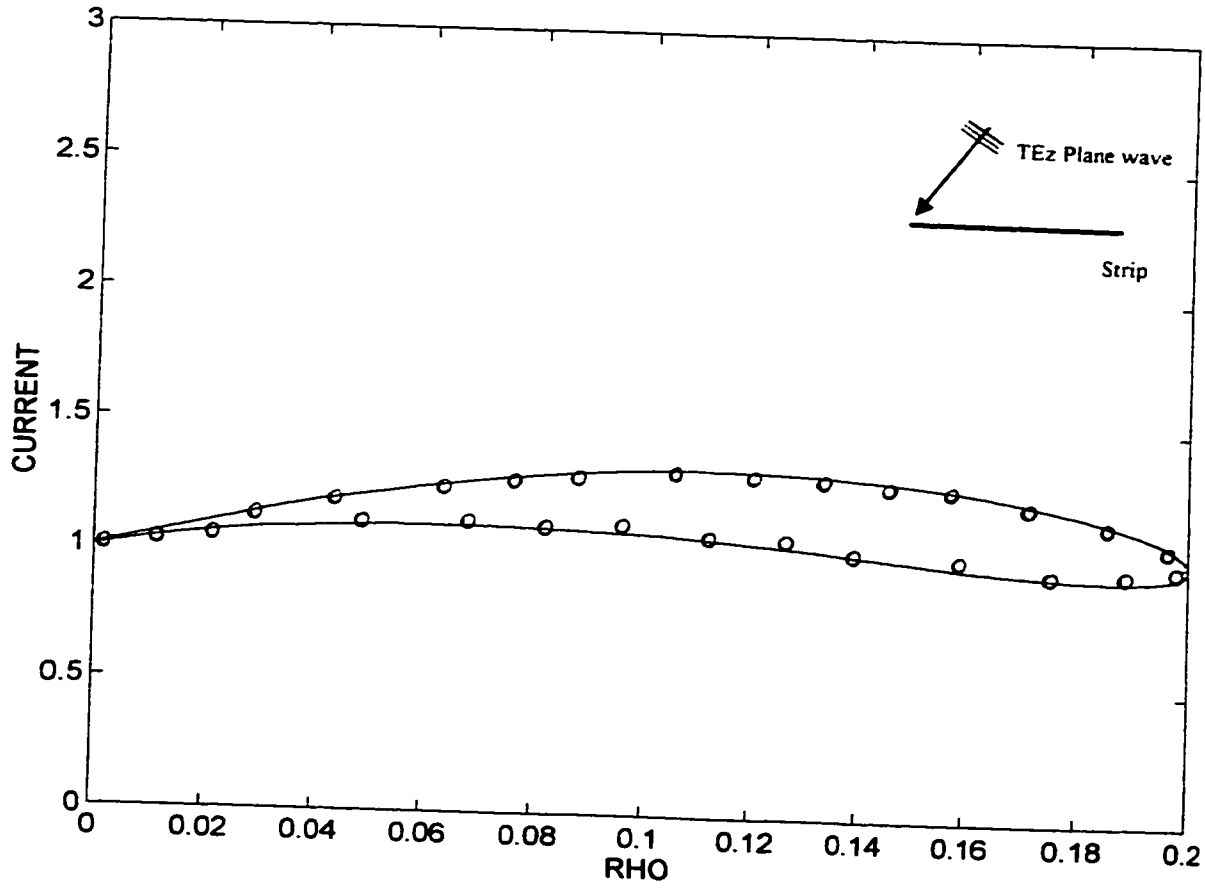

Fig 3.17: Magnitude of current density on a strip of width w=0.2 λ illuminated by a TEz plane wave incident at φ'=60° (J in A/m, ρ in λ). [— Multiple diffraction UTD solution, ooo MM with 200 segments]

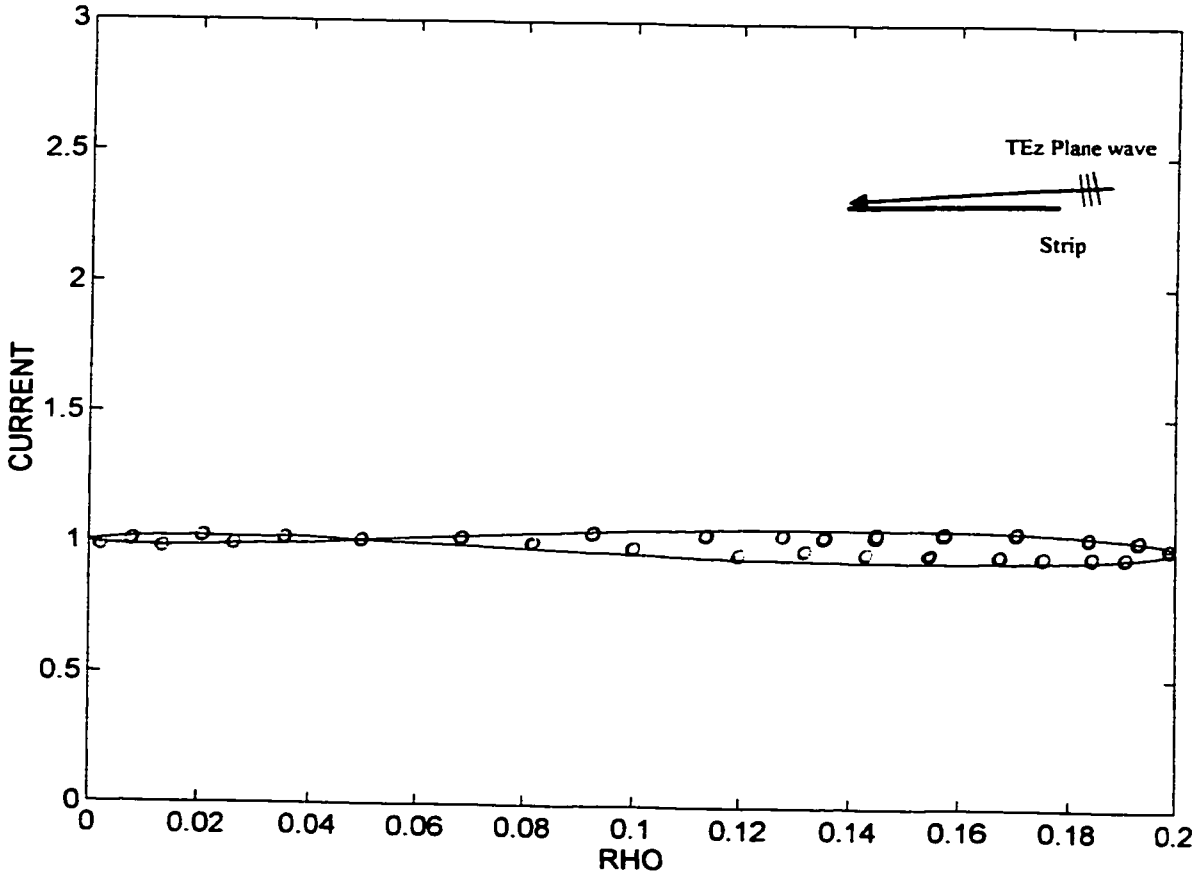

Fig 3.18: Magnitude of current distribution on a strip of width w=0.2 λ illuminated by a TEz plane wave incident at $\varphi^{i}=10°$ (J in A/m, ρ in λ). [— Multiple diffraction UTD solution, ooo MM with 200 segments]

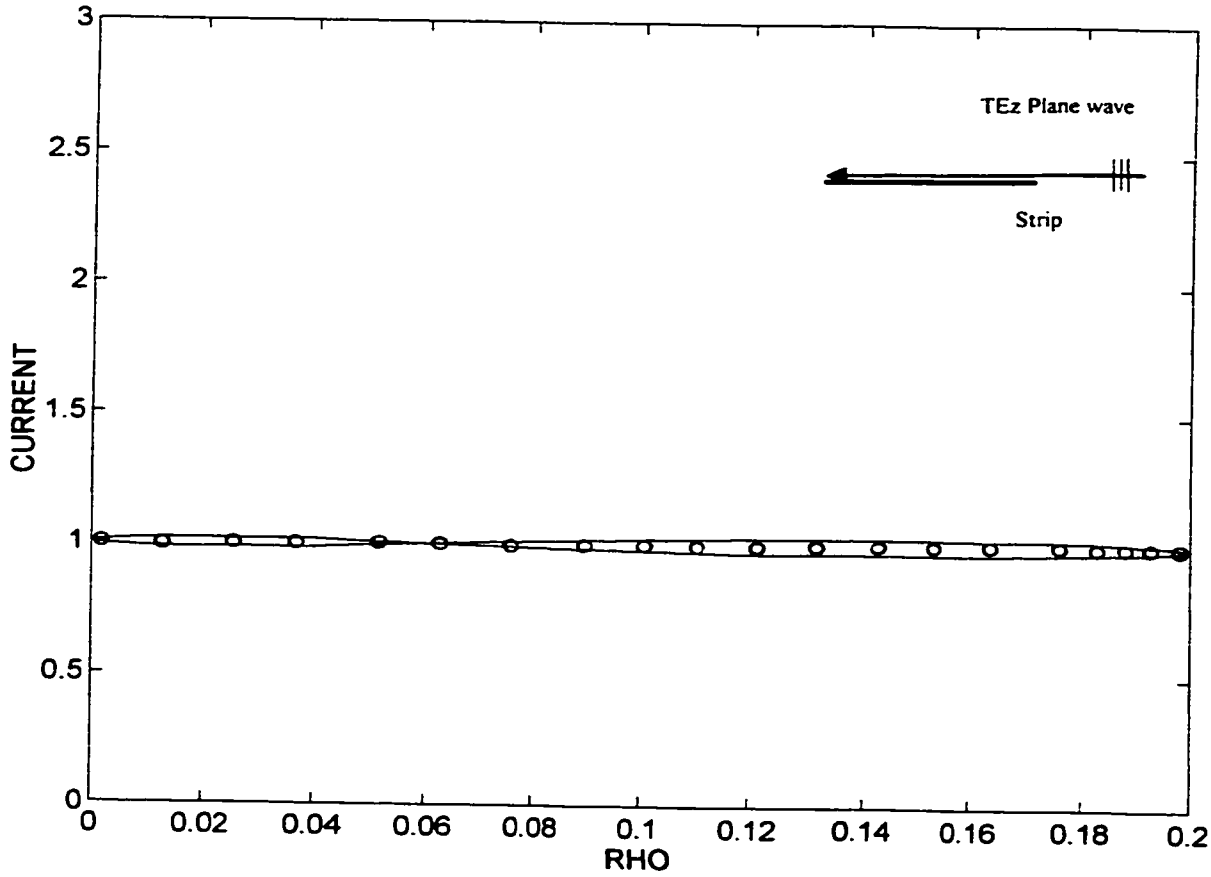

Fig 3.19: Magnitude of current distribution on a strip of width w=0.2 λ illuminated by a TEz plane wave incident at φ'=0.5° (J in A/m, ρ in λ). [— Multiple diffraction UTD solution, ooo MM with 200 segments]

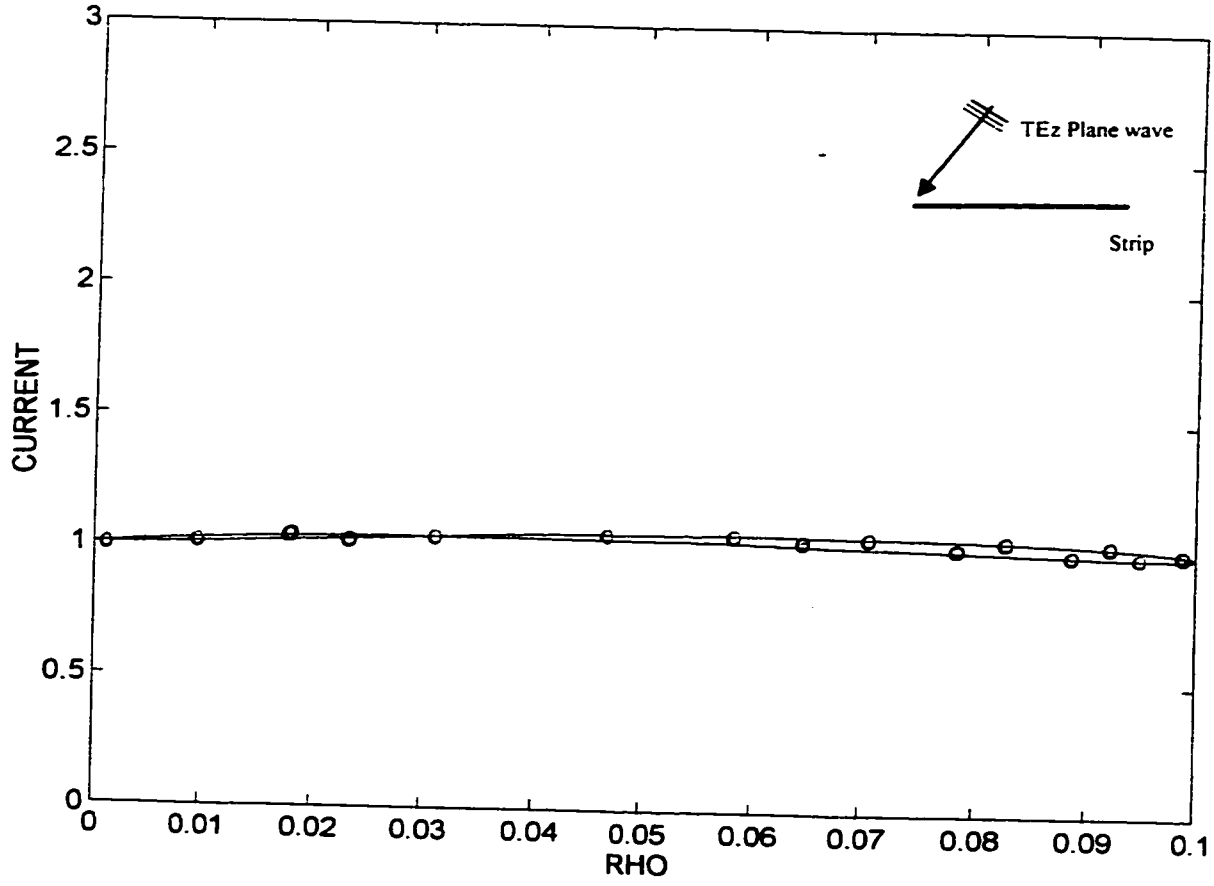

Fig 3.20: Magnitude of current distribution on a strip of width w=0.1 λ illuminated by a TEz plane wave incident at φ`=60° (J in A/m, ρ in λ). [— Multiple diffraction UTD solution. ooo MM with 200 segments]

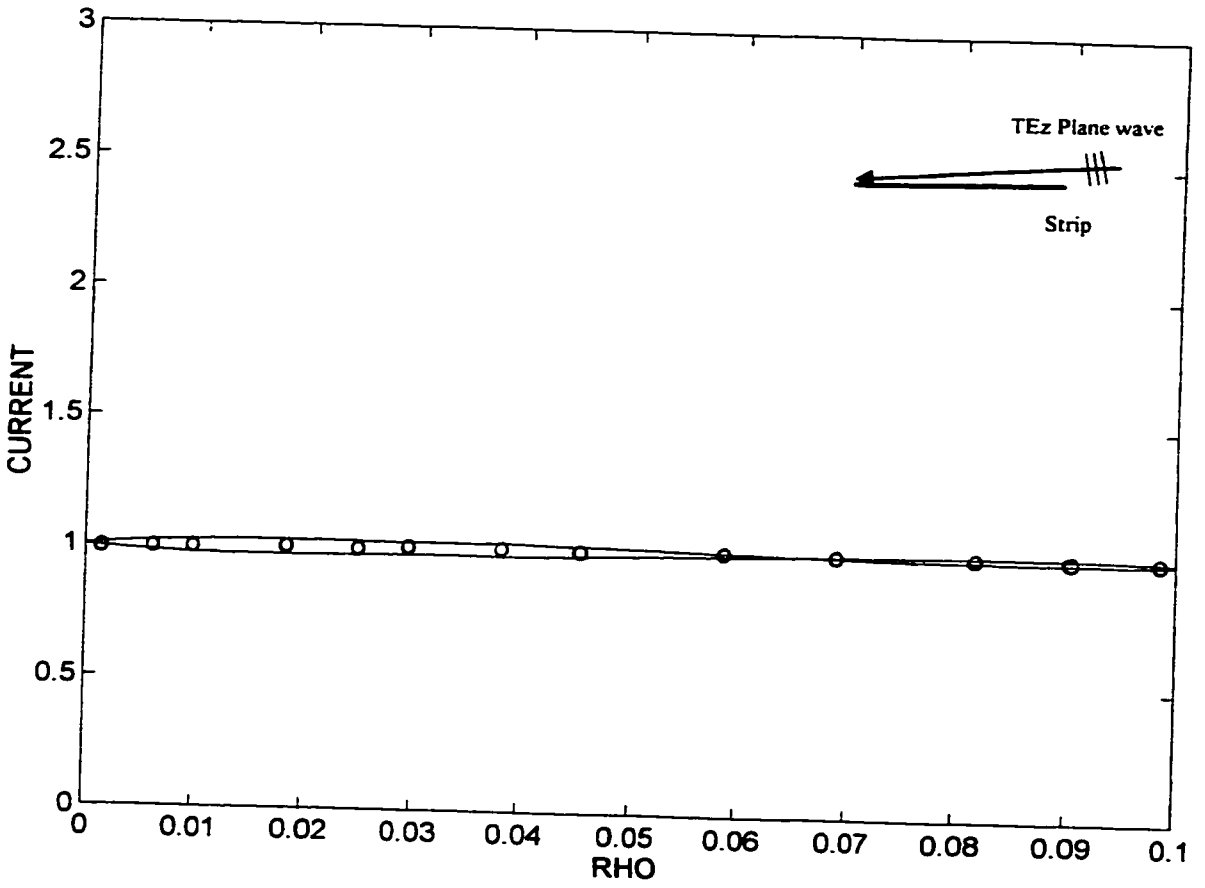

Fig 3.21: Magnitude of current distribution on a strip of width w=0.1λ illuminated by a TEz plane wave incident at φ'=10° (J in A/m, ρ in λ). [— Multiple diffraction UTD solution, ooo MM with 200 segments].

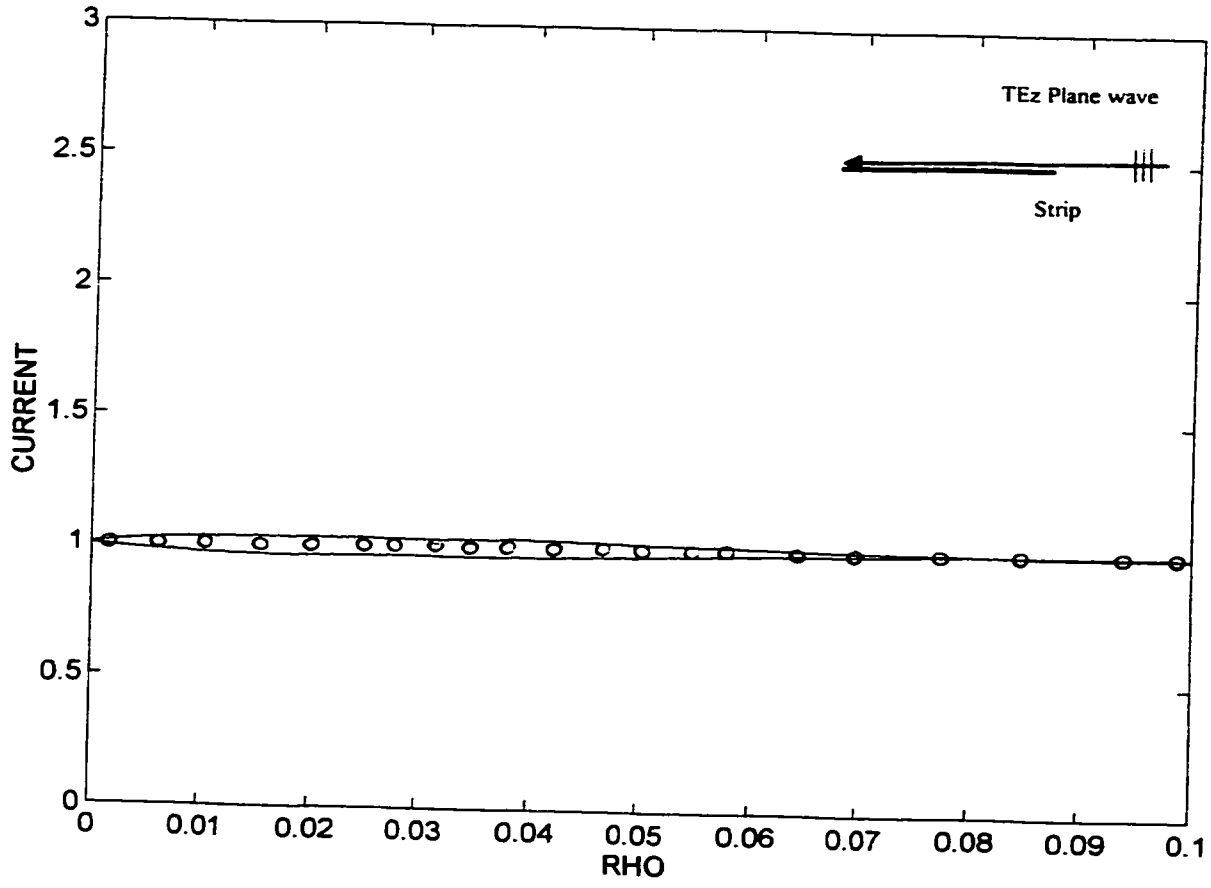

Fig 3.22: Magnitude of current distribution on a strip of width w=0.1 λ illuminated by a TEz plane wave incident at φ'=0.5° (J in A/m, ρ in λ). [— Multiple diffraction UTD solution, ooo MM with 200 segments]

3.3 STRIP SURFACE CURRENT USING THE MOMENT METHOD

In this section, the formulation of the EFIE and moment method solution (of the surface current density of a strip, illuminated by a TEz plane wave) will be derived first and the code based on this formulation will be described after.

3.3.1 Formulation

To establish the integral equation of the geometry of Figure 3.8, the incident and scattered tangential electric fields on the strip must be defined. Since the TEz plane wave has a unity magnetic field at the origin, the tangential fields at a point on the strip separated by a distance ρ from the origin are:

$$H_t^i = e^{jk\rho\cos\varphi'} \quad \text{(in the z direction)} \tag{3.7}$$

$$E_t^i = \eta e^{jk\rho\cos\varphi'} \times \sin\varphi' \quad \text{(in the x direction)} \tag{3.8}$$

From equation 2.18, the scattered tangential electric field (in the x direction) at a certain point m on the strip is (since φ"=0):

$$E_t^s = \frac{-k\eta}{8}\int_0^w J_x(\rho)\left[H_0^{(2)}(k|\rho_m-\rho|)+H_2^{(2)}(k|\rho_m-\rho|)\right]d\rho \tag{3.9}$$

The EFIE is : $$E_t^i = -E_t^s \tag{3.10}$$

Now let's represent the current density by the following series:

$$J_x(\rho) \cong \sum_{n=1}^{N} I_n\, g_n(\rho)$$

Equation 3.9 becomes:

$$E_t^s = \frac{k\eta}{8}\sum_{n=1}^{N} I_n \int_n g_n(\rho)\left[H_0^{(2)}(k|\rho_m-\rho|)+H_2^{(2)}(k|\rho_m-\rho|)\right]d\rho \tag{3.11}$$

If we divide the strip into N segments and if we take g_n to be a pulse function with unity amplitude along the n^{th} segment and zero elsewhere, equation 3.11 becomes,

$$E_t^s = \frac{k\eta}{8}\sum_{n=1}^{N} I_n \int_{\rho_n}^{\rho_{n+1}} \left[H_0^{(2)}\left(k|\rho_m - \rho|\right) + H_2^{(2)}\left(k|\rho_m - \rho|\right)\right] d\rho \qquad (3.12)$$

Equation 3.12 can be repeated for a number of points m equal to the number of segments with the observation being done at the middle of the segment (point matching). This will allow equation 3.10 to become,

$$Vm = \sum_{n=1}^{N} I_n Zmn, \qquad m = 1,2...N \qquad (3.13)$$

where,

$$Vm = \eta\, e^{jk\rho_m \cos\varphi'} \times \sin\varphi' \qquad (3.14)$$

$$Z_{mn} = \frac{k\eta}{8}\int_{\rho_n}^{\rho_{n+1}} \left[H_0^{(2)}\left(k|\rho_m - \rho|\right) + H_2^{(2)}\left(k|\rho_m - \rho|\right)\right] d\rho \qquad (3.15)$$

From equations 2.35 and 2.43, equation 3.15 can be written as(knowing that the segment width is $\Delta = \frac{w}{N}$) :

<u>for m=n</u>

$$Z_{mm} \cong \frac{k\eta\Delta}{8}\left\{1 - j\frac{1}{\pi}\left[-1 + 2In\left(\frac{1.781k\Delta}{4e}\right) + \frac{16}{(k\Delta)^2}\right]\right\} \qquad (3.16)$$

<u>for m ≠ n</u>

$$Z_{mn} = \frac{k\eta}{4}\int_{\rho_n}^{\rho_{n+1}} \frac{H_1^{(2)}\left(k|\rho_m - \rho|\right)}{k|\rho_m - \rho|} d\rho \qquad (3.17)$$

Equation 3.16 is a closed form accurate approximation of the self term. Equation (3.17) can be computed numerically as an integral.

Once the system of N linear equations with N unknowns is solved, the solution represents the total current on the strip scatterer (since it is of zero thickness). To obtain the current on the top and bottom surface of the strip the following must be used,

$$\vec{J}_{Total} = \vec{J}_{Top} + \vec{J}_{Bottom}$$

$$\vec{J}_{Total} = \hat{n} \times (\vec{H}_1^s - \vec{H}_2^s)$$

where,

$\hat{n}$ is the normal vector to the surface

$\vec{H}_1^s$ is the tangential scattered magnetic field just above the strip (region 1)

$\vec{H}_2^s$, is the tangential scattered magnetic field just below the strip (region 2)

since the geometry is symmetric

$$H_1^s = -H_2^s = H^s \qquad \Rightarrow |J_{Total}| = 2 \times H^s$$

$$\vec{J}_{Top} = \hat{n} \times (\vec{H}_i + \vec{H}_1^s) = \left(H_i + \frac{1}{2}|J_{Total}| \right) \hat{\rho}$$

$$\vec{J}_{Bottom} = \hat{n} \times (\vec{H}_i + \vec{H}_2^s) = \left(-H_i + \frac{1}{2}|J_{total}| \right) \hat{\rho}$$

Since H^s can be computed from equation 3.7, the current density on the top and bottom surface of the strip can be computed.

3.3.2 Code and Results

Computer code PSTRIP.FOR was created based on the formulation of the previous section. Numerical integration was done by Simpson rule and Crout's method was used to solve the N linear equations. Results of surface current densities on strips were plotted to be compared with UTD results in section 3.2.

3.4 RECTANGULAR CYLINDER SURFACE CURRENT USING UTD

After evaluating the strip, the rectangular cylinder illuminated by a TEz plane wave (refer to Figure 3.23) was chosen for evaluation. The choice of the rectangular cylinder was considered because it is halfway between the exact half plane solution (n=2) and no diffraction at all (n=1). It is also a simple geometry subject to multiple diffraction.

This section will formulate the solution of the problem first and cover the code and results afterward.

3.4.1 Formulation of the GO Fields

Let's suppose the TEz plane wave (refer to Figure 3.23) has a unit magnitude magnetic field at the origin and the incidence angle φ' can vary between 0^0 and 90^0. This means that the incident fields on points A, B, C, and D are:

$$H_A^i = e^{-j\bar{k}\bullet\bar{R}_A} = e^{-jk\left(\frac{wx}{2}\cos\varphi' - \frac{wy}{2}\sin\varphi'\right)} \quad (3.18)$$

$$H_B^i = e^{-j\bar{k}\bullet\bar{R}_B} = e^{-jk\left(-\frac{wx}{2}\cos\varphi' - \frac{wy}{2}\sin\varphi'\right)} \quad (3.19)$$

$$H_C^i = e^{-j\bar{k}\bullet\bar{R}_C} = e^{-jk\left(-\frac{wx}{2}\cos\varphi' + \frac{wy}{2}\sin\varphi'\right)} \quad (3.20)$$

$$H_D^i = 0 \qquad \text{since} \quad 0°<\varphi'<90° \quad (3.21$$

a) On surface AB (refer to fig 3.24):

The incident field at any point is:

$$H_{AB}^i = e^{-jk\left(-\left(\rho_A - \frac{wx}{2}\right)\cos\varphi' - \frac{wy}{2}\sin\varphi'\right)} \quad (3.22)$$

$$H_{AB}^{GO} = 2H_{AB}^i \qquad \text{(from image theory)} \quad (3.23)$$

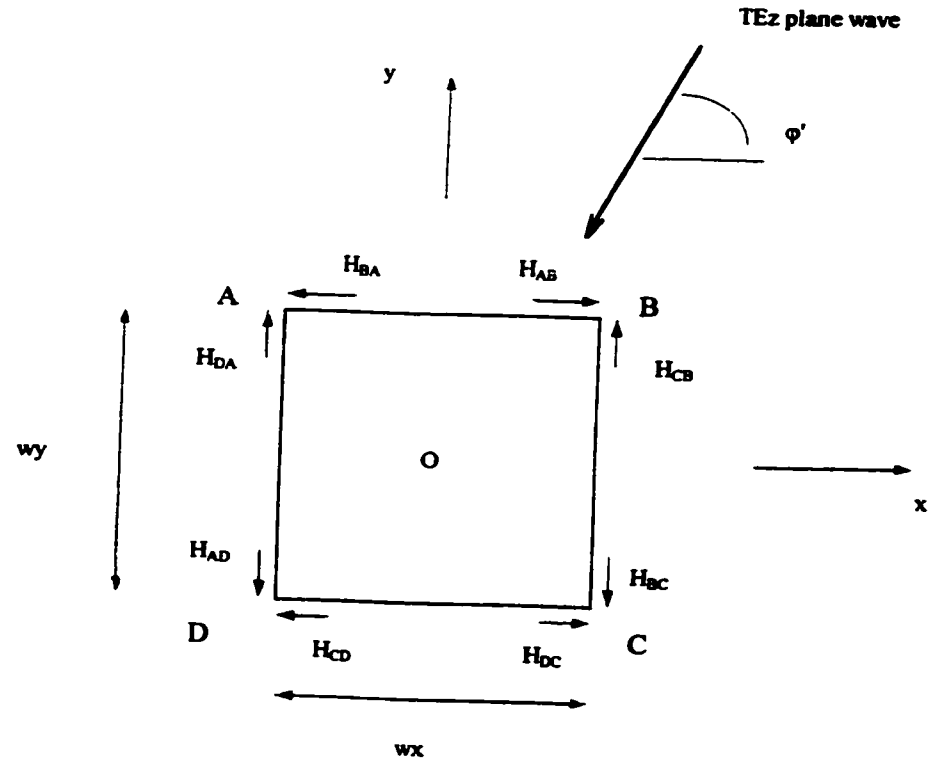

Figure 3.23: TEz plane wave incident on rectangular cylinder.

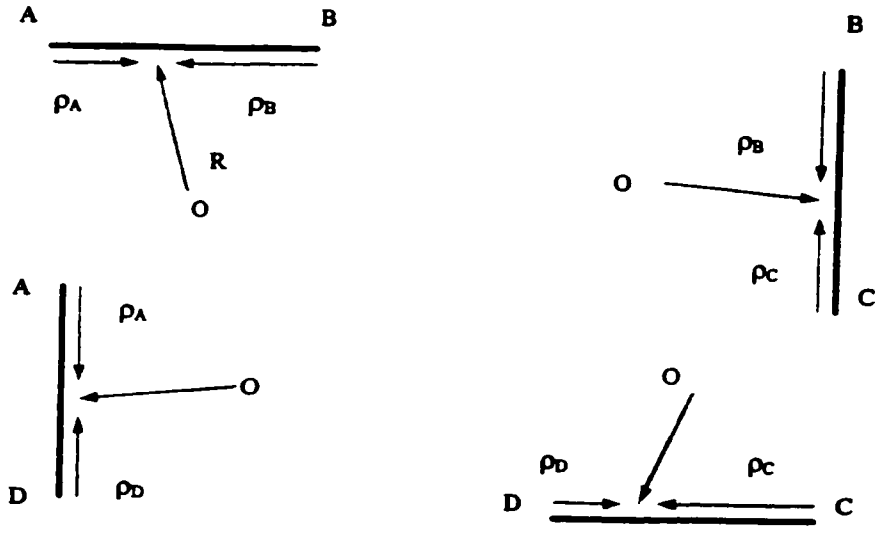

Figure 3.24: Cylinder sides geometry.

b) On surface BC:

$$H_{BC}^{i} = e^{-jk\left(-\left(\frac{wx}{2}\right)\cos\varphi'-\left(\frac{wy}{2}-\rho_B\right)\sin\varphi'\right)} \quad (3.24)$$

$$H_{BC}^{GO} = 2H_{BC}^{i} \quad (3.25)$$

c) On surface CD

$$H_{CD}^{i} = H_{CD}^{r} = 0 \quad (3.26)$$

d) On surface AD

$$H_{AD}^{i} = H_{AD}^{r} = 0 \quad (3.27)$$

3.4.2 Formulation of the Multiple Diffraction Terms

Since multiple diffraction is considered here (refer to Figure 3.23), the following definitions apply:

H_{BA}= Sum of all multiple diffractions due to all edges of the rectangular cylinder arriving at A from the B direction.

H_{DA}= Sum of all multiple diffractions due to all edges of the rectangular cylinder arriving at A from the D direction.

H_{AB}, H_{CB}, H_{BC}, H_{DC}, H_{CD} and H_{AD} have similar definitions depending on the edge.

- $Wxy = \frac{wx.wy}{wx+wy}$
- $D_h(\rho, L, \varphi, \varphi', n)$ is the hard diffraction coefficient.
- $K_x = \frac{e^{-jkwx}}{\sqrt{wx}}$, wx is the diameter of cylinder in x axis.
- $K_y = \frac{e^{-jkwy}}{\sqrt{wy}}$, wy is the diameter of cylinder in the y axis.

To find the multiple diffraction terms, a set of linear equations must be solved:

$$H_{AB} = H'_A K_x D_h(wx, wx, 0, \varphi', 1.5) + \frac{1}{2} H_{BA} K_x D_h\left(wx, \frac{wx}{2}, 0, 0, 1.5\right) + \frac{1}{2} H_{DA} K_x D_h(wx, wxy, 0, 1.5\pi, 1.5) \quad (3.28)$$

$$H_{BC} = H'_B K_y D_h(wy, wy, 1.5\pi, \pi - \varphi', 1.5) + \frac{1}{2} H_{CB} K_y D_h\left(wy, \frac{wy}{2}, 1.5\pi, 1.5\pi, 1.5\right) + \frac{1}{2} H_{AB} K_y D_h(wy, wxy, 1.5\pi, 0, 1.5) \quad (3.29)$$

$$H_{CD} = H'_C K_x D_h\left(wx, wx, 1.5\pi, \frac{\pi}{2} - \varphi', 1.5\right) + \frac{1}{2} H_{DC} K_x D_h\left(wx, \frac{wx}{2}, 1.5\pi, 1.5\pi, 1.5\right) + \frac{1}{2} H_{BC} K_x D_h(wx, wxy, 1.5\pi, 0, 1.5) \quad (3.30)$$

$$H_{DA} = \frac{1}{2} H_{AD} K_y D_h\left(wy, \frac{wy}{2}, 0, 0, 1.5\right) + \frac{1}{2} H_{CD} K_y D_h(wy, wxy, 1.5\pi, 0, 1.5) \quad (3.31)$$

$$H_{AD} = H'_A K_y D_h(wy, wy, 1.5\pi, \varphi', 1.5) + \frac{1}{2} H_{DA} K_y D_h\left(wy, \frac{wy}{2}, 1.5\pi, 1.5\pi, 1.5\right) + \frac{1}{2} H_{BA} K_y D_h(wy, wxy, 0, 1.5\pi, 1.5) \quad (3.32)$$

$$H_{BA} = H_B^i K_x D_h(wx, wx, 0, \pi - \varphi', 1.5)$$
$$\frac{1}{2} H_{AB} K_x D_h\left(wx, \frac{wx}{2}, 0, 0, 1.5\right) \qquad (3.33)$$
$$+ \frac{1}{2} H_{CB} K_x D_h(wx, wxy, 0, 1.5\pi, 1.5)$$

$$H_{CB} = H_C^i K_y D_h\left(wy, wy, 0, \frac{\pi}{2} - \varphi', 1.5\right)$$
$$+ \frac{1}{2} H_{BC} K_y D_h\left(wy, \frac{wy}{2}, 0, 0, 1.5\right) \qquad (3.34)$$
$$+ \frac{1}{2} H_{DC} K_y D_h(wy, wxy, 0, 1.5\pi, 1.5)$$

$$H_{DC} = +\frac{1}{2} H_{CD} K_x D_h\left(wy, \frac{wy}{2}, 1.5\pi, 1.5\pi, 1.5\right)$$
$$+ \frac{1}{2} H_{AD} K_x D_h(wy, wxy, 1.5\pi, 0, 1.5) \qquad (3.35)$$

Equations 3.28 to 3.35 constitute 8 equations with 8 unknowns and can be solved for H_{AB}, H_{BC}, H_{CD} H_{DA}, H_{AD}, H_{BA}, H_{CB}, and H_{DC}.

3.4.3 Formulation of the Total Field

a) on surface AB (refer to Figure 3.24):

If the following definitions are made,

$K_A = \dfrac{e^{-jk\rho_A}}{\sqrt{\rho_A}}$ $\qquad$ $K_B = \dfrac{e^{-jk\rho_B}}{\sqrt{\rho_B}}$

$wx\rho = \dfrac{wx \times \rho}{wx + \rho}$ $\qquad$ $wy\rho = \dfrac{wy \times \rho}{wy + \rho}$

the diffracted field on AB is then:

$$H^{D}_{AB} = \begin{aligned} & H'_{A} K_{A} D_{h}(\rho_{A}, \rho_{A}, 0, \varphi', 1.5) \\ & + \frac{1}{2} H_{BA} K_{A} D_{h}(\rho_{A}, wx\rho_{A}, 0, 0, 1.5) \\ & + \frac{1}{2} H_{BA} K_{A} D_{h}(\rho_{A}, wy\rho_{A}, 0, 1.5\pi, 1.5) \\ & + H'_{B} K_{B} D_{h}(\rho_{B}, \rho_{B}, 0, \pi - \varphi', 1.5) \\ & + \frac{1}{2} H_{AB} K_{B} D_{h}(\rho_{B}, wx\rho_{B}, 0, 0, 1.5) \\ & + \frac{1}{2} H_{CB} K_{B} D_{h}(\rho_{B}, wy\rho_{B}, 0, 1.5\pi, 1.5) \end{aligned} \qquad (3.36)$$

Solving equations 3.28 to 3.35 and using equations 3.22, 3.23 and 3.36 the total field on surface AB is

$$H^{T}_{AB} = H^{GO}_{AB} + H^{D}_{AB} \qquad (3.37)$$

b) On surface BC (refer to Figure 3.24)

Similar definitions to the ones done in a) lead to:

$$H^{D}_{BC} = \begin{aligned} & H'_{B} K_{B} D_{h}(\rho_{B}, \rho_{B}, 1.5\pi, \pi - \varphi', 1.5) \\ & \frac{1}{2} H_{CB} K_{B} D_{h}(\rho_{B}, wy\rho_{B}, 1.5\pi, 1.5\pi, 1.5) \\ & \frac{1}{2} H_{AB} K_{B} D_{h}(\rho_{B}, wx\rho_{B}, 1.5\pi, 0, 1.5) \\ & H'_{C} K_{C} D_{h}\left(\rho_{C}, \rho_{C}, 0, \frac{\pi}{2} - \varphi', 1.5\right) \\ & \frac{1}{2} H_{BC} K_{C} D_{h}(\rho_{C}, wy\rho_{C}, 0, 0, 1.5) \\ & \frac{1}{2} H_{DC} K_{C} D_{h}(\rho_{C}, wx\rho_{C}, 0, 1.5\pi, 1.5) \end{aligned} \qquad (3.38)$$

$$H^{T}_{BC} = H^{GO}_{BC} + H^{D}_{BC} \qquad (3.39)$$

c) On surface CD (refer to Figure 3.24)

$$
\begin{aligned}
H^{D}_{CD} = {} & H'_{C} K_{C} D_{k}\left(\rho_{C}, \rho_{C}, 1.5\pi, \frac{\pi}{2} - \varphi', 1.5\right) \\
& + \frac{1}{2} H_{DC} K_{C} D_{k}(\rho_{C}, wx\rho_{C}, 1.5\pi, 1.5\pi, 1.5) \\
& + \frac{1}{2} H_{BC} K_{C} D_{k}(\rho_{C}, wy\rho_{C}, 1.5\pi, 0, 1.5) \\
& + \frac{1}{2} H_{CD} K_{D} D_{k}(\rho_{D}, wx\rho_{D}, 1.5\pi, 1.5\pi, 1.5) \\
& + \frac{1}{2} H_{AD} K_{D} D_{k}(\rho_{D}, wy\rho_{D}, 0, 1.5\pi, 1.5)
\end{aligned}
\tag{3.40}
$$

$$
H^{T}_{CD} = H^{D}_{CD} \tag{3.41}
$$

d) On surface DA (refer to Figure 3.24)

$$
\begin{aligned}
H^{D}_{CD} = {} & H'_{A} K_{A} D_{k}(\rho_{A}, \rho_{A}, 1.5\pi, \varphi', 1.5) \\
& + \frac{1}{2} H_{DA} K_{A} D_{k}(\rho_{A}, wy\rho_{A}, 1.5\pi, 1.5\pi, 1.5) \\
& + \frac{1}{2} H_{BA} K_{A} D_{k}(\rho_{A}, wx\,\rho_{A}, 1.5\pi, 0, 1.5) \\
& + \frac{1}{2} H_{AD} K_{D} D_{k}(\rho_{D}, wy\rho_{D}, 0, 0, 1.5) \\
& + \frac{1}{2} H_{CD} K_{D} D_{k}(\rho_{D}, wx\rho_{D}, 0, 1.5\pi, 1.5)
\end{aligned}
\tag{3.42}
$$

$$
H^{T}_{CD} = H^{D}_{CD} \tag{3.43}
$$

Now since $\vec{J}_{x} = \vec{n} \times \vec{H}^{T}$ (3.44)

The current density can be computed at any point on the cylinder.

3.4.4 Code and Results

Based on the formulations in sections 3.4.1, 3.4.2 and 3.4.3 code MGTDBX.FOR was created. The code covers angles of incidence φ' between 0 and 90^0. It uses the generic UTD formulation for the diffraction coefficient. Results from the moment method solution described in section 3.5 are plotted (in small circles) also for comparison.

The results from MGTDBX.FOR chosen to be reproduced here, are for a square cylinder illuminated by a TEz plane wave. The radius of the cylinder = a. The plots of the current density are against ρ/a, where ρ is a linear distance on the surface of the cylinder from edge A moving clockwise. This means thus at $\rho/a=1$, the position is halfway between A and B, if $\rho/a=4$ the position is at C etc...
The idea behind this method of plotting is to compare the results obtained to plots already existent in the open literature.
Figures 3.25, 3.26, 3.27 and 3.28 show the current density distribution on the surface of a square cylinder (of radius a) with ka= 10, 5, 2 an 1 respectively and the TEz plane wave incident at 89.9^0.
These plots are in agreement with [21] [22] results (Note: [22] corrects some of the plots found in [21]).
Differences are noticeable at edges for the UTD solution but this is expected so close to the edge. For a = 0.1591λ, the difference is more noticeable on the shadow side with the UTD method. The difference between UTD and moment method results (as a percentage of the moment method result) is still however below 5% at 0.05λ from edge C.
Figures 3.29 and 3.30 show the current density distribution with 60^0 angle of incidence for ka=2 and 1 respectively.

There is no equivalent to these plots in [21][22] but there is a good agreement between the UTD and moment method results.

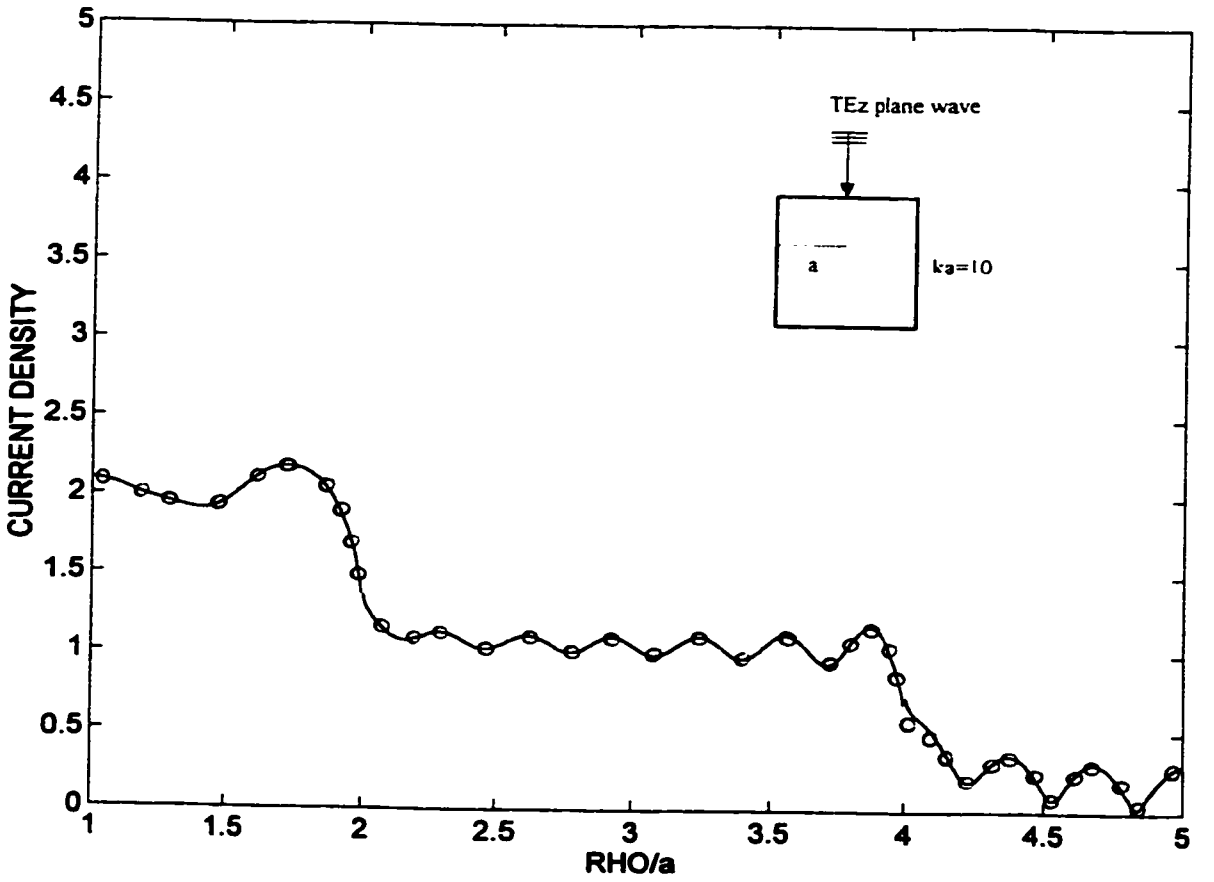

Figure 3.25: Magnitude of current density distribution (J in A/m) on the surface of a square cylinder (radius=a) illuminated by a TEz plane wave at an angle of incidence of 89.9^{0} (ka=10, a=1.5915 λ.). [— UTD, ooo MM]

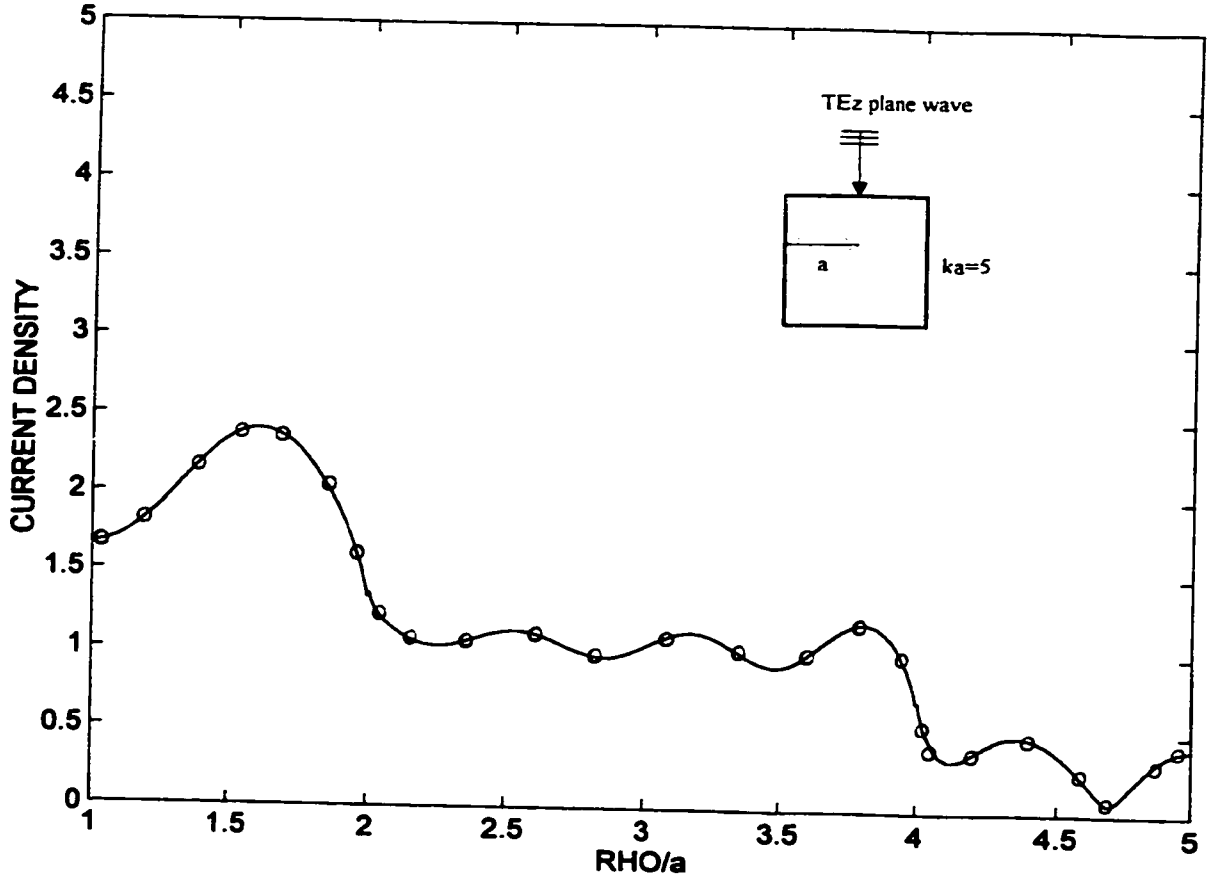

Figure 3.26: Magnitude of current density (J in A/m) on a square cylinder illuminated by a TEz plane wave at an angle of incidence of 89.9 ^{o} (ka=5, a=0.7958 λ). [— UTD, ooo MM]

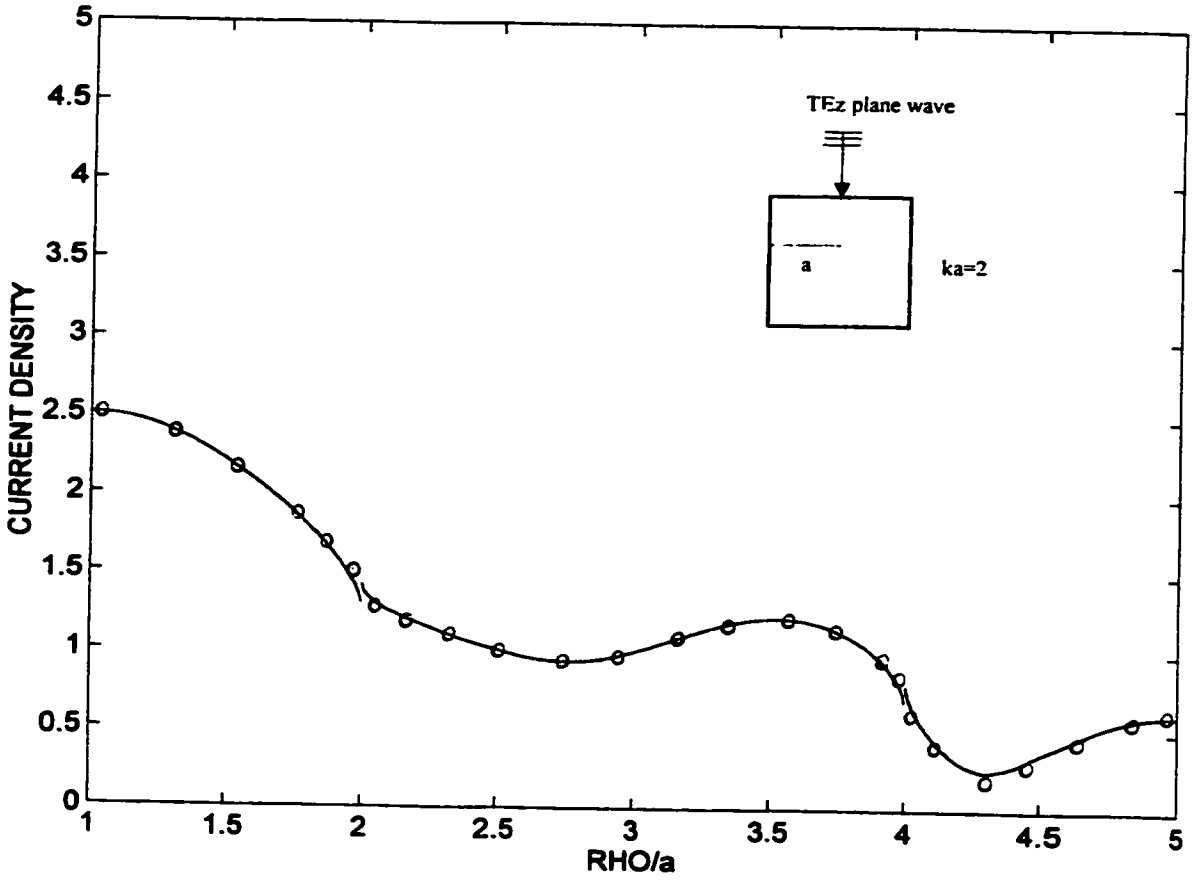

Figure 3.27: Magnitude of current density (J in A/m) on a square cylinder illuminated by a TEz plane wave at an angle of incidence of 89.9^{0} (ka=2, a=0.3183 λ). [— UTD, ooo MM]

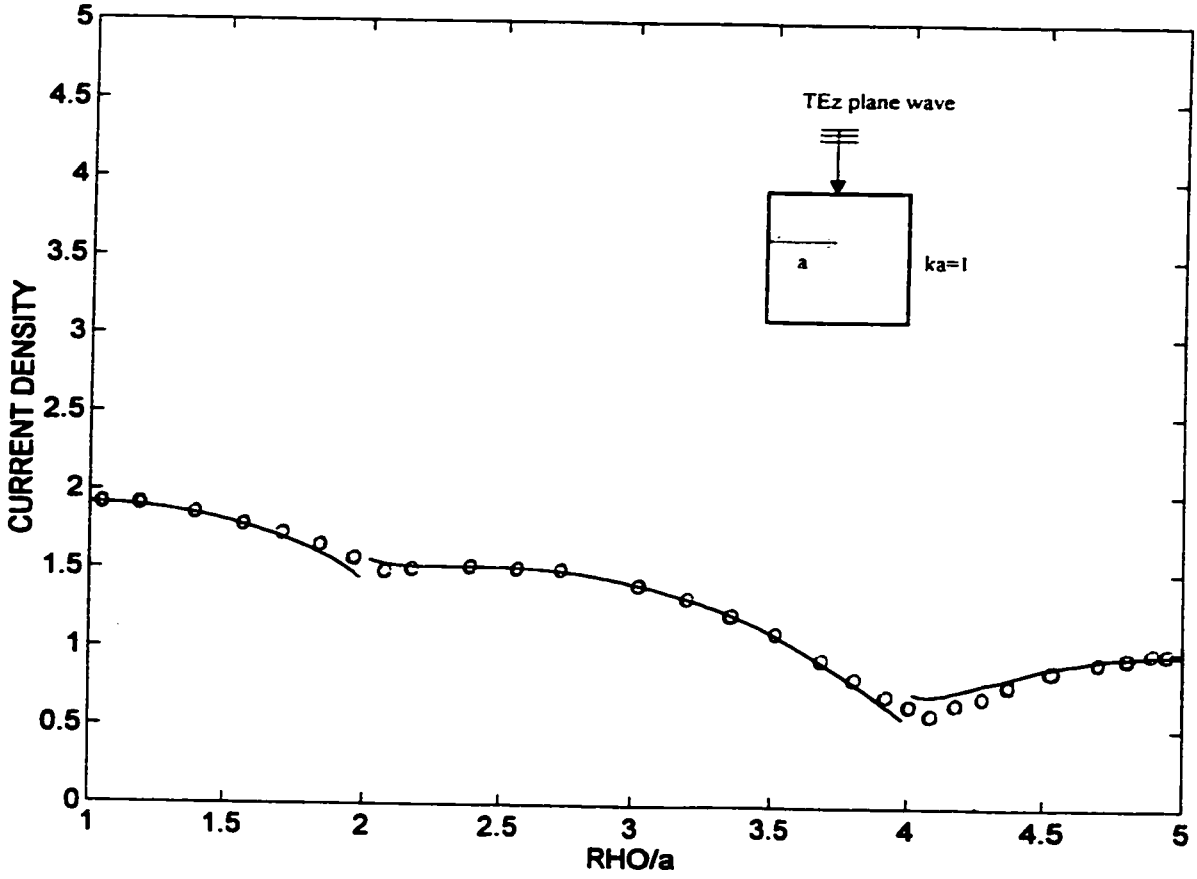

Figure 3.28: Magnitude of current density (J in A/m) on a square cylinder illuminated by a TEz plane wave at an angle of incidence of 89.9° (ka=1, a=0.1591 λ). [— UTD, ooo MM]

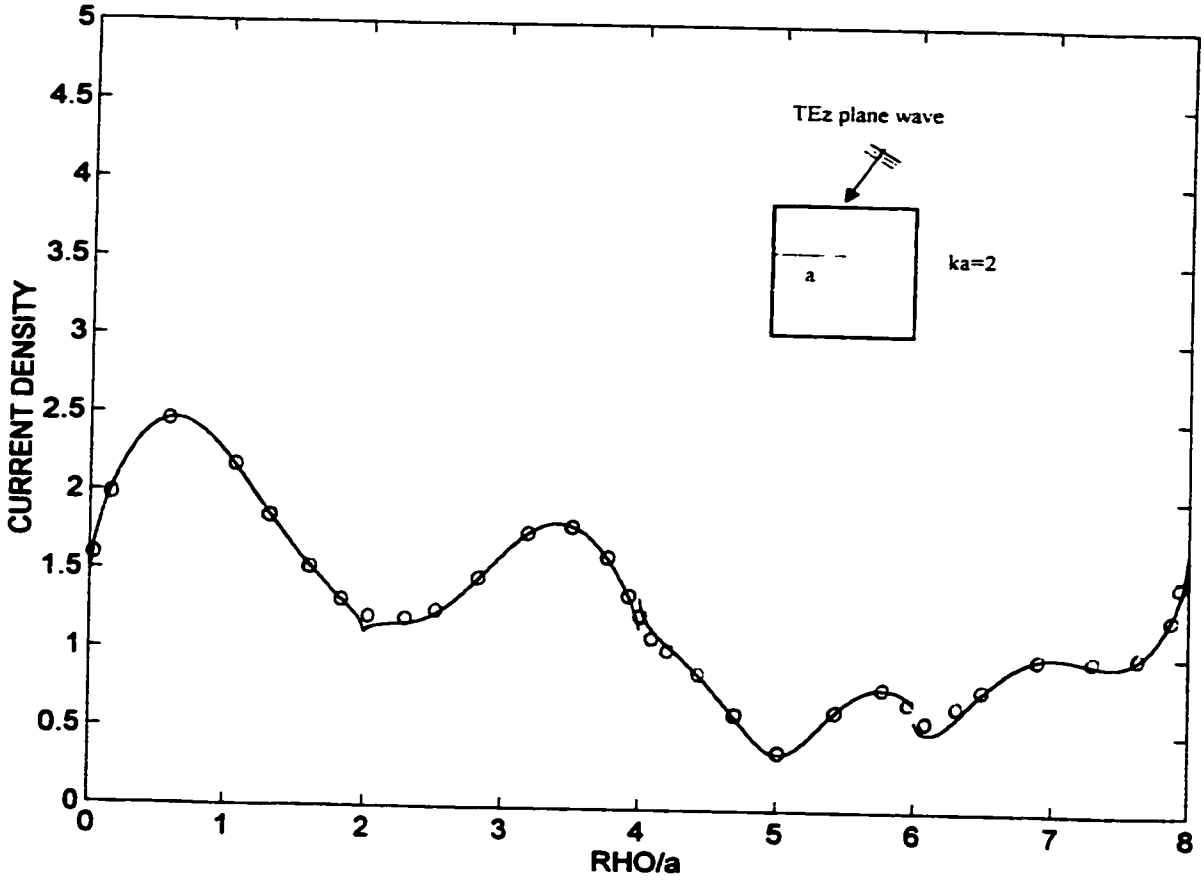

Figure 3.29 : Magnitude of current density (J in A/m) on a square cylinder illuminated by a TEz plane wave at an angle of incidence of 60^{0} (ka=2, a=0.3183 λ). [— UTD, ooo MM]

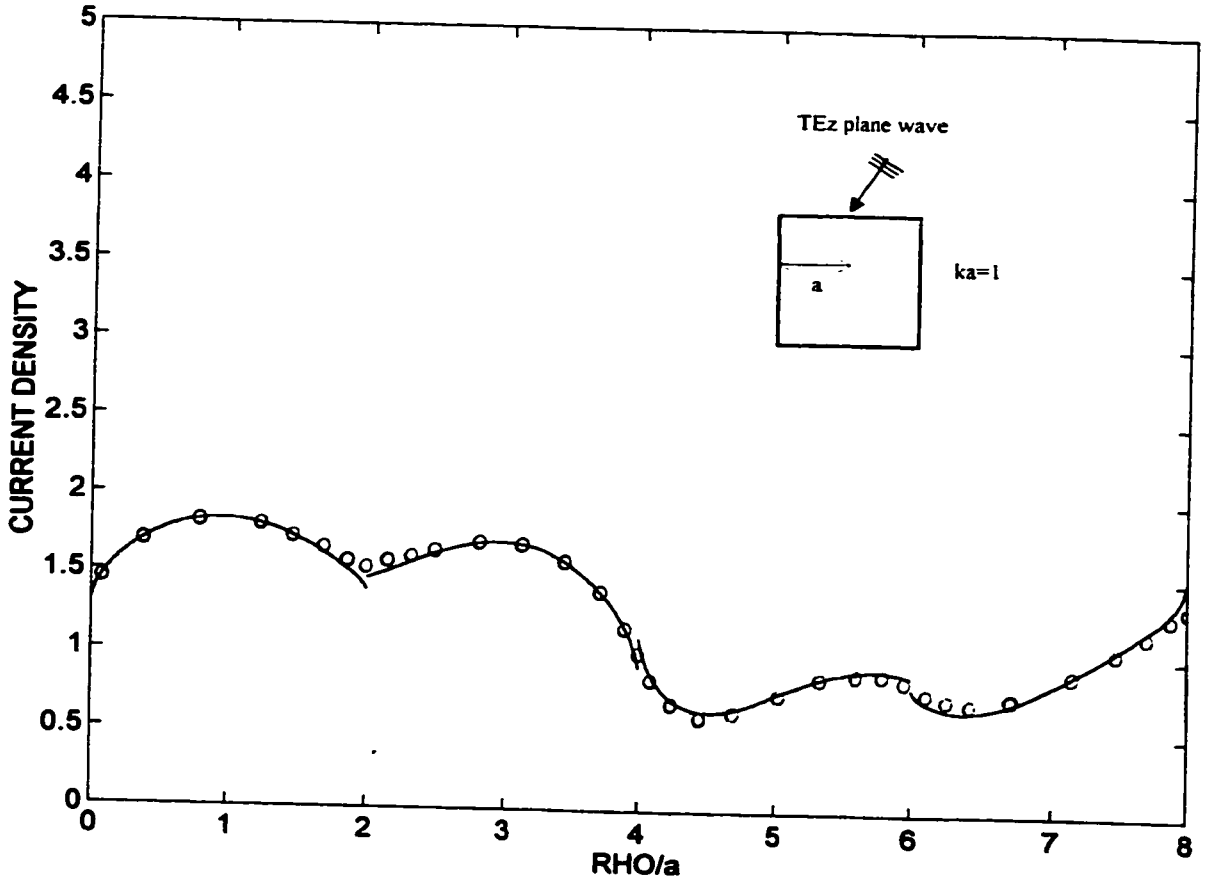

Figure 3.30: Magnitude of current density (J in A/m) on a square cylinder illuminated by a TEz plane wave at an angle of incidence of 60^0 (ka=1, a=0.1591 λ). [— UTD, ooo MM]

3.5 RECTANGULAR CYLINDER SURFACE CURRENT USING THE MOMENT METHOD

In this section the problem depicted in Figure 3.23 will be solved by the moment method. First, and to be able to establish the EFIE, the formulation of the incident and scattered fields is done followed by the EFIE moment method solution description. At the end, the created code is described.

3.5.1 Incident Field Formulation

The EFIE is used here even if it is the TEz case (refer to Figure 3.23). Since the incident TEz plane wave has a unit magnitude magnetic field at the origin, elsewhere the incident field is at a point (x,y):

$$H^{i}(x, y) = e^{-jk(-x\cos\varphi' - y\sin\varphi')}$$

The incident electric field is normal to both $\vec{H}$ and $\vec{k}$ and has an x and y component. They are at a certain point (x,y)

$$E_x^i = \eta \times \sin\varphi' \times e^{-jk(-x\cos\varphi' - y\sin\varphi')} \tag{3.45}$$

$$E_y^i = -\eta \times \cos\varphi' \times e^{-jk(-x\cos\varphi' - y\sin\varphi')} \tag{3.46}$$

3.5.2 Scattered Field Formulation

For the 2-D TEz scattering case, equation 2.18 gives the x and y component of the scattered electric field due to the surface current on a plate. This geometry is shown in Figure 3.31a.The axis of the plate coordinates system can be rotated 90^0 like in the case depicted in 3.31b so that the plate is on the y axis. In such a

case equation 2.18a is used to compute E_y^s with the integral along the y axis and equation 2.18b is used to compute E_y^s with the integral along the y axis. Rotating the coordinates axis again like in 3.31 c) will not change the formulation of E_y^s from the case in 3.31b but it will multiply the E_y^s formulation by a negative sign. It should be mentioned also that due to the axis rotation, φ' is positive in the case of 3.31a when $\vec{R}$ has a positive y component. It is however negative in the case of 3.31c when $\vec{R}$ has a positive x component.
If segments of current pulses are used to represent the current distribution on the plate, the scattered field becomes (based on equation 2.18):

a) <u>For a plate parallel to the x axis (refer to Figure 3.31a)</u>:
If the plate of width = wx is sliced to Nx segments and the current J_x on the plate is represented by: $J_x = \sum_{n=1}^{Nx} I_n g_n(x)$

Where $g_n(x)$ is a pulse function with unity amplitude at segment n and zero elsewhere, then

$$E_x^s = \sum_{n=1}^{Nx} I_n \left[-\frac{k\eta}{8} \int_{x_n-\frac{\Delta x}{2}}^{x_n+\frac{\Delta x}{2}} \left(H_0^{(2)}(kR_m) + H_2^{(2)}(kR_m)\cos(2\varphi'') \right) dx \right] \qquad \text{(3.47a)}$$

$$E_y^s = \sum_{n=1}^{Nx} I_n \left[-\frac{k\eta}{8} \int_{x_n-\frac{\Delta x}{2}}^{x_n+\frac{\Delta x}{2}} \left(H_2^{(2)}(kR_m)\sin(2\varphi'') \right) dx \right] \qquad \text{(3.47b)}$$

where x_n = is the middle of segment n

Δx = is wx/Nx = segment width

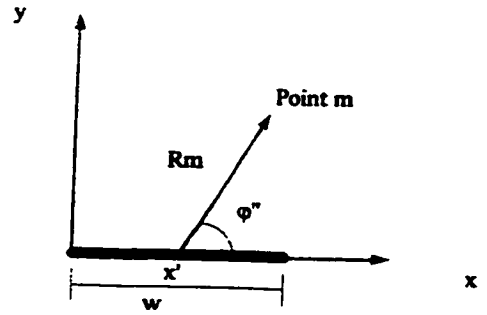

(a)

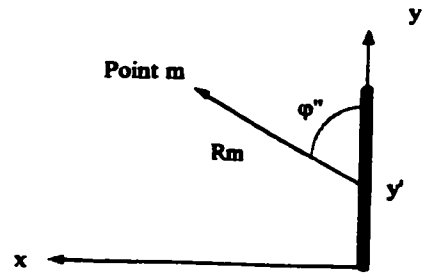

(b)

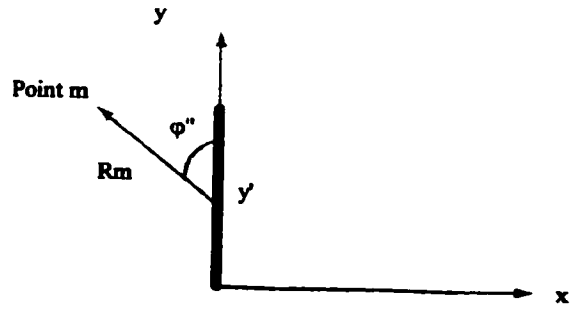

(c)

Figure 3.31 : Scattered fields geometries due to surface current on plates in the x and y axis.

b) <u>For a plate parallel to the y axis (refer to Figure 3.31c)</u>:

If the current is $J_y = \sum_{n=1}^{Ny} I_n g_n(y)$, then similarly to the previous case,

$$E_x^s = \sum_{n=1}^{Ny} I_n \left[+ \frac{k\eta}{8} \int_{y_n - \frac{\Delta y}{2}}^{y_n + \frac{\Delta y}{2}} \left(H_2^{(2)}(kR_m) \sin(2\varphi'') \right) dy \right] \qquad (3.48a)$$

$$E_y^s = \sum_{n=1}^{Ny} I_n \left[- \frac{k\eta}{8} \int_{y_n - \frac{\Delta x}{2}}^{y_n + \frac{\Delta x}{2}} \left(H_0^{(2)}(kR_m) + H_2^{(2)}(kR_m) \cos(2\varphi'') \right) dy \right] \qquad (3.48b)$$

where, y_n = middle of segment n

Δy = wy/Ny = segment width

Since the geometry dealt with here is a rectangular cylinder with its surfaces parallel to the x or y axis, the tangential electric field at a point on the cylinder generated by one side is E_x^s or E_y^s, hence due to a certain side of the cylinder the scattered tangential electric field at a certain point m on the surface on the cylinder is:

$$E_{tm}^s = \sum_{n=1}^{N} I_n Z_{mn} \qquad (3.49)$$

where,

N = is Nx or Ny.

Z_{mn} = is the term between brackets in equation 3.47a, 3.47b, 3.48a or 3.48b depending which side is the generating one (choice between equation 3.47 and 3.48) and on which side m is on (choice between a and b).

The Z_{mn} terms are generally computed by numerical integration, or closed form according to equations 2.34, 2.35, 2.36 or 2.43 .It should be remembered that depending how the EFIE is formulated $E^i_{tan} = -E^s_{tan}$ *or* $-E^i_{tan} = E^s_{tan}$, the Z_{mn} terms have to be multiplied by –1. Equations 2.34, 2.35, 2.36 and 2.43 were derived for the EFIE $E^i_{tan} = -E^s_{tan}$

3.5.3 Total Tangential Electric Field on AB

The geometry in Figure 3.23 is used to establish the total field on each segment. The perimeter of the rectangular cylinder is divided (starting from A, clockwise) into N segments. Each section of the perimeter parallel to the x axis is divided into Nx segments and each section parallel to the y axis is divided into Ny segments.

N = Nx + Ny + Nx + Ny = 2Nx + 2Ny.

Segment n = 1 is next to A and segment n = Nx is next to B and segment Nx + Ny is next to C etc... The dimensions of the cylinder are wx and wy.

The total tangential electric field at a point m (x_m, wy/2) on AB is the sum of the tangential incident field and tangential scattered field generated by AB itself, BC, CD and DA.

a) <u>Tangential incident electric field.</u>

From equation (3.45):

$$E^i_{tan} = E^i_x = \eta \times \sin\varphi' \times e^{-jk\left(-x_m \cos\varphi' - \frac{wy}{2}\sin\varphi'\right)}$$

b) <u>From AB:</u>

$$E^s_{tan} = E^s_x = \sum_{n=1}^{Nx} I_n Z_{mn}$$

where, Z_{mn} is the term between brackets in equation 2.47a)

$$R_m = \sqrt{|x_m - x|}$$

$\varphi"=0$, $\cos(2\varphi") = 1$

c) From BC (refer to Figure 3.32a):

$$E^s_{tan} = E^s_x = \sum_{n=Nx+1}^{Nx+Ny} I_n Z_{mn}$$

where, Z_{mn} is from equation 3.48a

$$R_m = \sqrt{\left(\frac{wx}{2} - x_m\right)^2 + \left(\frac{wy}{2} - y\right)^2}$$

$$\sin 2\varphi" = 2\sin\varphi"\cos\varphi" = 2\frac{\left(\frac{wx}{2} - x_m\right)}{R_m} \times \frac{\left(\frac{wy}{2} - y\right)}{R_m}$$

d) From CD (refer to Figure 3.32b):

$$E^s_{tan} = E^s_x = \sum_{n=Nx+Ny+1}^{2Nx+Ny} I_n Z_{mn}$$

where, Z_{mn} is from equation 3.47a

$$R_m = \sqrt{(x_m - x)^2 + (wy)^2}$$

$$\cos(2\varphi") = -1 + 2\cos^2(\varphi") = -1 + 2\left(\frac{x_m - x}{R_m}\right)^2$$

e) From AD (refer to Figure 3.32c)

$$E^s_{tan} = E^s_x = \sum_{n=2Nx+Ny+1}^{2Nx+2Ny} I_n Z_{mn}$$

where, Z_{mn} is from equation 3.48a

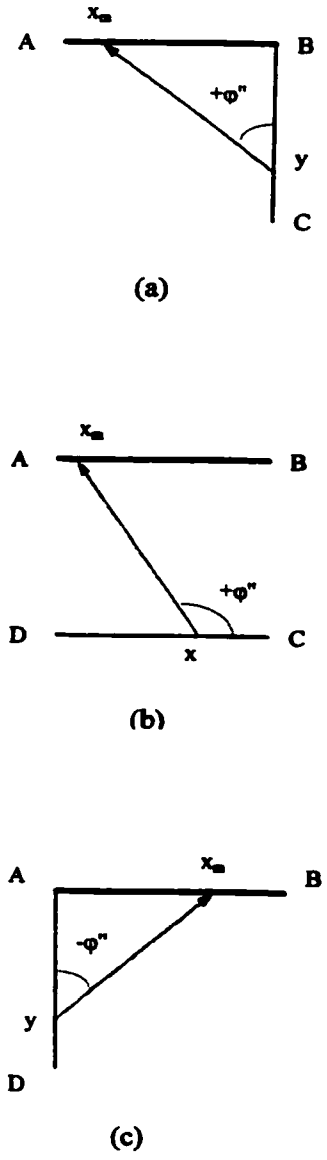

Figure 3.32 : Scattered field on AB due to other cylinder segments.

$$R_m = \sqrt{\left(\frac{wx}{2} + x_m\right)^2 + \left(\frac{wy}{2} - y\right)^2}$$

$$\sin(2\varphi'') = 2\sin(\varphi'')\cos(\varphi'') = -2\left(\frac{x_m + \frac{wx}{2}}{R_m}\right)\left(\frac{\frac{wy}{2} - y}{R_m}\right)$$

3.5.4 Total Tangential Electric Field on BC

A point m on BC has coordinate $\left(\frac{wx}{2}, y_m\right)$

a) Incident field:

$$E^i_{tan} = E^i_y = -\eta \times \cos\varphi' \times e^{-jk\left(-\frac{wx}{2}\cos\varphi' - y_m \sin\varphi'\right)}$$

b) From AB:

$$E^s_{tan} = E^s_y = \sum_{n=1}^{N_x} I_n Z_{mn}$$

where, Z_{mn} = is from equation 3.47b

$$R_m = \sqrt{\left(\frac{wx}{2} - x\right)^2 + \left(\frac{wy}{2} - y_m\right)^2}$$

$$\sin(2\varphi'') = 2\sin(\varphi'')\cos(\varphi'') = -2\left(\frac{\frac{wy}{2} - y_m}{R_m}\right)\left(\frac{\frac{wx}{2} - x}{R_m}\right)$$

c) From BC:

$$E^s_{tan} = E^s_y = \sum_{n=N_x+1}^{N_x+N_y} I_n Z_{mn}$$

where, Z_{mn} = is from equation 2.48b

$$R_m = |y_m - y|$$

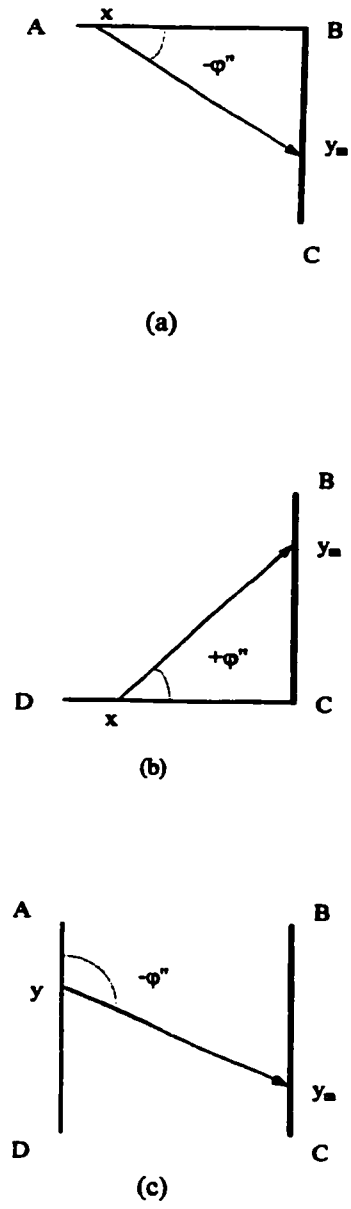

Figure 3.33 : Scattered fields on BC due to other cylinder segments

$$\varphi'' = 0, \quad \cos(2\varphi'') = 1$$

d) From CD (refer to Figure 3.33b):

$$E^s_{tan} = E^s_y = \sum_{n=Nx+Ny+1}^{2Nx+Ny} I_n Z_{mn}$$

where Z_{mn} = is from equation 3.47b

$$R_m = \sqrt{\left(\frac{wx}{2} - x\right)^2 + \left(\frac{wy}{2} + y_m\right)^2}$$

$$\sin(2\varphi'') = 2\sin(\varphi'')\cos(\varphi'') = 2\left(\frac{\frac{wy}{2} + y_m}{R_m}\right)\left(\frac{\frac{wx}{2} - x}{R_m}\right)$$

e) From DA (refer to Figure 3.33c):

$$E^s_{tan} = E^s_y = \sum_{n=2Nx+Ny+1}^{2Nx+2Ny} I_n Z_{mn}$$

where Z_{mn} = is from equation 3.48b)

$$R_m = \sqrt{(wx)^2 + (y_m - y)^2}$$

$$\cos(2\varphi'') = -1 + 2\cos^2(\varphi'') = -1 + 2\left(\frac{y_m - y}{R_m}\right)^2$$

3.5.5 Total Tangential Electric Field on CD

A point m on CD has coordinates $\left(x_m, \frac{-wy}{2}\right)$

a) incident field:

$$E^i_{tan} = E^i_x = \eta \times \sin\varphi' \times e^{-jk\left(-x_m \cos\varphi' + \frac{wy}{2}\sin\varphi'\right)}$$

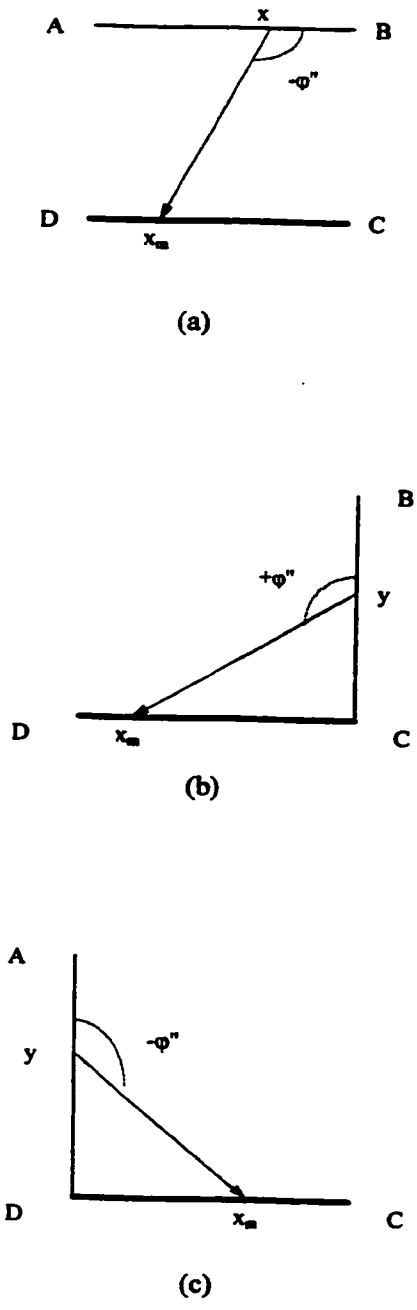

Figure 3.34 : Scattered fields on CD due to other cylinder segments

b) From AB (refer to Figure 3.34a):

$$E^s_{tan} = E^s_x = \sum_{n=1}^{N_x} I_n Z_{mn}$$

where Z_{mn} = is from equation 3.47a

$$R_m = \sqrt{(x_m - x)^2 + (wy)^2}$$

$$\cos(2\varphi'') = -1 + 2\cos^2(\varphi'') = -1 + 2\left(\frac{x_m - x}{R_m}\right)^2$$

c) From BC (refer to Figure 3.34b):

$$E^s_{tan} = E^s_x = \sum_{n=N_x+1}^{N_x+N_y} I_n Z_{mn}$$

where, Z_{mn} = is from equation 3.48a

$$R_m = \sqrt{\left(x_m - \frac{wx}{2}\right)^2 + \left(y + \frac{wy}{2}\right)^2}$$

$$\sin(2\varphi'') = 2\sin(\varphi'')\cos(\varphi'') = -2\left(\frac{\frac{wx}{2} - x_m}{R_m}\right)\left(\frac{\frac{wy}{2} + y}{R_m}\right)$$

d) From CD :

$$E^s_{tan} = E^s_x = \sum_{n=N_x+N_y+1}^{2N_x+N_y} I_n Z_{mn}$$

where, Z_{mn} = is from equation 3.47a

$$R_m = |x_m - x|$$

$$\cos(2\varphi'') = 1, \quad \varphi'' = 0$$

e) From AD (refer to Figure 3.34c):

$$E^s_{\tan} = E^s_x = \sum_{n=2N_x+N_y+1}^{2N_x+2N_y} I_n Z_{mn}$$

where, Z_{mn} = is from equation 3.48a

$$R_m = \sqrt{\left(x_m + \frac{wx}{2}\right)^2 + \left(y + \frac{wy}{2}\right)^2}$$

$$\sin(2\varphi'') = 2\sin(\varphi'')\cos(\varphi'') = -2\left(\frac{\frac{wy}{2} + y}{R_m}\right)\left(\frac{\frac{wx}{2} + x_m}{R_m}\right)$$

3.5.6 Total Tangential Electric Field on DA

A point m on DA has coordinate $\left(\frac{-wx}{2}, y_m\right)$

a) Incident field:

$$E^i_{\tan} = E^i_y = -\eta \times \cos\varphi' \times e^{-jk\left(+\frac{wx}{2}\cos\varphi' - ym\sin\varphi'\right)}$$

b) From AB (refer to Figure 3.35a):

$$E^s_{\tan} = E^s_y = \sum_{n=1}^{N_x} I_n Z_{mn}$$

where, Z_{mn} = is from equation 3.47b)

$$R_m = \sqrt{\left(x_m + \frac{wx}{2}\right)^2 + \left(y - \frac{wy}{2}\right)^2}$$

$$\sin(2\varphi'') = 2\sin(\varphi'')\cos(\varphi'') = 2\left(\frac{\frac{wy}{2} - y_m}{R_m}\right)\left(\frac{\frac{wx}{2} + x}{R_m}\right)$$

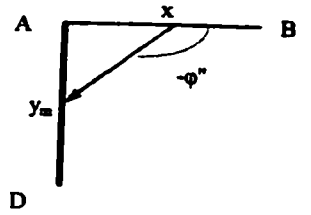

(a)

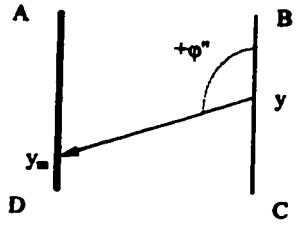

(b)

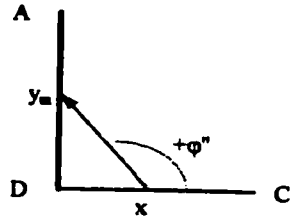

(c)

Figure 3.35: Scattered fields on DA due to other cylinder segments

c) From BC (refer to Figure 3.35b):

$$E_{tan}^{s} = E_{y}^{s} = \sum_{n=N_{y+1}}^{N_{x+Ny}} I_n Z_{mn}$$

where, Z_{mn} = is from equation 3.48b

$$R_m = \sqrt{(wx)^2 + (y_m - y)^2}$$

$$\cos(2\varphi'') = -1 + 2\cos^2(\varphi'') = -1 + 2\left(\frac{y_m - y}{R_m}\right)^2$$

d) From CD (refer to Figure 3.35b):

$$E_{tan}^{s} = E_{y}^{s} = \sum_{n=Ny+N_{y+1}}^{2N_{x+Ny}} I_n Z_{mn}$$

where, Z_{mn} = is from equation 3.47b

$$R_m = \sqrt{\left(x + \frac{wx}{2}\right)^2 + \left(y_m + \frac{wy}{2}\right)^2}$$

$$\sin(2\varphi'') = 2\sin(\varphi'')\cos(\varphi'') = -2\left(\frac{\frac{wy}{2} + y_m}{R_m}\right)\left(\frac{\frac{wx}{2} + x}{R_m}\right)$$

e) From DA:

$$E_{tan}^{s} = E_{y}^{s} = \sum_{n=2Ny+N_{y+1}}^{2N_{x+2Ny}} I_n Z_{mn}$$

where, Z_{mn} = is from equation 3.48b

$$R_m = |y_m - y|$$

$$\varphi'' = 0, \quad \cos(2\varphi'') = 1$$

3.5.7 EFIE and the Moment Method

The EFIE can be written as:

$$V_m = Z_{mn} I_n \qquad \begin{matrix} n=1,2...N \\ m=1,2...N \end{matrix} \qquad (3.50)$$

where,

V_m = E^i_{tan} at a certain point m

Z_{mn} = the impedance term from a sub segment n to a point m.

I_n = Current at sub segment n.

N = Nx + Ny + Nx + Ny = 2Nx + 2Ny

Nx = number of segments for each AB and CD

Ny = number of segments for each BC and DA

Additionally the subscript m or n indicates that the observer or the source respectively is present at:

AB if $1 \leq m$ or $n \leq Nx$

BC if $Nx + 1 \leq m$ or $n \leq Nx + Ny$

CD if $Nx + Ny + 1 \leq m$ or $n \leq 2Nx + Ny$

DA if $2Nx + Ny + 1 \leq m$ or $n \leq 2Nx + 2Ny$

Equation 3.50 represents the pulse basis / point matching case of the moment method solution of the EFIE.

3.5.8 Code and Results

Computer Code PBOX.FOR was created based on the formulations of the previous sections. The code computes the Z_{mn} terms (except the self term) by numerical integration of each sub segment n along its width Δ using Simpson's rule. The results were plotted in section 3.4 for comparison with UTD plots.

4 SCATTERING - TMz CASE

4.1 EDGE SURFACE CURRENT USING UTD

Obtaining the surface current on an infinite wedge illuminated by a TMz plane wave (refer to Figure 2.1) requires the total tangential magnetic field on the surface of the wedge. Equation 2.1 and 2.3 gives the total and the diffracted electric fields respectively. The magnetic field needs to be derived from the electric field in this case.

From Maxwell's equations:

$$\nabla \times \vec{E} = -j\omega\mu\vec{H}$$

Since E has a z component only,

$$\frac{1}{\rho}\frac{\partial E_z}{\partial \varphi}\cdot\hat{a}_\rho - \frac{\partial E_z}{\partial \rho}\cdot\hat{a}_\varphi = -j\omega\mu\vec{H}$$

then, the tangential magnetic field to the surface is

$$\vec{H}_{\tan} = \vec{H}_\rho = \frac{j}{k\eta}\frac{1}{\rho}\frac{\partial E_z}{\partial \varphi}\cdot\hat{a}_\rho \qquad (4.1)$$

4.1.1 Incident and Reflected Magnetic Tangential Fields

A TMz incident plane wave with unit magnitude electric field at the edge of the wedge is assumed. It is assumed also that φ' varies between 0° and $n\pi/2$, all other cases being able to be deduced by symmetry. Each face of the wedge will be treated separately here.

a) '0' face fields:

$\varphi=0°$

$$E_z^i = e^{jk\rho\cos(\varphi-\varphi')}$$

$$E_z^r = -e^{jk\rho\cos(\varphi+\varphi')}$$

from equation 4.1,

$$H_\rho^i = \frac{1}{\eta}\sin(\varphi-\varphi')e^{jk\rho\cos(\varphi-\varphi')} = -\frac{1}{\eta}\sin(\varphi')e^{jk\rho\cos(\varphi')} \quad (4.2a)$$

$$H_\rho^r = \frac{1}{\eta}\sin(\varphi+\varphi')e^{jk\rho\cos(\varphi+\varphi')} = -\frac{1}{\eta}\sin(\varphi')e^{jk\rho\cos(\varphi')} \quad (4.2b)$$

b) 'n' face fields:

Let's define: $\psi = n\pi - \varphi$ *and* $\psi' = n\pi - \varphi'$

With variables ψ *and* ψ' the 'n' face become the '0' face and vice versa

$$E_z^i = U(\varphi'-(n-1)\pi)\times e^{jk\rho\cos(\psi-\psi')}$$

$$E_z^r = U(\varphi'-(n-1)\pi)\times e^{jk\rho\cos(\psi+\psi')}$$

from equation 4.1 we have (since $\partial\varphi = -\partial\psi$),

$$H_\rho^i = U(\varphi'-(n-1)\pi)\times\frac{1}{\eta}\sin(\psi-\psi')\times e^{jk\rho\cos(\psi-\psi')} \quad (4.3\ a)$$

$$H_\rho^r = -U(\varphi'-(n-1)\pi)\times\frac{1}{\eta}\sin(\psi+\psi')\times e^{jk\rho\cos(\psi+\psi')} \quad (4.3\ b)$$

4.1.2 Diffracted field

From equations 2.3 and 4.1

$$H_\rho^d = \frac{j}{k\eta}\frac{1}{\rho}\times E_z^i(Q_E)\times\frac{e^{-jk\rho}}{\sqrt{\rho}}\times\frac{\partial D_s(\rho,\rho,\varphi,\varphi',n)}{\partial\varphi} \quad (4.4)$$

where $\varphi = 0°$ for the 'o'face and $\varphi = n\pi$ for the 'n' face

Equation 4.4 can be evaluated if $\frac{\partial D_s}{\partial \varphi}$ is known. A practical way to compute it is by using the already existing method and subroutine for the slope diffraction coefficient. Both are not totally equivalent and one should be derived from the other as it will be explained below.

a) Slope diffraction

In chapter 2, formulas for UTD were introduced. As stated in equation 2.3 and 2.4, the diffracted field depends on the incident field at the edge. According to this formula, the diffracted field will be zero if the incident field at the edge is zero also. There are some instances where this situation occurs (zero incident field) at the edge itself only and the incident field is not zero nearby.

This situation is dealt with by introducing a higher order diffraction dependent not on the magnitude of the incident field but rather on its rate of change (slope). The diffracted field due to slope diffraction is represented by an equation similar to equations 2.3 and 2.4 but the incident field term is replaced by its derivative (rate of change) relatively to the normal and $D_{s,h}$ is replaced by $\frac{\partial D_{s,h}}{\partial \varphi'}$.

The majority of existing codes dealing with diffraction coefficients, have also subroutine for the slope diffraction coefficient.

Evaluation of slope diffraction is not in the scope of this work but it will be shown below how to use $\frac{\partial D_s}{\partial \varphi'}$ to get $\frac{\partial D_s}{\partial \varphi}$ with an easy manipulation.

b) Derivative of D_s with respect to φ instead φ'

The slope diffraction coefficient formulation can be found easily in the literature[2][[23][24].

The interest here, however is to use the output of a subroutine for this coefficient and to transform it into $\frac{\partial D_s}{\partial \varphi}$.

Since the slope diffraction coefficient is $\frac{\partial D_s}{\partial \varphi'}$, where D_s is given by equation 2.5, the main goal is to derive each term between the brackets in equation 2.5 with respect to φ'.

If we define $\beta^- = \varphi - \varphi'$ and $\beta^+ = \varphi + \varphi'$, the term to be evaluated is,

$$\frac{\partial}{\partial \beta}\left(\cot\left(\frac{\pi \pm \beta}{2n}\right)F\left(kLa^{\pm}(\beta)\right)\right)$$

Now since $\frac{\partial \beta^-}{\partial \varphi'} = -1$ and $\frac{\partial \beta^+}{\partial \varphi'} = 1$,

once evaluated, the terms derived with respect to β^- need to be multiplied by –1 to obtain the derivative with respect to φ'. Since the diffraction coefficient has the general form of: $D_s = K \times \left(D_1 + D_2 - \left(D_3 + D_4\right)\right)$ where the first two D terms only include β^-.

If we define $\frac{\partial D_n}{\partial \beta^{\pm}} = d_n$, then

$$\frac{\partial D_s}{\partial \varphi'} = K \times \left(-d_1 - d_2 - \left(d_3 + d_4\right)\right) \qquad (4.5)$$

To obtain the derivative with respect to φ and Since $\frac{\partial \beta^-}{\partial \varphi} = +1$ and $\frac{\partial \beta^+}{\partial \varphi} = +1$

Then $$\frac{\partial D_s}{\partial \varphi} = Kern \times = \left(d_1 + d_2 - \left(d_3 + d_4\right)\right) \tag{4.6}$$

Usually subroutines will give the result of the slope diffraction as an array of d_n. It is easy to multiply the relevant terms with a minus sign to get equation 4.6 from equation 4.5 to evaluate finally equation 4.4.

The incident, reflected and diffracted tangential magnetic fields have been formulated, the surface current on the wedge can be obtained, from

$$\begin{aligned} &\vec{J}_z = \hat{n} \times \vec{H} \\ &\Rightarrow \ |J_z| = |H_\rho| \end{aligned} \tag{4.7}$$

4.1.3 Code and Results

Computer Code EEDGE.FOR was created based on the preceding formulation using the modified slope diffraction coefficient.

Figures 4.1 and 4.2 show the surface current density distribution on the '0' face and 'n' face of a half plane and a 90° wedge respectively, illuminated by a TMz plane wave (with a unit magnitude electric field at the edge) at 90° incidence. Note that in Figure 4.2, physical optics predicts $|J_z| = 2/\eta \cong 0.0053\ A/m$. Figure 4.3 shows both current curves superimposed because the illumination (incidence 135°) is symmetrical on the edge (n=1.5). Figure 4.4 shows the case of the half plane with almost grazing incidence (0.05°), as expected the current magnitude is low.

In all Figures (4.1 to 4.4), the current at the edge seems to go singular and unbounded. This is a known [6] singularity for the TMz case. Since the UTD code using the slope diffraction coefficient subroutine is used for the first time in this work, an independent check was considered preferable. Figure 4.5 shows the current distribution for the same case as in Figure 4.1 but the method used to produce it is based on the modal solution computed by a fractional order

Bessel functions subroutine[25]. Figures 4.1 and 4.5 are identical even at the edge.

Meixner [6] has studied this singularity for the TMz case and has introduced a suitable condition to make sure the solution is unique. Meixner's edge condition requires the energy density to be integrable at the edge. Figure 4.6 shows the current density (representing only H_{tan}) multiplied by $\sqrt{\rho}$ for the case of Figure 4.1, the value converges and is finite near the edge.

The code EEDGE.FOR is considered adequate for the present evaluation and its formulation will be used as a building block for the solution of more complex shapes in the next sections.

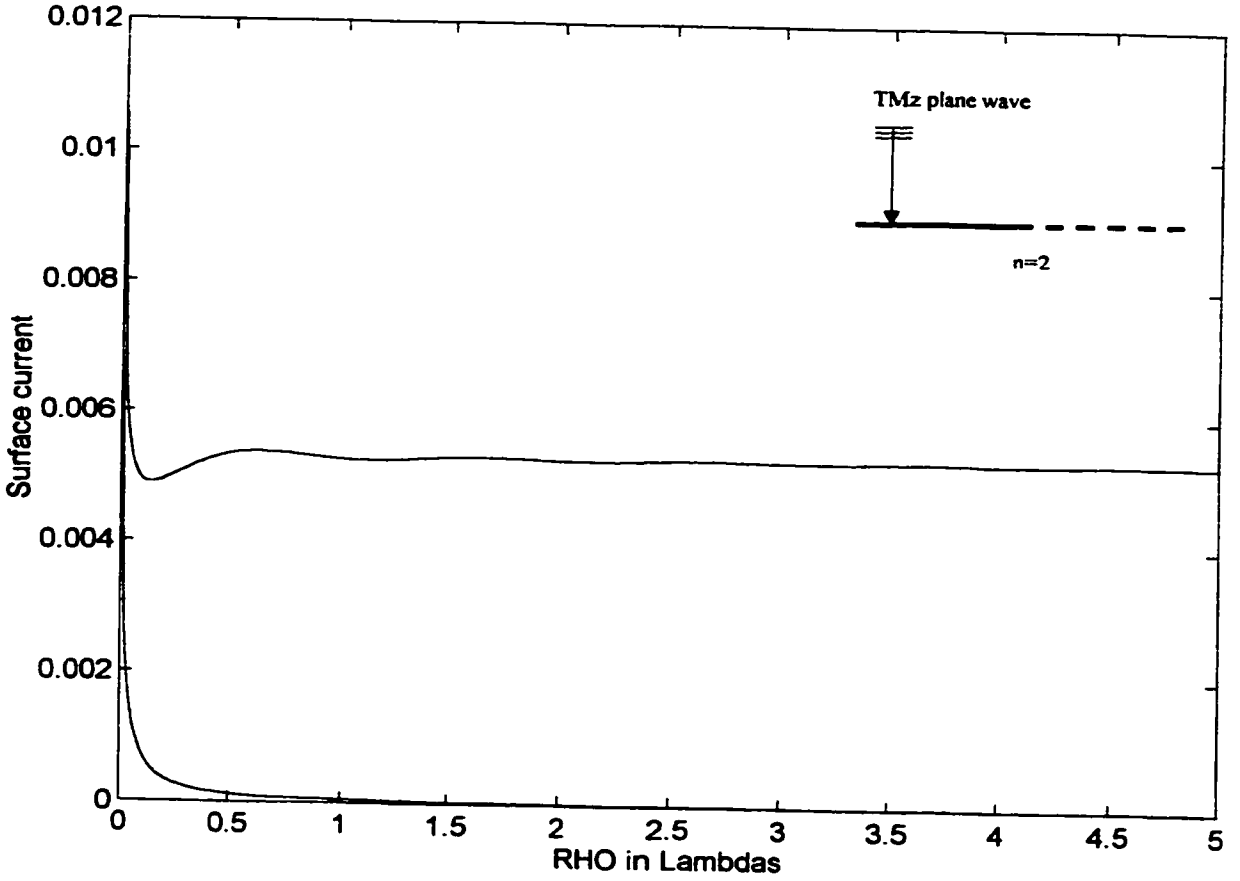

Figure 4.1: Magnitude of current distribution on the surface of a half plane (n=2) illuminated by a TMz plane wave at $\varphi' = 90°$ (J in A/m, ρ in λ)-UTD.

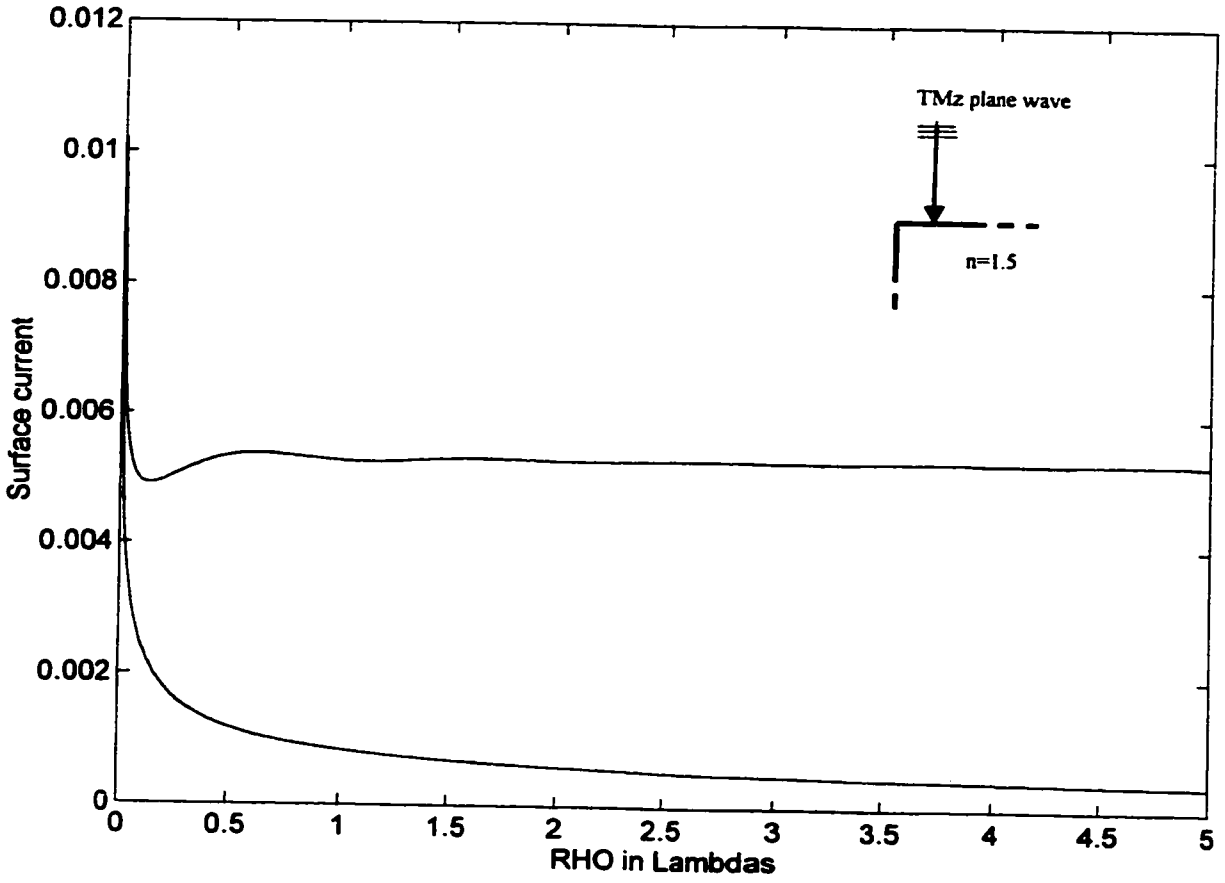

Figure 4.2: Magnitude of current distribution on the surface of a straight edge (n=1.5) illuminated by a TMz plane wave at $\varphi' = 90°$ (J in A/m,ρ in λ.)-UTD.

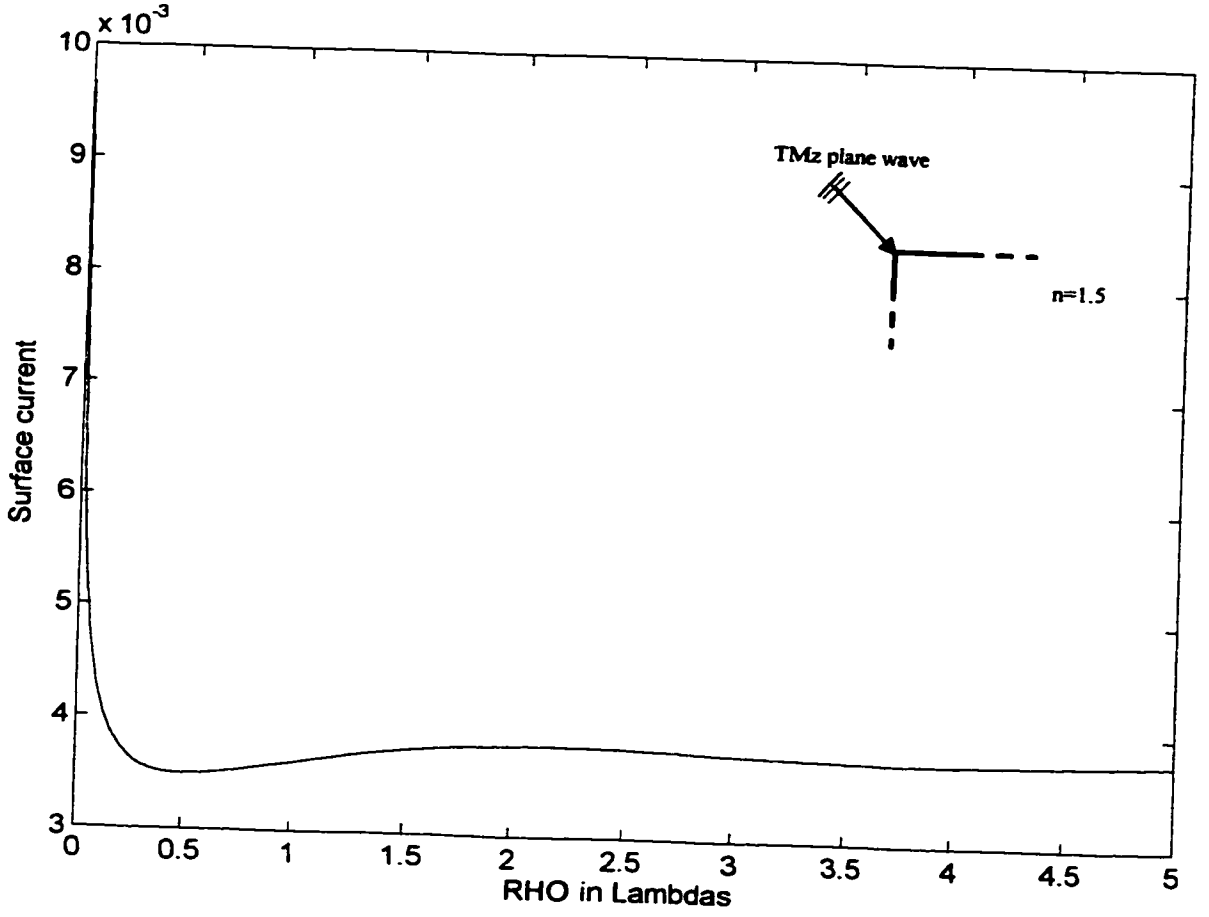

Figure 4.3: Magnitude of current distribution on the surface of a straight edge (n=1.5) illuminated by a TMz plane wave at $\varphi' = 135°$ (J in A/m.ρ in λ.)-UTD.

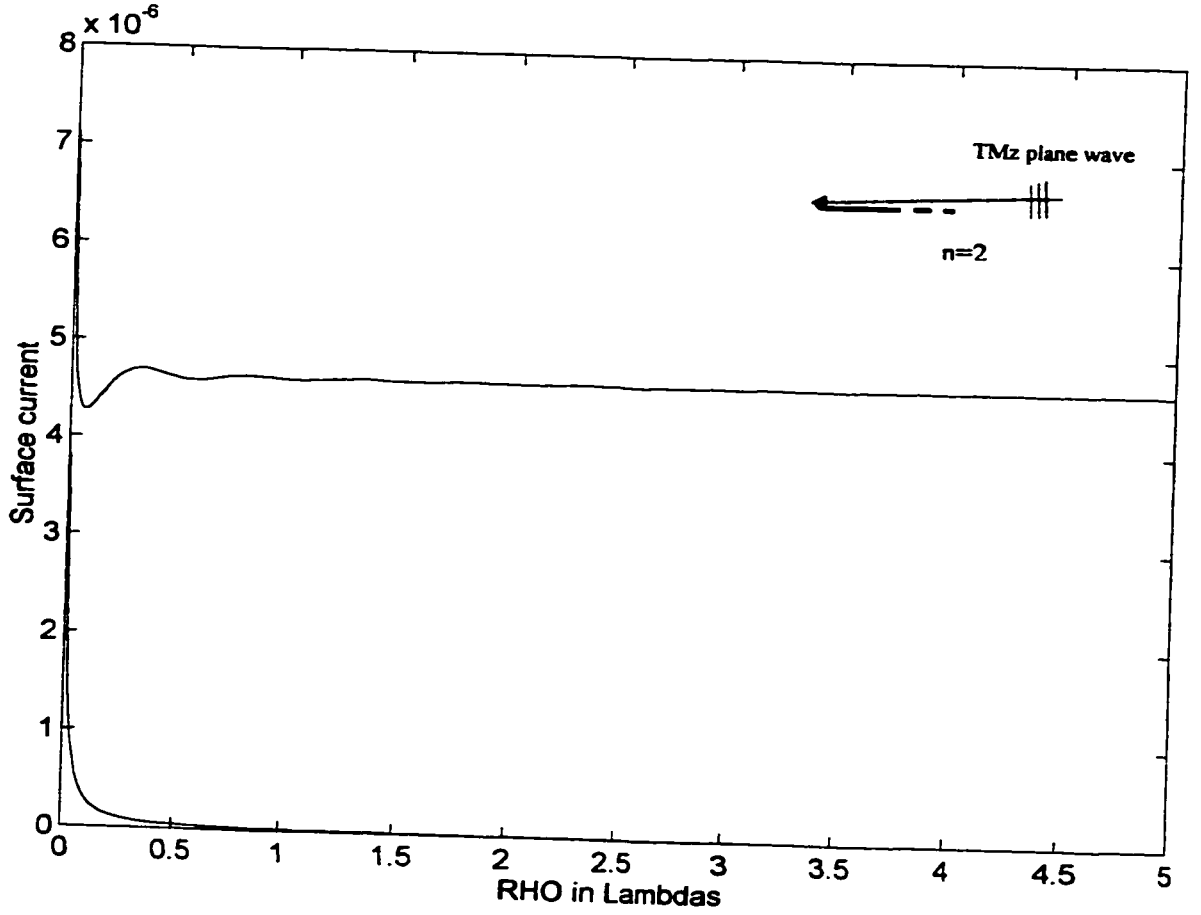

Figure 4.4: Magnitude of current distribution on the surface of a half plane illuminated by a TMz plane wave at almost grazing incidence $\varphi'=0.05^{\circ}$ (J in A/m, ρ in λ.)- (UTD).

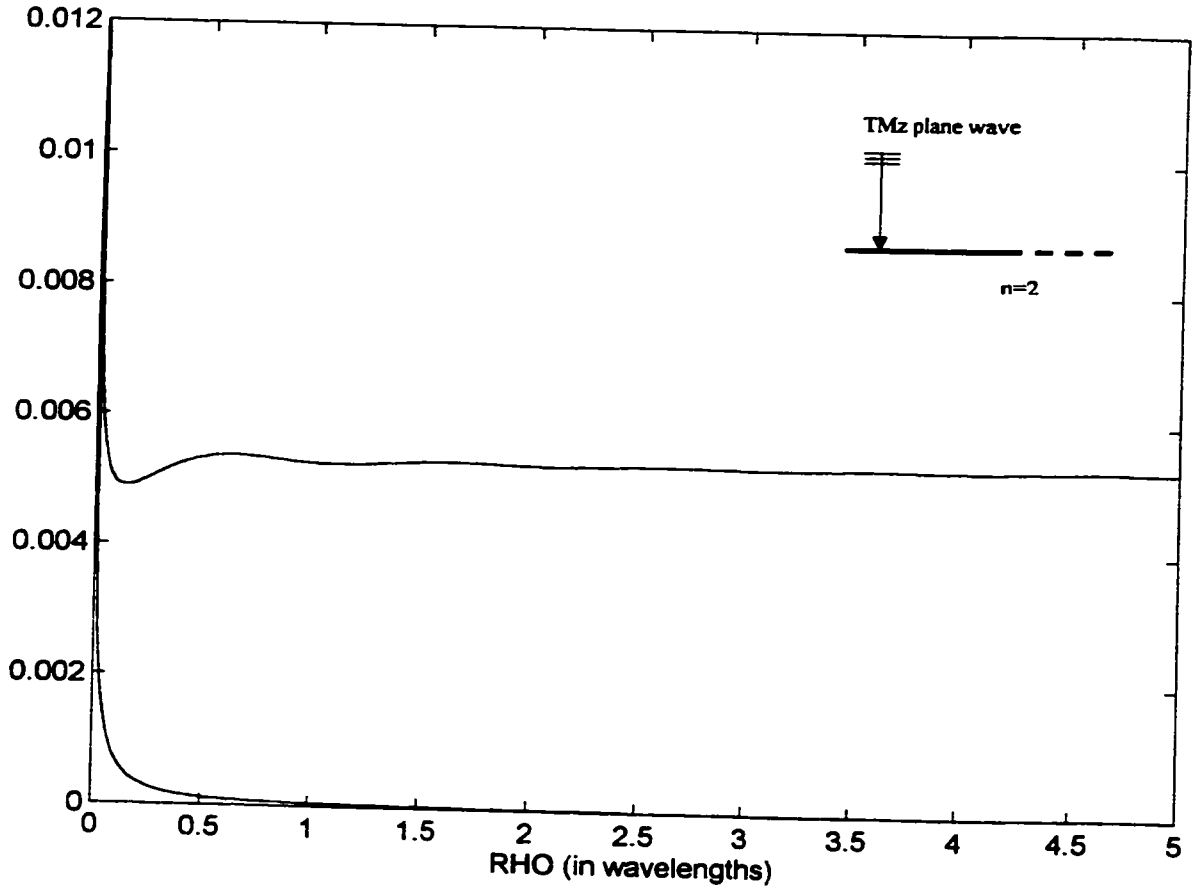

Figure 4.5: Magnitude of current density distribution on the surface of a half plane illuminated by a TMz plane wave at $\varphi' = 90°$ (J in A/m, ρ in λ)-Modal solution using fractional Bessel functions.

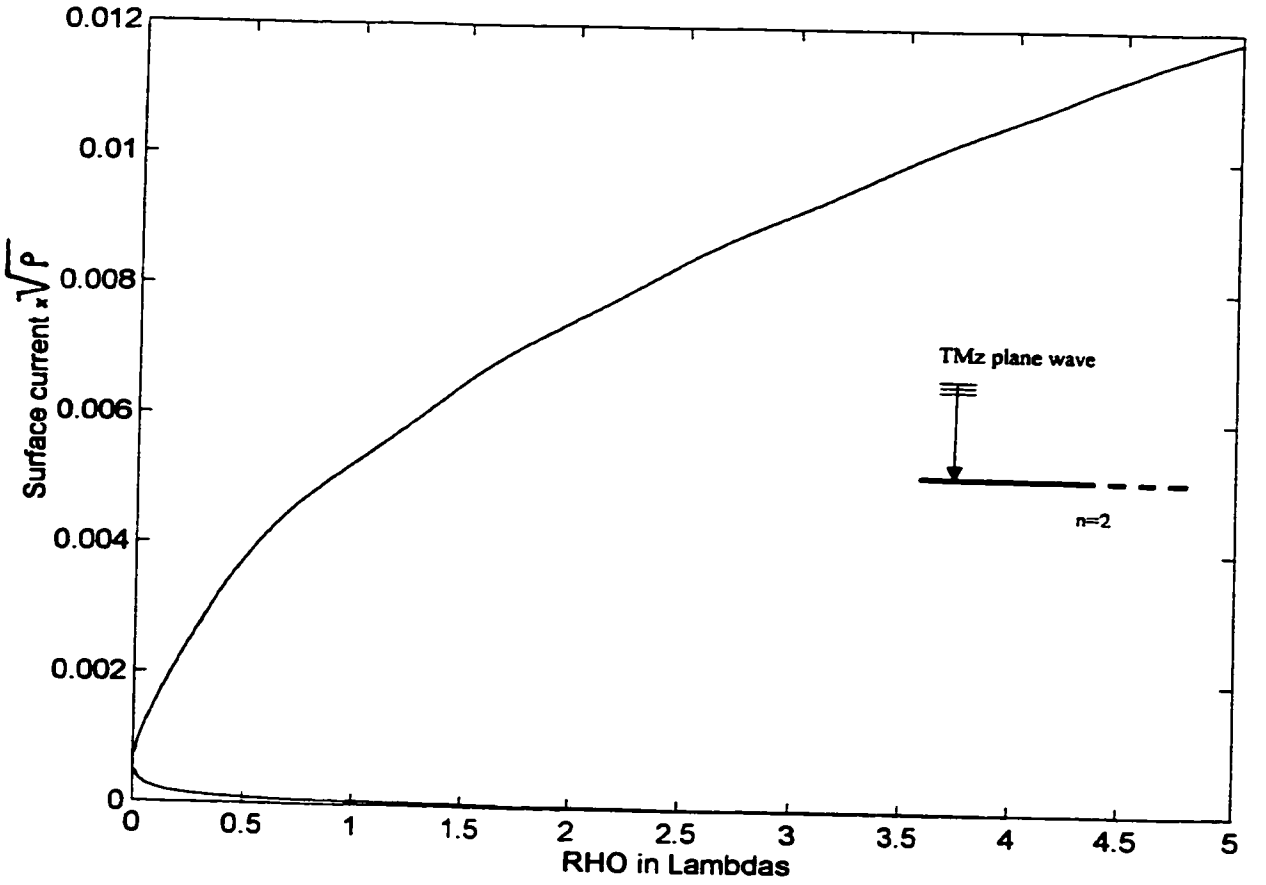

Figure 4.6: Magnitude of current density (J in A/m) multiplied by $\sqrt{\rho}$ along the surface of a half plane illuminated by a TMz plane wave at $\varphi' = 90°$ (ρ in λ)-.

4.2 STRIP SURFACE CURRENT USING UTD

4.2.1 Formulation

The same case of section 3.2.1 will be taken here with the incident wave being a TMz plane wave (refer to Figure 3.8). The incident wave has a unit magnitude electric field at edge A (the origin). The solution considers the present geometry as a combination of two edges, one at A and the other at B. Both edge contributions will be taken into consideration to get the diffracted field to be added to the GO field. All of this however is to get the total electric field. To obtain the surface current on the strip, the tangential magnetic field is needed. Using Maxwell's equation H_{tan} will be derived from E_z (TMz case):

$$\nabla \times \vec{E} = -j\omega\mu\vec{H}$$

Since E has a z component only,

$$\frac{1}{\rho}\frac{\partial E_z}{\partial \varphi}\cdot\hat{a}_\rho - \frac{\partial E_z}{\partial \rho}\cdot\hat{a}_\varphi = -j\omega\mu\vec{H}$$

then, the tangential magnetic field to the surface is

$$\vec{H}_{\tan} = \vec{H}_\rho = \frac{j}{k\eta}\frac{1}{\rho}\frac{\partial E_z}{\partial \varphi}\cdot\hat{a}_\rho \tag{4.8}$$

a) GO fields

-on the lit side:

$$E_z^i = e^{jk\rho\cos(\varphi-\varphi')}$$

$$E_z^r = -e^{jk\rho\cos(\varphi+\varphi')}$$

from equation 4.8,

$$H_\rho^i = \frac{1}{\eta}\sin(\varphi-\varphi')e^{jk\rho\cos(\varphi-\varphi')} \tag{4.9}$$

$$H_\rho^r = -\frac{1}{\eta}\sin(\varphi+\varphi')e^{jk\rho\cos(\varphi+\varphi')} \tag{4.10}$$

-On the shadow side:

$H^i = H^r = 0$ since $0° < \varphi' < 180°$

b) Diffracted fields

Since at A the field magnitude is unity, at B the incident field is:

$$E^i(Q_B) = e^{jkw\cos\varphi'}$$

-On the lit side:

from equation (2.3):

$$E_A^d = 1 \times \frac{e^{-jk\rho}}{\sqrt{\rho}} \times D_s(\rho, \rho, 0, \varphi', 2)$$

$$E_B^d = e^{jkw\cos\varphi'} \times \frac{e^{-jk(w-\rho)}}{\sqrt{(w-\rho)}} \times D_s(w-\rho, w-\rho, 2\pi, \pi+\varphi', 2)$$

then from equation 4.8, the diffracted tangential magnetic fields are (lit side):

$$H_A^d = \frac{j}{k\eta}\frac{1}{\rho} \times \frac{e^{-jk\rho}}{\sqrt{\rho}} \times \frac{\partial D_s(\rho, \rho, 0, \varphi', 2)}{\partial\varphi} \quad (4.11)$$

$$H_B^d = \frac{-j}{k\eta}\frac{1}{(w-\rho)} \times \frac{e^{jk(w\cos\varphi'-(w-\rho))}}{\sqrt{w-\rho}} \times \frac{\partial D_s(w-\rho, w-\rho, 2\pi, \pi+\varphi', 2)}{\partial\varphi} \quad (4.12)$$

-On the shadow side:

$$E_A^d = 1 \times \frac{e^{-jk\rho}}{\sqrt{\rho}} \times D_s(\rho, \rho, 2\pi, \varphi', 2)$$

$$E_B^d = e^{jkw\cos\varphi'} \times \frac{e^{-jk(w-\rho)}}{\sqrt{(w-\rho)}} \times D_s(w-\rho, w-\rho, 0, \pi+\varphi', 2)$$

then from equation 4.8, the diffracted tangential magnetic fields are (shadow side):

$$H_A^d = \frac{j}{k\eta}\frac{1}{\rho} \times \frac{e^{-jk\rho}}{\sqrt{\rho}} \times \frac{\partial D_s(\rho, \rho, 2\pi, \varphi', 2)}{\partial\varphi} \quad (4.13)$$

$$H_B^d = \frac{-j}{k\eta}\frac{1}{(w-\rho)} \times \frac{e^{jk(w\cos\varphi'-(w-\rho))}}{\sqrt{w-\rho}} \times \frac{\partial D_s(w-\rho, w-\rho, 0, \pi+\varphi', 2)}{\partial\varphi} \quad (4.14)$$

As shown in the previous section, computing $\frac{\partial D_s}{\partial\varphi}$ is a matter of multiplying two terms out of the four terms of the slope diffraction coefficient by a minus sign. It should be noted here that no multiple diffraction is considered in the present case, since the diffracted field is zero at the surface.

From equation 4.9 to 4.14, the total tangential magnetic field is

$$H_\rho^{Total} = H_\rho^i + H_\rho^r + H_A^d + H_B^d \quad (4.15)$$

and the current density can be evaluated from

$$\vec{J}_z = \hat{n} \times \vec{H}$$
$$\Rightarrow \quad |J_z| = |H_\rho| \quad (4.16)$$

4.2.2 Code and Results

A computer code TMzGTD1.FOR was created based on the formulation of section 4.2.1. It uses the modified slope diffraction coefficient subroutine to compute $\frac{\partial D_s}{\partial\varphi}$.

A large number of plots were produced to verify the code, only few will be included here. As an independent check with open literature, the code reproduced exactly Figure 12.15 in [2]. Results from the moment method solution described in section 4.3 are plotted (in small circles) also for comparison.

It is worth noting that multiple diffraction was not necessary to get a good result for the TMz case.

As for the plots included here they all represent the surface current density on a strip of different width illuminated by a TM_z plane wave at different angles of incidence:

Figure 4.7 shows the case of a strip width of 0.5λ and an angle of incidence of 90°. The results of both methods are identical and exhibit the same singularity at the edges.

Figure 4.8 is for a strip of width of 0.2λ with angle of incidence of 90°. The results of both methods are identical.

Figure 4.9 is for a strip of width of 0.2λ with angle of 0.5° (almost grazing). The results of both methods are very similar. They look alike at edge B and stay almost identical until 0.03 λ from edge A where the moment method values seems to go singular before the UTD ones. A large number of points were used on the strip (using UTD) and this showed that the curve also goes singular but much closer to the edge at A

Figure 4.10 is for a strip of width of 0.1λ with angle of incidence of 90°. The plots of both methods are almost identical in shape except that the UTD one gives slightly higher amplitudes (around 8%).

Figure 4.11 is for a strip of width of 0.1λ with angle of incidence of 10°. Both plots look alike at edge B and stay very similar up until 0.03λ from edge A where the moment method plot seems to go singular before the UTD plot. At A, the UTD plot goes singular also but much closer to the edge itself.

In general the UTD plots and Moment method plots are similar at low frequency with the singular behavior difference at the edge being incidence angle sensitive. It seems that the rate at which the singularity is reached drops tremendously with decreasing angle of incidence (near grazing) for the edge which is farther away from the source of the illumination. This could be explained

by the fact that the current density depends on a modified slope diffraction coefficient. A quick analysis of this modified coefficient (refer to sec 4.1.2) shows that it is equivalent to the normal diffraction coefficient with ϕ and ϕ' swapped. This means that with an illumination coming from the right side (almost at grazing incidence), the left edge diffraction contribution depends on the derivative of a coefficient with less variations unlike the opposite side which is at higher rate of change next to the boundaries. This again could be the cause of the leading term of the asymptotic solution not being the most prominent of all. It is however understood that this difference between UTD and moment method is on how to represent a singularity by itself and as long as these singularities are understood the final result could be acceptable.

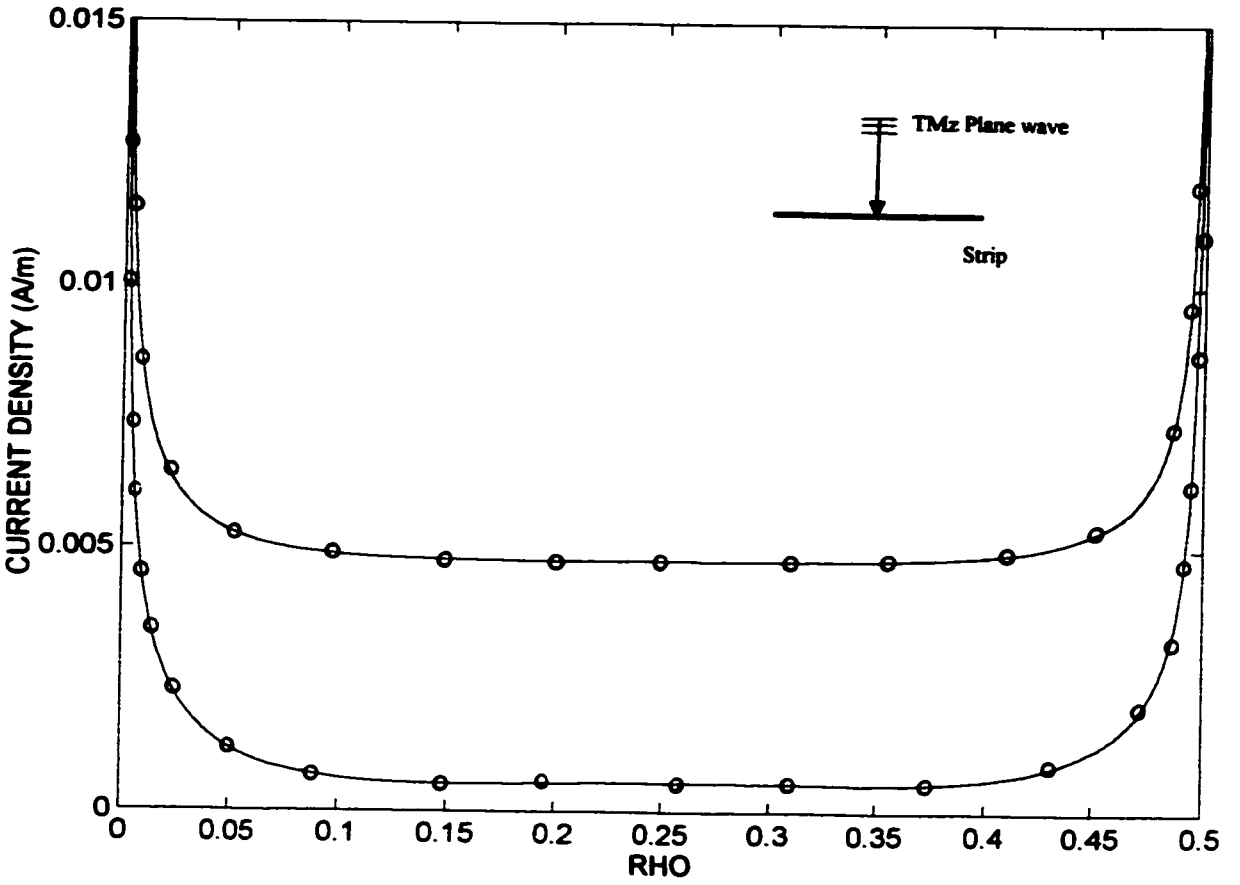

Fig. 4.7: Magnitude of current density distribution on the surface of a strip (w=0.5λ) illuminated by a TMz plane wave incident at φ^{i} =90 ° (J in A/m, ρ in λ). [— UTD, ooo MM]

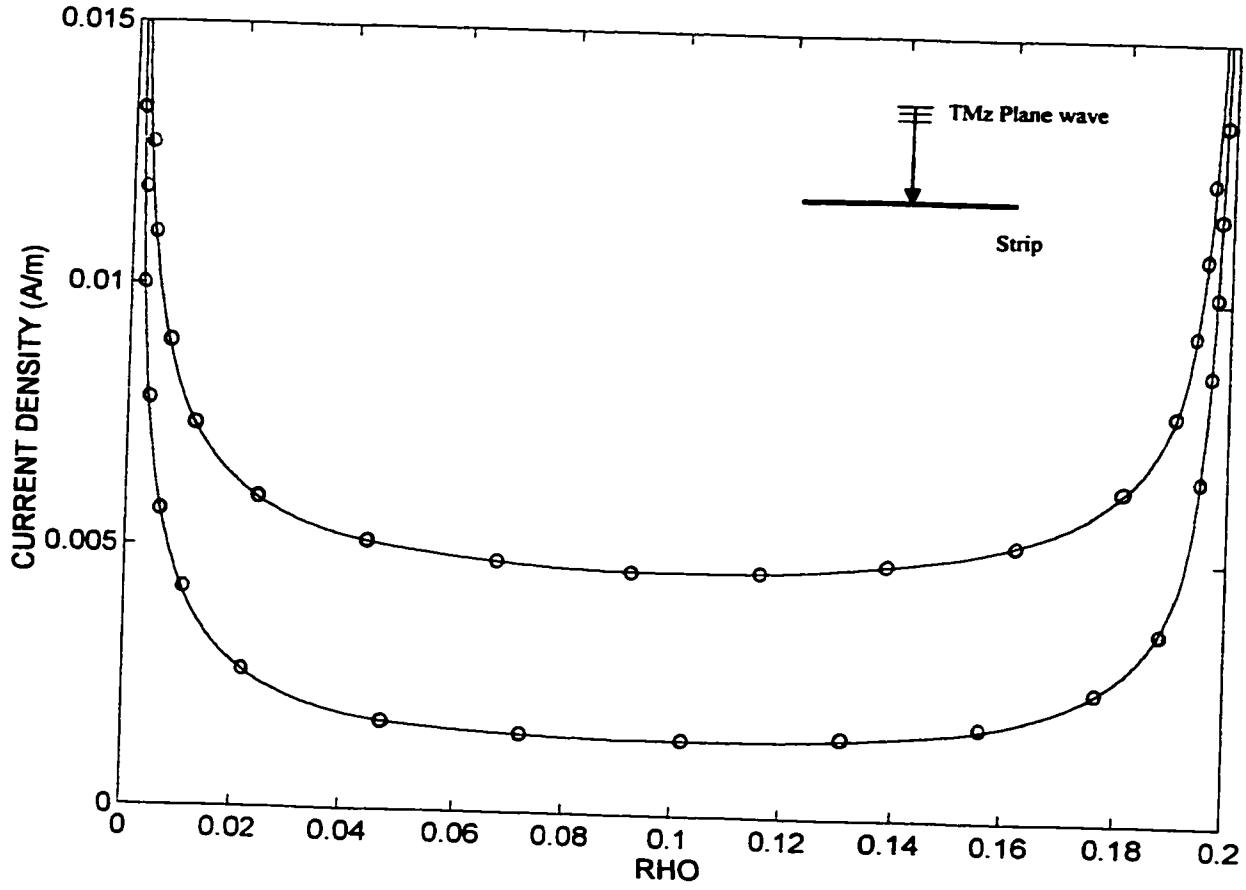

Fig. 4.8: Magnitude of current density distribution on the surface of a strip (w=0.2λ) illuminated by a TMz plane wave incident at φ' =90 ° (J in A/m,ρ in λ). [— UTD. ooo MM]

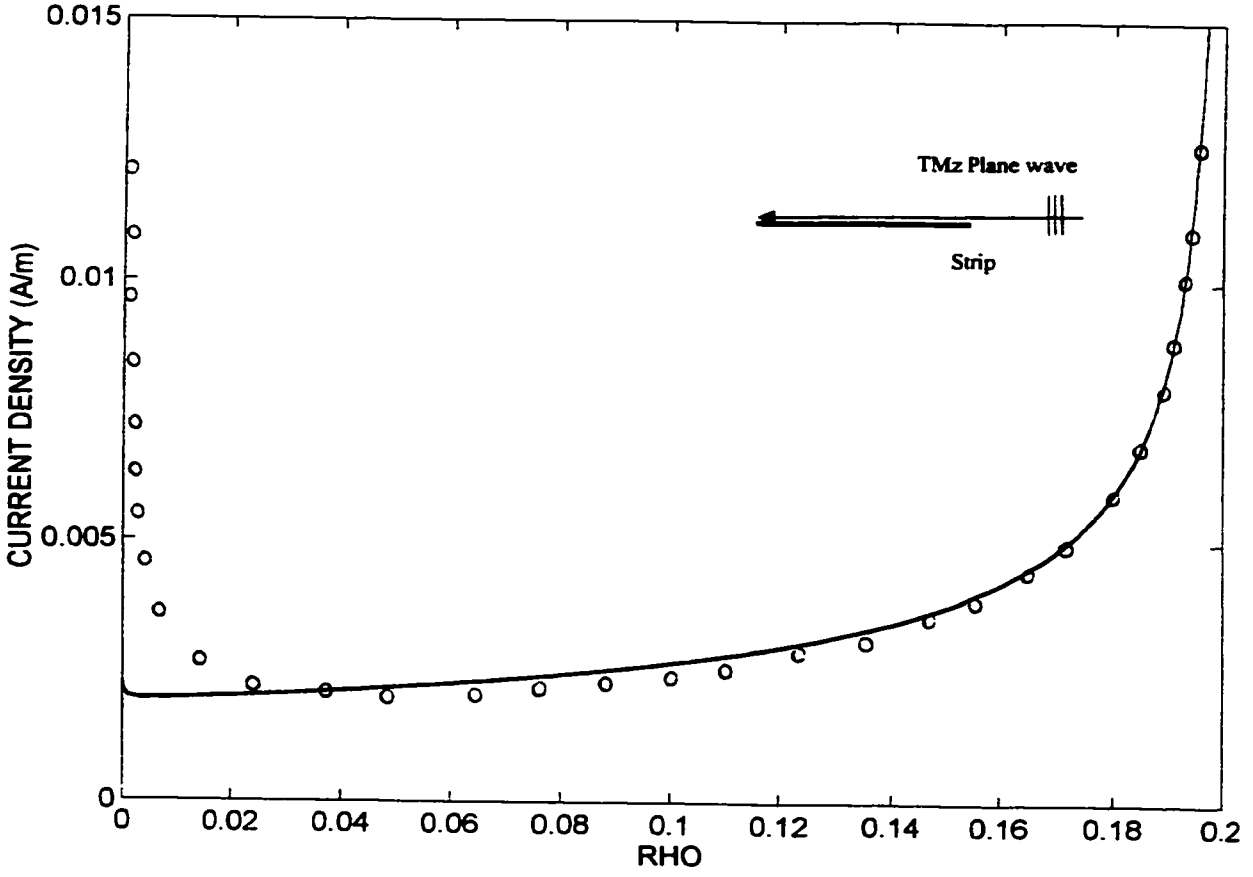

Fig. 4.9: Magnitude of current density distribution on the surface of a strip (w=0.2λ) illuminated by a TMz plane wave incident at $\varphi' = 0.5°$ (J in A/m, ρ in λ). [— UTD, ooo MM]

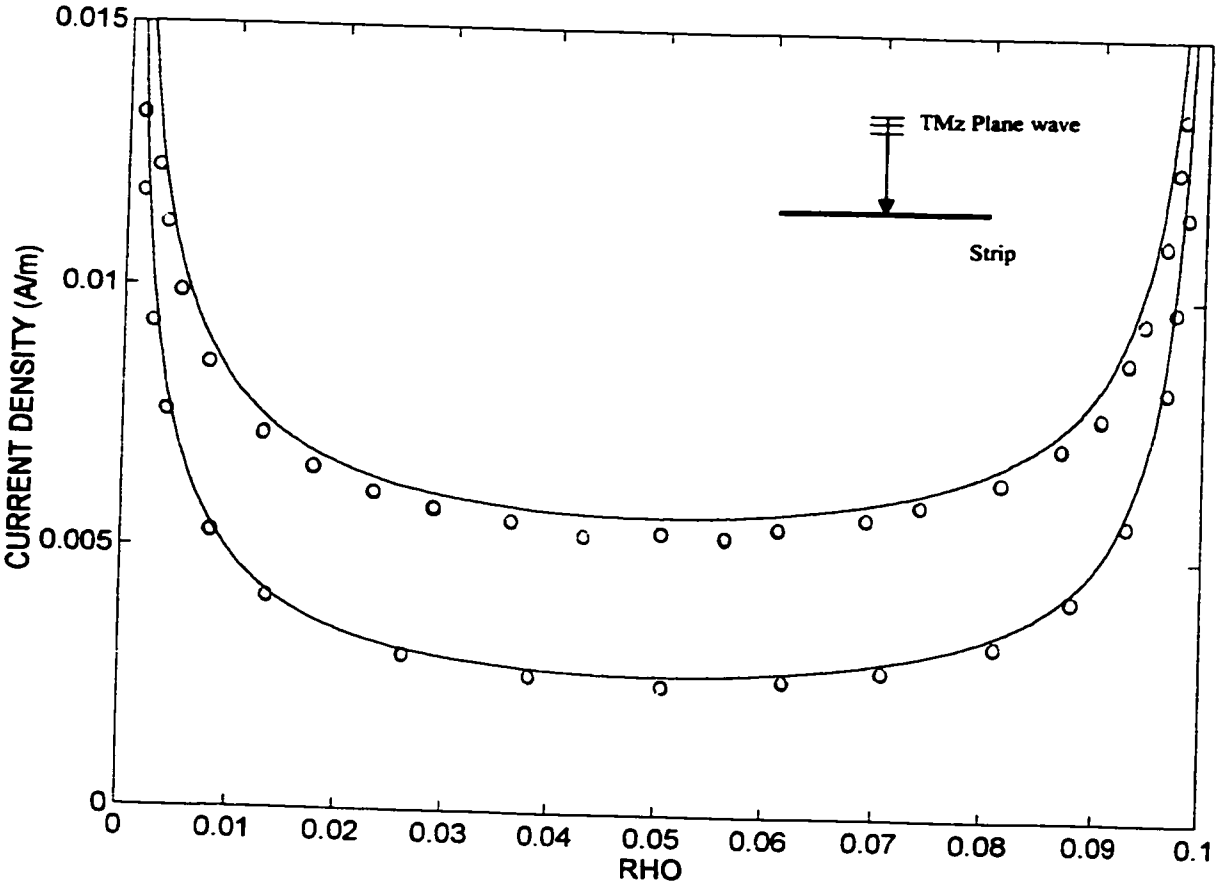

Fig. 4.10: Magnitude of current density distribution on the surface of a strip (w=0.1λ) illuminated by a TMz plane wave incident at φ^{i} =90 ° (J in A/m, ρ in λ). [— UTD, ooo MM]

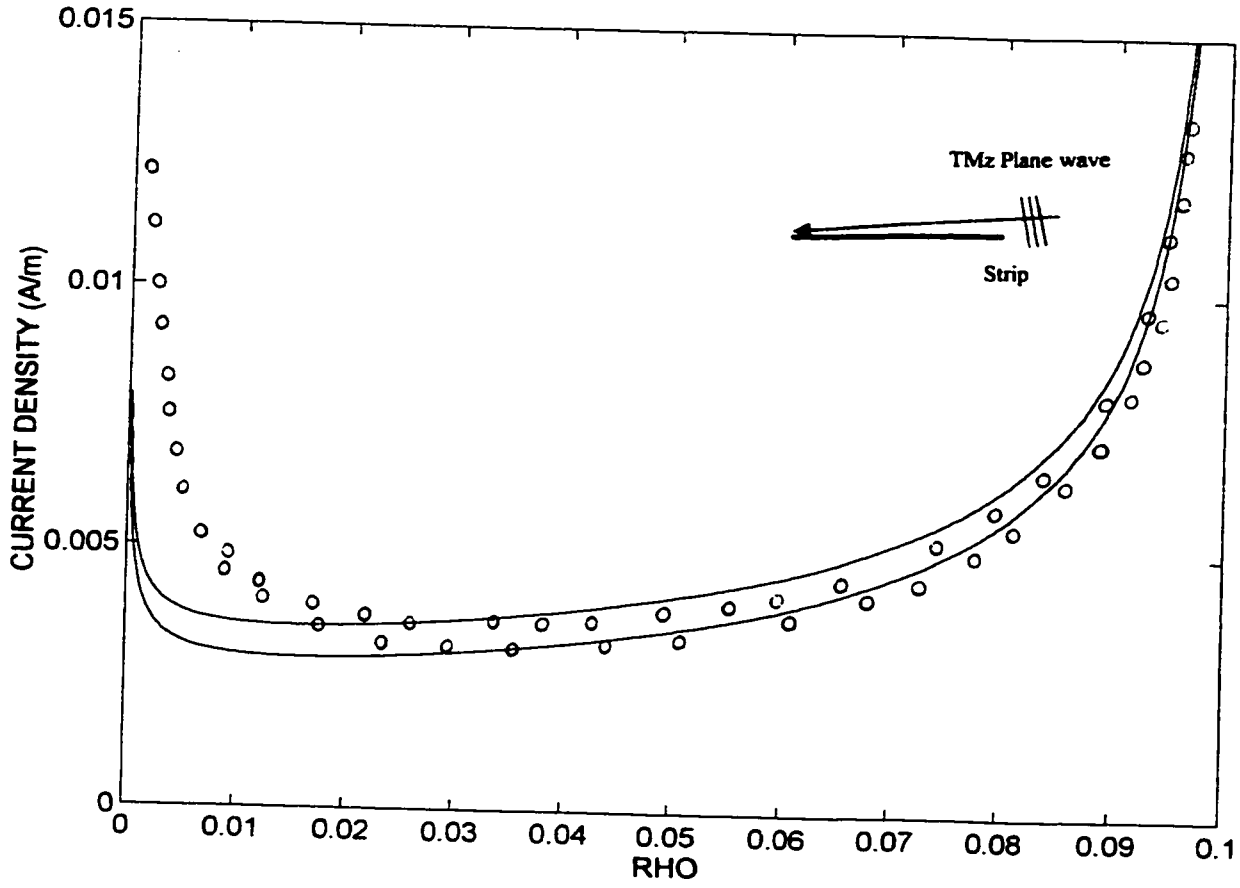

Fig. 4.11: Magnitude of current density distribution on the surface of a strip (w=0.1λ) illuminated by a TMz plane wave incident at φ' =10 ° (J in A/m, ρ in λ).[— UTD. ooo MM]

4.3 STRIP SURFACE CURRENT USING THE MOMENT METHOD

4.3.1 EFIE Formulation

The incident electric field on the strip (refer to fig. 3.8) illuminated by a TMz plane wave is :

$$E^i = E_z^i = e^{jk\rho\cos(\varphi-\varphi')}$$

this field is tangent to the strip since it is the TMz case. The current induced on the strip also has only a z component.

The scattered field is produced by the current J_z on the strip. From equation (2.17) and at a certain point m on the strip

$$-E^s(\vec{\rho}_m) = E_z^i(\vec{\rho}_m) = \frac{k\eta}{4}\int_0^w J_z(\rho)H_0^{(2)}(|\vec{\rho}_m - \vec{\rho}|)d\rho \qquad (4.17)$$

If the current is represented by $J(\rho) \cong \sum_{n=1}^{N} I_n g_n(\rho)$ and we take g_n to be a pulse function equal to unity on segment n and zero elsewhere, then equation 2.17 can be written as:

$$-E^s(\vec{\rho}_m) = E_z^i(\vec{\rho}_m) = \frac{k\eta}{4}\sum_{n=1}^{N} I_n \int_{\rho_n}^{\rho_n+1} H_0^{(2)}(|\vec{\rho}_m - \vec{\rho}|)d\rho \qquad (4.18)$$

4.3.2 Moment Method Formulation

Since pulse basis functions and point matching is used here, equation 4.18 can be repeated for several points m. If we subdivide the strip into N segments with width $\Delta = \frac{w}{N}$ and we apply equation 4.18 once to the mid point of each segment, we can write

$[V_m]=[Z_{mn}][I_n]$ (4.19)

where, m and n = 1,2...N

$V_m = E_z^i(\vec{\rho}_m)$

$$Z_{mn} = = \frac{k\eta}{4}\int_{\rho n}^{\rho n+1} H_0^{(2)}(|\vec{\rho}_m - \vec{\rho}|)d\rho \ .$$

From equations 2.31 and 2.33, Z_{mn} takes the form of

$$Z_{mn} \cong \begin{cases} \frac{k\pi}{4}\Delta\left[1 - j\frac{2}{\pi}\ln\left(\frac{\gamma k\Delta}{4e}\right)\right] & m = n \quad \text{(4.20 a)} \\ \frac{k\eta}{4}\Delta H_0^{(2)}(|\vec{\rho}_m - \vec{\rho}_n|) & m \neq n \quad \text{(4.20 b)} \end{cases}$$

The term (4.20b) can be changed to be a numerical integration of the Hankel function over the segments and not only taking the average distance between segment n and m. As it will be seen in the next section, even such an approximation will be lead to good results. It should be remembered that the scatterers dealt with here are electrically small and the number of segments is relatively high and hence the segment width is small.

Since equation (4.19) represents a set of N equations with N unknowns, and all V_m and Z_{mn} can be computed, it is possible to solve for all I_n.
Once all the I_n are known, the current on the strip is known. It must be remembered however that this current represents the total current on the strip (upper and lower side). As shown in section 3.3.1, a similar method could be used to get the top current and the bottom current from the total current:

$$\vec{J}_{Top} = -\left(H_x^i + \frac{1}{2}|J_{total}| \right) \hat{z}$$

$$\vec{J}_{Bottom} = -\left(-H_x^i + \frac{1}{2}|J_{total}| \right) \hat{z}$$

4.3.3 Code and Results

The computer code PSTRIP.FOR was modified to include the TMz case. Figure 12.15 in [2] could also be reproduced exactly with PSTRIP. A number of plots were produced to assess if the approximation in 4.20b is crude and would require very fine slicing in segments. It was concluded that 4.20b is adequate for the cases dealt with here. The results were plotted in section 4.2 for comparison with UTD plots.

4.4 RECTANGULAR CYLINDER SURFACE CURRENT USING UTD

The geometry to be considered is the rectangular cylinder of Figure 3.23 but illuminated by a TMz plane wave incident at an angle φ' between 0° an 90°. The plane wave has a unit magnitude electric field at the origin.

The total magnetic field must be known so that current can be obtained. The solution considers the rectangular cylinder a combination of four edges. GO fields and diffraction from edges are combined to get the total electric field. Since we are dealing here with the TMz case, obtaining the magnetic field from the electric field will be required.

4.4.1 Incident and Reflected Fields

The incident fields at A, B, C and D are:

$$E_A^i = e^{-j\bar{k}.\bar{R}_A} = e^{-jk\left(\frac{wx}{2}\cos\varphi' - \frac{wy}{2}\sin\varphi'\right)}$$

$$E_B^i = e^{-j\bar{k}.\bar{R}_B} = e^{-jk\left(-\frac{wx}{2}\cos\varphi' - \frac{wy}{2}\sin\varphi'\right)}$$

$$E_C^i = e^{-j\bar{k}.\bar{R}_C} = e^{-jk\left(-\frac{wx}{2}\cos\varphi' + \frac{wy}{2}\sin\varphi'\right)}$$

$$E_D^i = 0 \qquad \text{(since } 0<\varphi'<90\text{)}$$

a) On surface AB:

The incident fields at a certain point m (refer to Figure 3.24) are:

$$E^i = e^{-jk\left(-\left(\rho_A - \frac{wx}{2}\right)\cos\varphi' - \frac{wy}{2}\sin\varphi'\right)}$$

$$H_{\tau m}^i = -\eta \sin\varphi' E^i$$

From image theory

$$H_{\tau m}^{GO} = 2 H_{\tau m}^i$$

b) On surface BC:

$$E^i = e^{-jk\left(-\frac{wx}{2}\cos\varphi' - \left(\frac{wy}{2} - \rho_B\right)\sin\varphi'\right)}$$

$H^i_{tan} = \eta \cos\varphi' E^i$

From image theory

$H^{GO}_{Tan} = 2 H^i_{Tan}$

c) On surface CD and DA:

$E^i = H^i = 0$ (since $0<\varphi'<90$)

4.4.2 Diffracted Field

Since the first diffraction will have a zero value at the surface, no multiple diffractions will be considered here.

Since the electric field has only a z component, from Maxwell's equations:

$$\vec{H} = \frac{j}{k\eta} \nabla \times \vec{E} = \frac{j}{k\eta} \left[\frac{1}{\rho} \frac{\partial E_z}{\partial \varphi} \cdot \hat{a}_\rho - \frac{\partial E_z}{\partial \rho} \cdot \hat{a}_\varphi \right]$$

this means that the tangential magnetic field to a certain edge surface is (as long as the origin is taken as the edge tip)

$$\vec{H}_{\tan} = \vec{H}_\rho = \frac{j}{k\eta} \frac{1}{\rho} \frac{\partial E_z}{\partial \varphi} \cdot \hat{a}_\rho \qquad (4.21)$$

Depending on the geometry, the sign will be adjusted if $\hat{\rho}$ is in the $-\hat{x}$ or $-\hat{y}$ directions. Each surface will be considered separately (refer to Figure 3.24).

a) On surface AB:

$$E^d_A = E^i_A \times \frac{e^{-jk\rho_A}}{\sqrt{\rho_A}} \times D_s(\rho_A, \rho_A, 0, \varphi', 1.5)$$

$$E^d_B = E^i_B \times \frac{e^{-jk\rho_B}}{\sqrt{\rho_B}} \times D_s\left(\rho_B, \rho_B, 1.5\pi, \frac{\pi}{2} + \varphi', 1.5\right)$$

from equation (4.21)

$$H^{tan}_{AB} = \frac{j}{k\eta} \left[\frac{1}{\rho_A} \frac{\partial E^d_A}{\partial \varphi} - \frac{1}{\rho_B} \frac{\partial E^d_B}{\partial \varphi} \right]$$

b) On surface BC:

At a certain point m on BC:

$$E_B^d = E_B^i \times \frac{e^{-jk\rho_B}}{\sqrt{\rho_B}} \times D_s\left(\rho_B, \rho_B, 0, \frac{\pi}{2} + \varphi', 1.5\right)$$

$$E_C^d = E_C^i \times \frac{e^{-jk\rho_C}}{\sqrt{\rho_C}} \times D_s\left(\rho_C, \rho_C, 1.5\pi, \pi + \varphi', 1.5\right)$$

from equation (4.21)

$$H_{BC}^{tan} = \frac{j}{k\eta}\left[-\frac{1}{\rho_B}\frac{\partial E_B^d}{\partial \varphi} + \frac{1}{\rho_C}\frac{\partial E_C^d}{\partial \varphi}\right]$$

c) On surface CD:

$$E_C^d = E_C^i \times \frac{e^{-jk\rho_C}}{\sqrt{\rho_C}} \times D_s\left(\rho_C, \rho_C, 0, \pi + \varphi', 1.5\right)$$

$E_D^d = 0$ **(since 0<φ'<90)**

from equation (4.21)

$$H_{CD}^{tan} = \frac{j}{k\eta}\left[-\frac{1}{\rho_C}\frac{\partial E_C^d}{\partial \varphi}\right]$$

d) On surface DA:

$$E_A^d = E_A^i \times \frac{e^{-jk\rho_A}}{\sqrt{\rho_A}} \times D_s\left(\rho_A, \rho_A, 1.5\pi, \varphi', 1.5\right)$$

$E_D^d = 0$ **(since 0<φ'<90)**

from equation (4.21)

$$H_{DA}^{\tan} = \frac{j}{k\eta}\left[-\frac{1}{\rho_A}\frac{\partial E_A^d}{\partial \varphi}\right]$$

On any surface, In paragraphs a) to d),

$H_{\tan}^{Total} = H_{\tan}^{GO} + H_{\tan}^{diffracted}$

the evaluation of $\frac{\partial E^d}{\partial \varphi}$ requires the evaluation of $\frac{\partial D_z}{\partial \varphi}$. As seen previously, this is easily obtained from the slope diffraction coefficient.

4.4.3 Code and Results

A computer code HGTDBX.FOR was created based on the formulation of sections 4.3.1 and 4.3.2. It uses the same slope diffraction coefficient subroutine used for the strip.

As for the TEz case, current density distributions will be shown for a square cylinder illuminated by a TMz plane wave. The diameter of the cylinder =2a. The plots of the current densities are against ρ/a, where ρ is a linear distance on the surface of the cylinder from edge A moving clockwise. This means that for ρ/a =1, the position is halfway between A and B and if ρ/a = 4, the position is at C. The reason for this representation is to be able to compare the results with plots already existent in the open literature [21][22]. The results from the moment method solution described in section 4.5. are plotted (in small circles) also for comparison.

Figures 4.12, 4.13, 4.14 and 4.15 show the current density distribution for ka= 10, 5, 2 and 1 respectively at a 89.5° angle of incidence.

UTD plots compare well with moment method plots and with references [21][22] for all the cylinder surfaces except for side CD . It should be noted here that edge D is receiving a grazing incidence and the effect of multiple diffraction was not considered, hence edge D does not contribute in anyway to the field on CD.

Figures 4.16, 4.17 and 4.18 show the current density distribution for ka= 5, 2 and 1 respectively at a 60° angle of incidence (these cases are not covered in [21][22]). UTD and moment method plots are in agreement except at the edge D. Since with a 60° of incidence edges A, B and C are illuminated by non grazing fields and since the effect of multiple diffraction is not accounted for here, only edge D does not have any contribution to the field on CD and AD. The singular behavior at edges is also similar for both methods except for edge D.

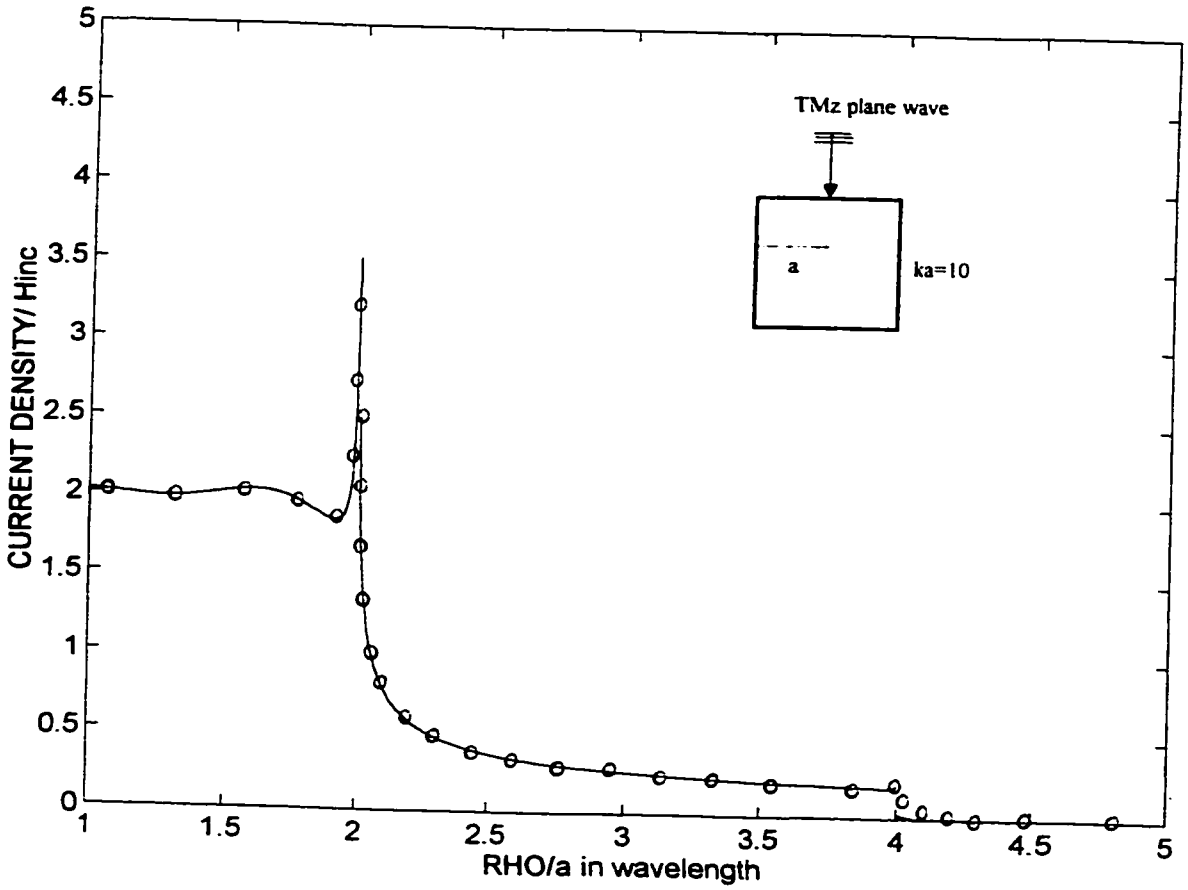

Fig. 4.12 : Normalized current density on the surface of a square cylinder (ka=10. a=1.5915λ) illuminated by a TMz plane wave at φ' =89.5°. [— UTD. ooo MM]

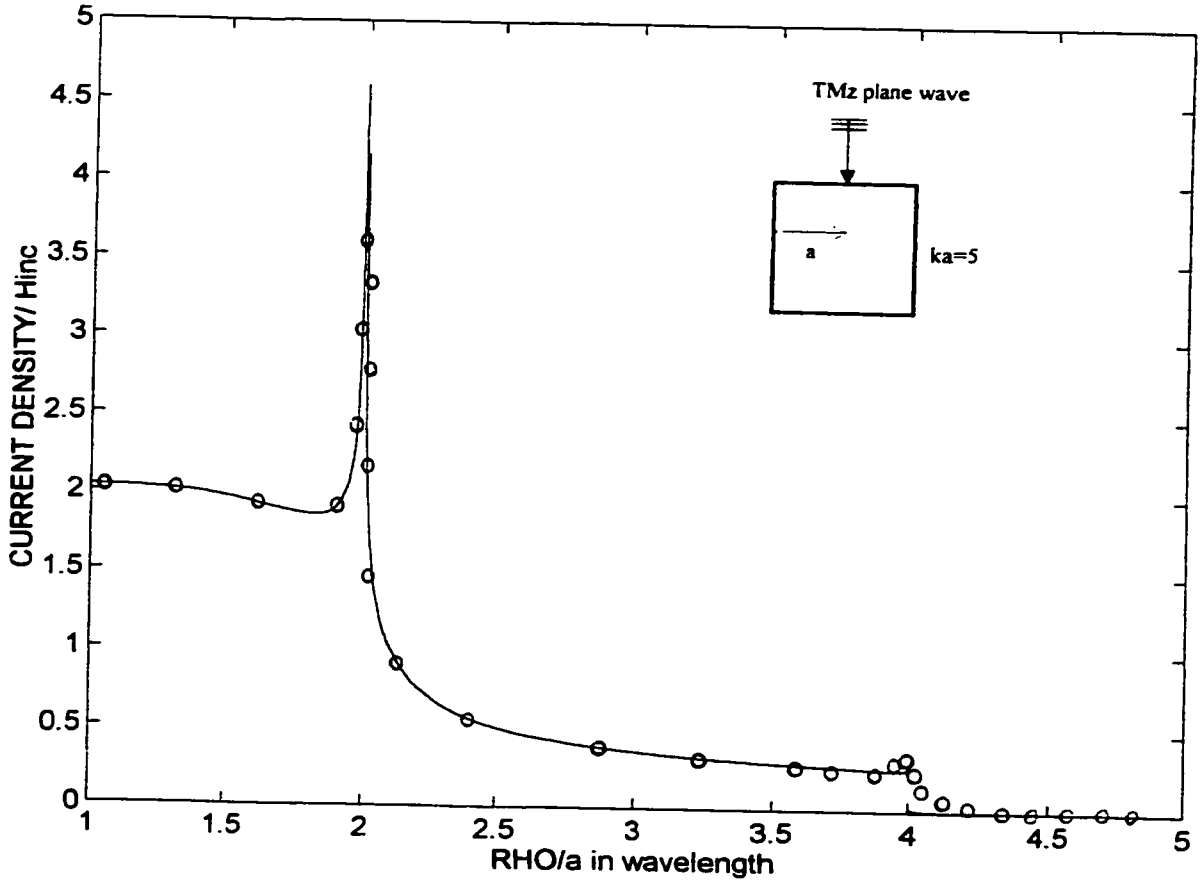

Fig. 4.13 : Normalized current density on the surface of a square cylinder (ka=5, a=0.796λ) illuminated by a TMz plane wave at φ' =89.5°. [— UTD, ooo MM]

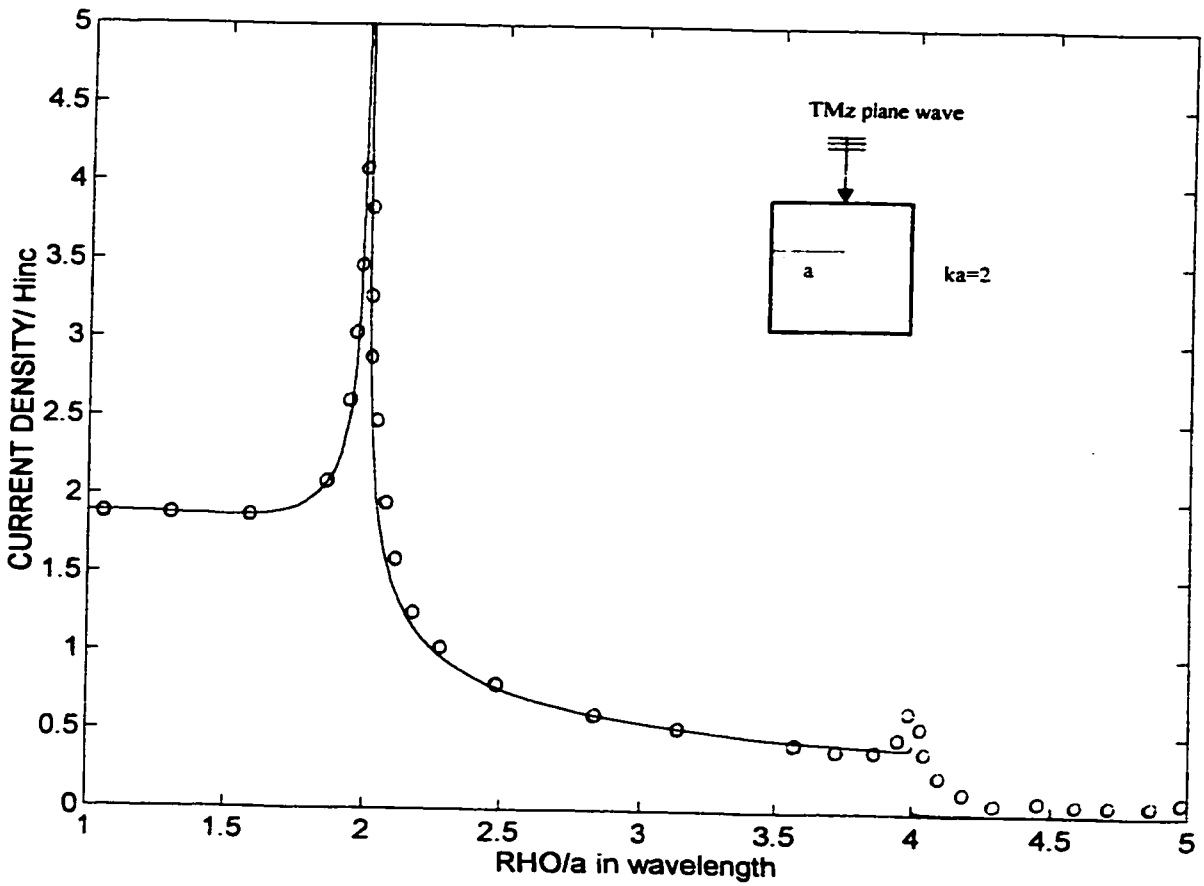

Fig. 4.14 : Normalized current density on the surface of a square cylinder (ka=2, a=0.3183λ) illuminated by a TMz plane wave at φ^{i} =89.5°. [— UTD, ooo MM]

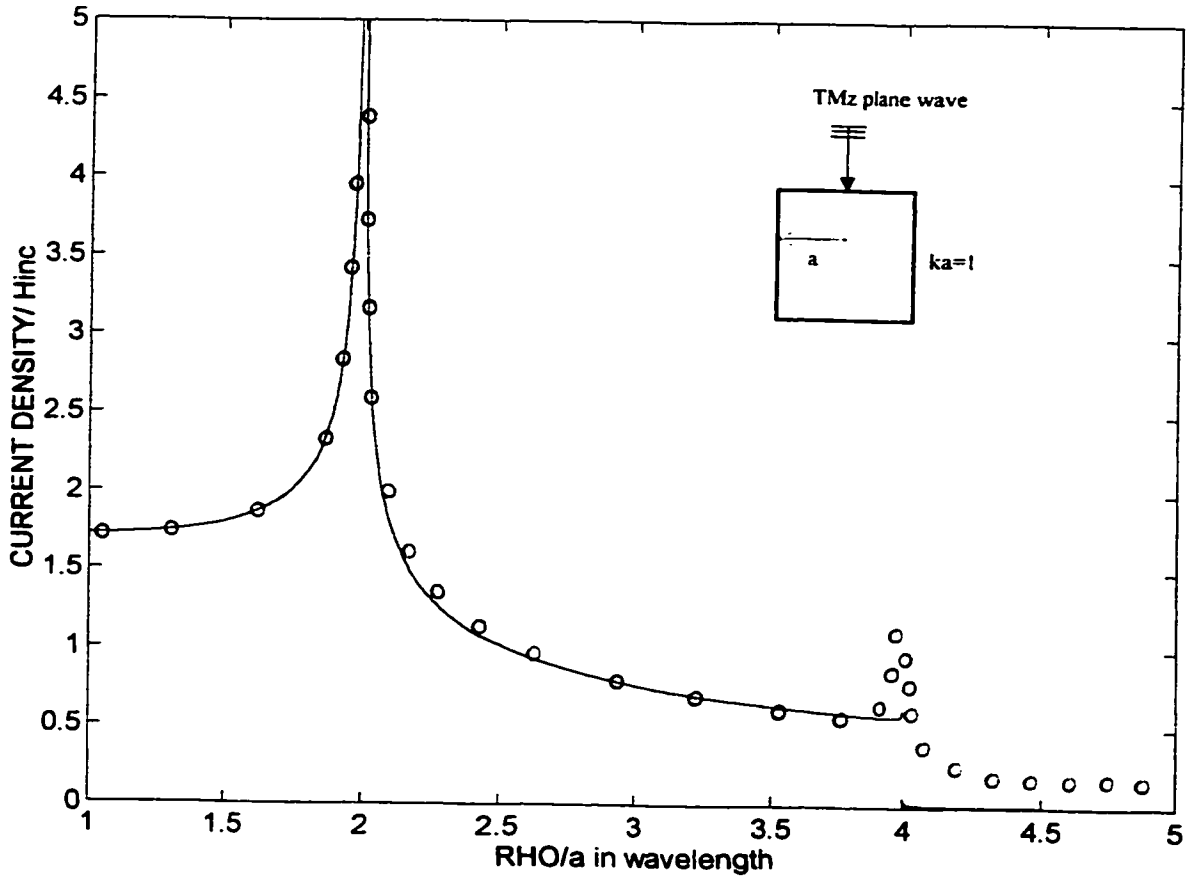

Fig. 4.15 : Normalized current density on the surface of a square cylinder (ka=1, a=0.15915λ) illuminated by a TMz plane wave at φ' =89.5°.[— UTD. ooo MM]

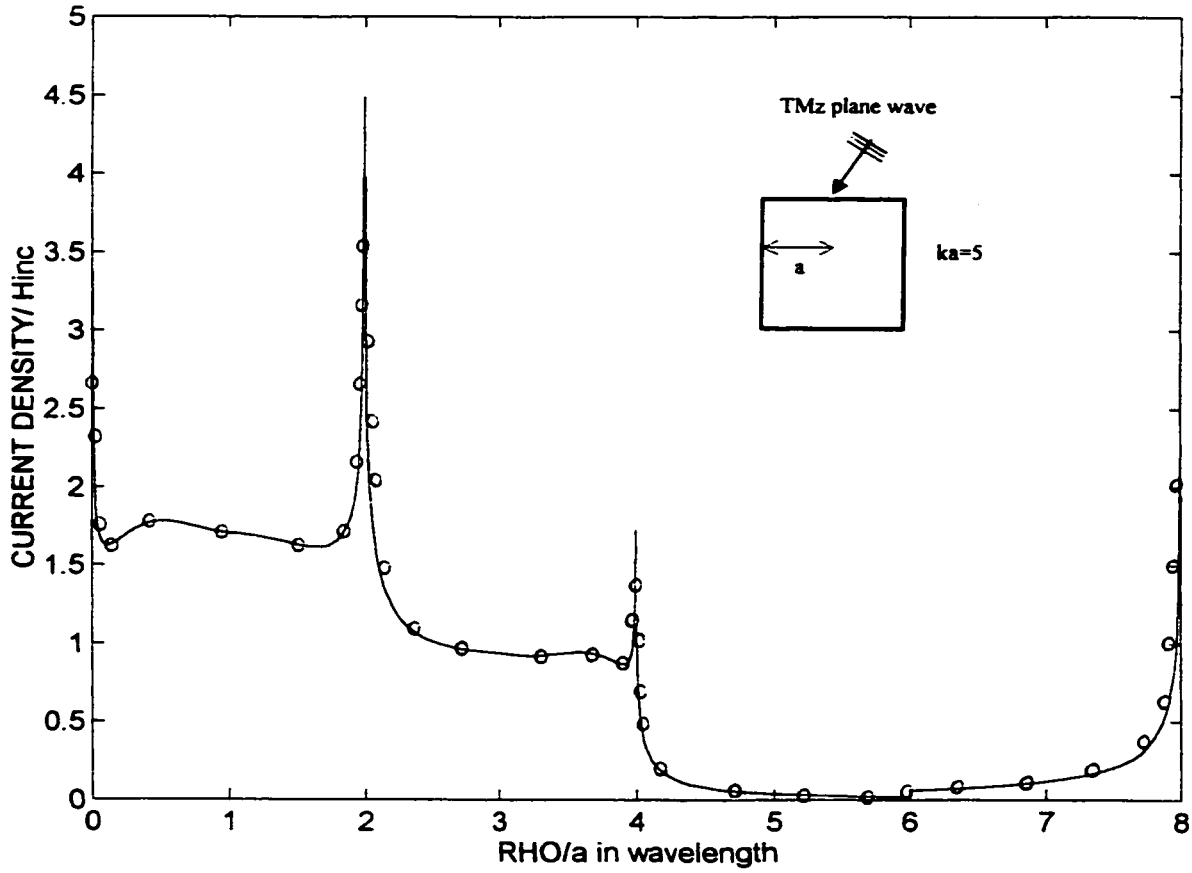

Fig. 4.16 : Normalized current density on the surface of a square cylinder (ka=5, a=0.796λ) illuminated by a TMz plane wave at φ^{i} =60°. [— UTD, ooo MM]

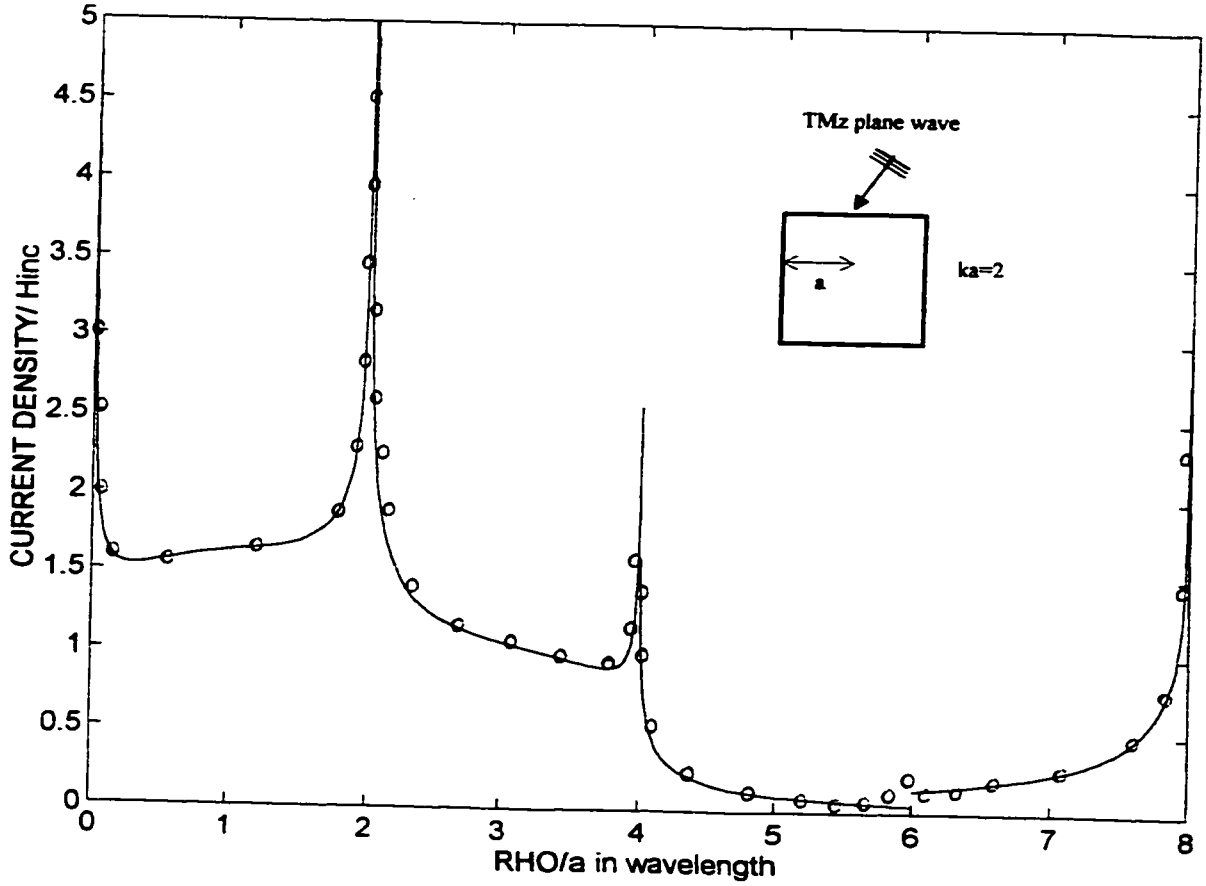

Fig. 4.17 : Normalized current density on the surface of a square cylinder (ka=2, a=0.3183λ) illuminated by a TMz plane wave at φ' =60°. [— UTD, ooo MM]

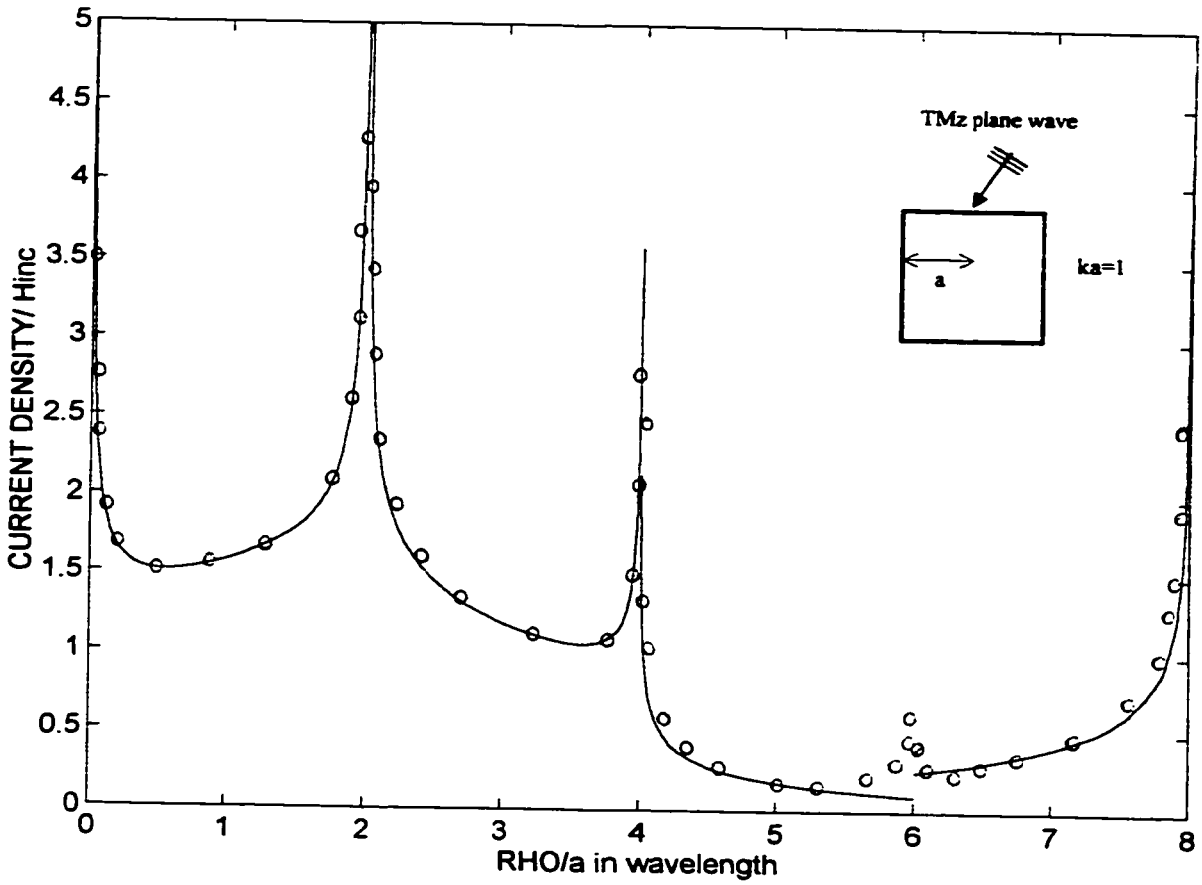

Fig. 4.18 : Normalized current density on the surface of a square cylinder (ka=1. a=0.15915λ) illuminated by a TMz plane was at φ^{i} =60°. [— UTD. ooo MM]

4.5 RECTANGULAR CYLINDER SURFACE CURRENT USING THE MOMENT METHOD

The geometry to be considered is the same as for section 4.3. (refer to Figures 3.23 and 3.24) with a TMz plane wave illumination.

4.5.1 Incident Electric Fields

At any point m on the surface of the rectangular cylinder, the incident electric field is :

$$E_z^i(m) = e^{-j\bar{k}.\bar{R}_m} = e^{-jk(-x_m \cos\varphi' - y_m \sin\varphi')}$$

Since we are dealing with the TMz case there is only a z component for incident and scattered electric fields. Hence the incident field is tangential to the surface of the cylinder.

a) On surface AB:

$$E^i = e^{-jk\left(-\left(\rho_A - \frac{wx}{2}\right)\cos\varphi' - \frac{wy}{2}\sin\varphi'\right)}$$

b) On surface BC:

$$E^i = e^{-jk\left(-\frac{wx}{2}\cos\varphi' - \left(\frac{wy}{2} - \rho_B\right)\sin\varphi'\right)}$$

c) On surface CD:

$$E^i = e^{-jk\left(-\left(\frac{wx}{2} - \rho_C\right)\cos\varphi' + \frac{wy}{2}\sin\varphi'\right)}$$

d) On surface DA:

$$E^i = e^{-jk\left(\frac{wx}{2}\cos\varphi' - \left(\frac{-wy}{2} + \rho_D\right)\sin\varphi'\right)}$$

4.5.2 Scattered Field

From equation 2.17, the scattered TMz field due to a strip is

$$E_z^s(\rho_m) = -\frac{k\eta}{4}\int_0^w J_z(\rho)H_0^{(2)}\left(|\vec{\rho}_m - \vec{\rho}|\right)d\rho$$

The rectangular cylinder is made of 4 surfaces, each to be considered as a strip (aligned in the x or y direction). If each strip now is divided to Nx or Ny segments and if we consider the current on a certain segment n to be of pulse shape, the strip contribution to the scattered field at a certain point m is :

a) From an x aligned strip

$$-E^s(m) = \frac{k\eta}{4}\sum_{n=1}^{N_x} I_n \int_{x_n-\frac{\Delta x}{2}}^{x_n+\frac{\Delta x}{2}} H_0^{(2)}(kR_m)dx \qquad (4.22)$$

where,

x_n= middle of segment n

$$R_m = \sqrt{(x_m - x)^2 + (y_m - y_n)^2}, \qquad y_n = \pm\frac{wy}{2}$$

$$\Delta x = \frac{wx}{Nx}$$

b) From a y aligned strip:

$$-E^s(m) = \frac{k\eta}{4}\sum_{n=1}^{N_y} I_n \int_{y_n-\frac{\Delta y}{2}}^{y_n+\frac{\Delta y}{2}} H_0^{(2)}(kR_m)dx \qquad (4.23)$$

where,

y_n= middle of segment n

$$R_m = \sqrt{(x_m - x_n)^2 + (y_m - y)^2}, \qquad x_n = \pm\frac{wx}{2}$$

$$\Delta y = \frac{wy}{Ny}$$

4.5.3 EFIE and Moment Method

The EFIE can be written as:

$$V_m = Z_{mn} I_n \qquad n=1,2...N \qquad m=1,2...N \qquad (4.24)$$

Where,

V_m = is the incident electric field at point m of the surface of the cylinder

I_n = Current at segment n

N = Nx+Ny+Nx+Ny=2Nx+2Ny=Total number of segments.

Nx = Number of segments for each AB and CD

Ny = Number of segments for each BC and DA.

Additionally the subscript m or n indicates that the observer or the source respectively is present at:

AB if $1 \leq m$ or $n \leq Nx$

BC if $Nx \leq m$ or $n \leq Nx+Ny$

CD if $Nx+Ny+1 \leq m$ or $n \leq 2Nx+Ny$

DA if $2Nx+2Ny+1 \leq m$ or $n \leq 2Nx+2Ny$

From equations 2.31 and 2.33, the formulation of the Z_{mn} terms can be written as:

$$Z_{mn} = \begin{cases} \frac{k\pi}{4}\Delta\left[1 - j\frac{2}{\pi}\ln\left(\frac{\gamma k\Delta}{4e}\right)\right] & m = n \qquad (4.25\ (a)) \\ \frac{k\eta}{4}\int_{\rho_n - \frac{\Delta}{2}}^{\rho_n + \frac{\Delta}{2}} H_0^{(2)}(kR_m)\,d\rho & m \neq n \qquad (4.25\ (b)) \end{cases}$$

where,

$\Delta = \Delta x$ *or* Δy

$\rho_n = x_n$ *or* y_n

$R_m = \sqrt{(x_m - x)^2 + (y_m - y_n)^2}$ *or* $\sqrt{(x_m - x_n)^2 + (y_m - y)^2}$

point m is taken to be at the middle of the segment.

Equation 4.25a is a closed form and equation 4.25b can be evaluated by numerical integration.

4.5.4 Code and Results

A computer code HPBOX.FOR was created based on the formulation in sections 4.5.1 to 4.5.3. The results were plotted in section 4.4 for comparison with UTD plots.

5 CONCLUSION

The results obtained in Chapters 3 and 4 permit the statement of several conclusions regarding the sensitivity of UTD edge diffraction to certain conditions when used at low frequency.

5.1 TEz SCATERRING

Chapter 3 demonstrated that as close as 0.05 λ near an edge, the value of the current density predicted by UTD was still quite adequate. At such a low frequency, UTD was still not sensitive to any angle of edges and their consideration as a source of a local diffraction phenomenon and their interaction together. All of this is true, on the condition that multiple diffraction contribution is taken into account in the computation of the total field. It is true that solving for multiple diffraction terms involves solving linear equations for unknowns but it should be remembered that the number of equations is proportional to the number of edges and not the number of current segments.

UTD accuracy seems to be affected very slightly by the incidence angle (especially near grazing), this is noticeable usually (in the case of the strip) on the edge which is farther from the illumination source. In such a case the edge diffraction coefficient is for the incidence angle which is almost at 180 degrees from both the incident/shadow and the reflection/shadow boundaries and hence much lower in magnitude than the diffraction coefficient of the other edge which is for an angle in the vicinity to both boundaries. This situation affects both the first diffraction and multiple diffractions and the leading term in the asymptotic solution might not be as predominant over other terms on one edge compared to the other.

Plane wave illumination was used exclusively in this work since the interest is for low frequencies and hence electrically small scatterers. It should be noted however that the contribution of waves of cylindrical type were introduced in the total field computation. These were introduced by taking into consideration multiple diffraction to obtain an accurate solution at low frequency. This is by itself a very good indicator that the type of incident wave seems not to be a parameter affecting accuracy.

It is also of general interest to state that even though UTD current density values directly at the edge exhibited a noticeable error, they were at no time unbounded and kept at least a faithful representation of the trend of the current density curve.

5.2 TMz SCATTERING

As seen in Chapter 4, TMz is the most delicate case to deal with. The fundamental difference here is that in the TMz case, the diffracted electric field must be zero on the surfaces of an edge. This means that the first time a field is diffracted and reaches another edge it is zero directly at the edge. This situation prevents the straight forward evaluation of multiple diffraction. The only way at that point to evaluate the effect of multiple diffraction is by introducing slope diffraction which is considered as second order diffraction. The penalty imposed by this situation on accuracy does not seem to be tremendous for directly illuminated surfaces where first diffraction and GO fields exist (less than 10% error). It is significant however when the only contribution to the total field comes from multiple diffraction (on deep shadow surfaces). Usually however these fields are very weak in intensity in this region.

It is of great importance to note also that the UTD solution represents faithfully the singularity at the edge of the TMz case and respects the Miexner condition

of finite energy. It is however very sensitive to the angle of incidence in representing this singularity. It is however understood that this difference between UTD and moment method is on how to represent a singularity by itself and as long as these singularities are understood the final result could be acceptable.

5.3 GENERAL CONCLUSION

A general overview of the variables that could affect UTD solutions at low frequency was done and these included the wedge angle, the interaction between the edges, the size of the scatterers the type of illuminating wave and its polarization and incidence angle. This study showed that for the TEz case, low frequency scattering problems can be solved by UTD with adequate accuracy. The TMz case however should be treated with care. UTD solutions for this polarization are still considered adequate as long as the edge singularity is understood and that surfaces in deep shadow are considered not to be adequately represented.

Multiple diffraction was quite important for the TEz case, but was less important for the TMz case. In the TMz case, multiple diffraction effects become more important as the frequency is lowered.

REFERENCES

[1] R. J. Marhefka and W. D. Burnside, "Antennas on Complex Platforms", *Proceedings of the IEEE*, Vol. 80, No 1, January 1992, pp 204-208.

[2] C. A. Balanis, *Advanced Engineering Electromagnetics,* John Wiley and Sons, Inc,1989.

[3] R. G. Kouyoumjian and P. H. Pathak, "A Uniform Geometrical Theory of Diffraction for an Edge in a Perfectly Conducting Surface", *Proc IEEE*, vol 62, November 1974, pp 1448-1461.

[4] J.A. Aas, "On The Accuracy of The Uniform Theory of Diffraction Close to a 90 deg Wedge", *IEEE Transactions on Antennas and Propagation,* Vol. AP-27, No 5, September 1979, pp 704-705.

[5] E. Kreyzig, *Advanced Engineering Mathematics,* John Wiley & Sons Inc, fifth edition 1983.

[6] J. Van Bladel, *Electromagnetic Fields,* Hemisphere Publication Corporation, Washington,1985.

[7] A. Sommerfeld, *Vorlesungen über Theoretische Physik-English-(Lectures on Theoretical Physics),*Academic Press, New York, 1950.

[8] M. Abramowitz, *Handbook of Mathematical Functions*, Dover Publications Inc New York, 1972.

[9] A. Jeffrey, *Handbook of Mathematical Formulas and Integrals,* Academic Press, San Diego,1995.

[10] W.L. Stuzman and G.A Thiele, *Antenna Theory and Design*, J. Whiley, New York, 1998.

[11] R.E. Collin, *Foundations for Microwave Engineering*, 2nd edition, McGraw-Hill, New York, 1992.

[12] R.F. Harrington, *Field Computations by Moment Methods*, IEEE Press 1993.

[13] W. Perry Wheless and T. Wurtz, "Introducing Undergraduates to the Moment Method", *IEEE Transactions on Education, Vol.38,No. 4, November 1995, pp 385-390*

[14] A.F. Peterson, S.L. Ray and R. Mittra, *Computational Methods for Electromagnetics,* IEEE Press, 1997.

[15] A.F. Peterson, R. Wilton and R. E. Jorgenson, "Variational Nature of Galerkin and Non-Galerkin Moment Method Solutions", *IEEE Transactions on Antennas and Propagation,* Vol. AP-44, No 4, April 1996, pp 500-503

[16] J. H. Richmond,"An Integral-Equation For TE Radiation and Scattering From Conducting Cylinders", Report 2902-7, The Ohio State University ElecroScience Laboratory, October 1972.

[17] J.H. Richmond, "A Reaction Theorem and Its application to Antenna Impedance Claculations", *IEEE Transactions on Antennas and Propagation,*pp 515-520.

[18] J.H. Richmond, "Scattering by a Dielectric Cylinder of Arbitrary Cross Section Shape", *IEEE Transactions on Antennas and Propagation,* Vol 13, No 3, May 1965, pp 334-341.

[19] N. N. Wang, "Self Consistent GTD Formulation For Conducting Cylinders with Arbitrary Convex Cross Section", *IEEE Transactions on Antennas and Propagation,* Vol. AP-24,No. 4, July 1976, pp 463-468.

[20] C.A. Balanis, *Antenna Theory Analysis and Design*, 2nd edition, John Whiley & Sons, Inc,1997.

[21] K. K. Mei and J.G. Van Bladel, "Scattering by Perfectly-Conducting Rectangular Cylinders", *IEEE Transactions on Antennas and Propagation,* March 1963, pp 185-192.

[22] M.G. Andreasen, Comments on" Scattering by Conducting Rectangular Cylinders", *IEEE Transactions on Antennas and Propagation,* March 1964 pp 235-236.

[23] D.A. McNamara, C.W.I. Pistorius and J.A.G. Malherbe, *Introduction to The Uniform Geometrical Theory of Diffraction,* Artech house , Boston, 1990.

[24] T. Veruttipong, "Diffraction at Edges and Convex Surfaces Illuminated by Fields with a Rapid Spatial Variation", Ph.D. Thesis, Ohio State University, 1982.

[25] "Advanced Electromagnetics ELEC 630",*Course Notes*, Concordia University Fall 1997.